

https://dspace.org/

Conceptualisation of hydrogeological system in the crystalline aquifer of the Hout River Catchment, Limpopo Province

Tshipala, Despina

2018

https://hdl.handle.net/10539/26896

Tshipala, Despina Azwinndini (2018) Conceptualisation of a hydrogeological system in the crystalline aquifer of the Hout River Catchment, Limpopo Province, University of the Witwatersrand, Johannesburg, https://hdl.handle.net/10539/26896

Downloaded from a DSpace repository. https://dspace.org/

Conceptualisation of hydrogeological system in the crystalline aquifer of the Hout River Catchment, Limpopo Province

By

Despina Tshipala

Student number: 559339



WITS
UNIVERSITY

A Research Report submitted to the Faculty of Science, University of the Witwatersrand, Johannesburg, in partial fulfilment of the requirements for the degree of Master of Science in Hydrogeology

School of Geosciences

Supervisor: Prof. Tamiru Abiye

October 2018

DECLARATION

I, Despina Azwinndini Tshipala, declare that this research report is my own work and is going to be submitted for the Master of Science in Hydrogeology at the Faculty of Science, University of the Witwatersrand, Johannesburg. It has never been submitted for a degree or examination in any other university.

_____

(Signature)

_____ Day of _____ 20_____ in _____

ABSTRACT

The research focused on conceptualisation of a hydrogeological system in the Hout River Catchment, Limpopo Province. The hydrogeological system in this area is characterised by crystalline aquifer within the Hout-Goudplaats Granite Gneiss, greenstone remnants and younger granite plutons. Like other semi-arid environment, groundwater is the main source of water for agricultural activities and livelihoods. However, normal annual rainfall seems to be insignificant to the overall aquifer replenishment. Aquifer replenishment in these settings has been associated with major rainfall events. The main objective of this study was to develop a feasible hydrogeological model to represent recharge estimation rates and sources, groundwater flow and occurrence and anthropogenic influence within the catchment.

The structural and geophysical analyses showed that dominant dolerite dykes and other lineaments trends are in the NE and NW directions and the measured dolerite dykes have strikes ranging between 088^{o} and 075^{o} and dip angle between 50^{o} and 55^{o}. The lineaments and mafic dykes are highly fractured and weathered. Some of these structures are magnetic and some are non-magnetic. Groundwater levels distribution suggest high levels related to lineaments and dykes, thus indicating structures allowing groundwater flow. There is no clear correlation between structural orientation and physicochemical parameters distribution. Groundwater with high TDS and EC are related to deeply weathered and fractured parts of the aquifer like the Mogwadi area. This groundwater will be less palatable if calcium and magnesium form large constituents of the TDS. Towards the surface headwaters of the Hout River, groundwater shows low TDS and EC. The highest observed mean annual rainfall for the years analysed in this study is 335.02 mm. The catchment is largely receiving rainfall from a regional moisture source shown by lower average deuterium excess of 2.77 ‰. This shows that very little rainfall is recharging the aquifer and the overall aquifer replenishment occurred during humid colder climates from a regional source of moisture possibly the Indian Ocean. The highest mean annual groundwater recharge rate estimated using WTF method is 39.33% of the MAP. The surface water runoff is 13.38% of the MAP. In 2015, groundwater abstractions were estimated at 25.501 Mm^{3}. The ^{14}C activity for the groundwater samples is highest in the north-western part of the catchment at 100 pMC and decreases towards the southern and southern-east part of the catchment at a range between 84.3 to 87.7 pMC. The radiogenic isotopes have shown that older groundwater occurs in pockets of identified weathered and deep fractured

Goudplaats-Hout River Gneiss areas. In contrast, a spring along the northern part of the catchment has a ^{3}H value of 2.2 TU, which shows recharge that occurred 4 years ago. The TDS and EC of this spring water are also low showing less mineralised and dissolved solids; there was no barium-carbonate precipitate formed during sampling of radiogenic carbon, which is indicative of abundant bicarbonate and hence availability of meteoric water. Groundwater sources are emerging from the northern, southern and north-western part of the catchment. Based on ^{3}H and ^{14}C, there are two aquifers within the catchment, which shows interconnectedness along the northern part of the catchment and more disconnected towards the south-eastern part of the catchment.

ACKNOWLEDGMENTS

- This research was financed by the USAID and National Academy of Sciences (USA) and Department of Science and Technology (RSA) through the PEER Program led by Prof. Tamiru Abiye and Dr. Karen Villholth. I would like to give a special thanks to my supervisor Prof Abiye for the immense support and knowledge that he gave throughout the research.
- A special thanks to Mr Mike Buttler form the iThemba Labs, Gauteng for the ^{14}C and ^{3}H analyses.
- I would also like to thank Mr Letsoalo and Mrs Dube from the Council of Geoscience for assisting with structural and geophysical data.
- A special thanks to Mr Lucky from the South African Weather Services (SAWS) and Mrs Irene Joubert from Agricultural Research Council Institute of Soil, Climate and Water (ISCW) for providing climatic data for the project.
- I would like to thank Mr Vester Hyens from the Department of Water and Sanitation, Polokwane for advices and hydrogeological talk he gave us during the site visit. I would also like to thank Mr. Khahliso Leketa from School of Geosciences, Wits and Dr. Karen Villholth, Dr Girma Ebrahim and Dr. Manuel Magombeyi from International Water Management Institute (IWMI- South Africa) who assisted in the field sampling.
- A special thanks to Mr. Botha for collecting rainfall samples for the project.
- Most importantly I would like to thank my family, friends and mentors who believed in me through the challenging times and gave me all the support during the course of this study.
- Above all I would like to thank the God all mighty to see me through the research. To God be the glory.

Table of contents

DECLARATION i

ABSTRACT ii

ACKNOWLEDGMENTS iv

Table of contents v

List of Tables x

Abbreviations xi

Units of Measurements xii

CHAPTER 1 : INTRODUCTION 1

1.1. Background 1

1.2. Problem statement 2

1.3. Research questions 3

1.4. Aims and objectives 3

CHAPTER 2 : LITERATURE REVIEW 4

2.1. Groundwater conceptualisation in basement aquifer 4

2.2. Hydrogeology of the basement crystalline aquifer 6

2.2.1. Crystalline rock aquifer occurrence 6

2.2.2. Basement aquifer recharge 9

2.2.3. Groundwater flow and occurrence 12

2.2.4. Groundwater quality in semi-arid environments 16

2.3. Groundwater abstractions history 17

2.4. Geophysical application in hydrogeology 18

CHAPTER 3 : DESCRIPTION OF THE STUDY AREA 20

3.1. Location 20

3.2. Climate 21

3.3. Geomorphology and drainage system 22

3.4. Land Use 23

3.5. Groundwater Use 23

CHAPTER 4 : GEOLOGICAL SETTING 24

4.1. The Limpopo Mobile Belt 24
4.1.2. The Southern Marginal Zone 24
4.2. Local Geology 26
4.2.1. Paleoarchean Gneiss (3500-3000 Ma) 26
4.2.2. Greenstone Belts (2.8-2.7 Ga) and supracrustal (2.67 Ga) 27
4.2.3. Neoarchean Intrusions (2800-2500 Ma) 28
4.2.4. The Soutpansberg Group (1.85 Ga) 28
4.3. Structural setting 32
4.3.1. Dykes and lineaments 32
4.3.3. Hout River Shear Zone 35
4.4 Hydrogeological Setting of the Hout River Catchment 37
CHAPTER 5 : METHODOLOGY 39
5.1 Structures and Groundwater analyses 41
5.1.1 Aeromagnetic and structural data 41
5.1.2 Groundwater level analyses 42
5.2. Catchment Water Balance Calculation 42
5.3. Water Table Fluctuation (WTF) Method 44
5.4. Physicochemical variables analyses 45
5.5. Environmental isotopes analyses 47
5.5.1. Stable isotopes ($\delta^{18}O$ and $\delta^{2}H$) 47
5.5.2. Radiogenic isotopes (^{14}C and ^{3}H) and stable carbon isotope (^{13}C) 50
CHAPTER 6 : RESULTS AND DISCUSSION 54
6.1. Structures and Groundwater flow patterns 54
6.1.1. Magnetic anomalies signatures and superimposed geological structures 54
6.1.2. The groundwater flow patterns and effects of lineaments on borehole yields 57
6.2. Physico-chemical parameters 59
6.3. Environmental isotopes ($\delta^{18}O$, $\delta^{2}H$, ^{3}H, ^{14}C and ^{13}C) 64
6.3.1. Stable isotopes (^{18}O and ^{2}H) composition 65
6.3.2. Radiogenic isotopes (^{14}C and ^{3}H) and stable carbon (^{13}C) 73
6.4. Water balance and recharge 82
6.4.1. Catchment water balance calculation 82
6.4.2. Water Table Fluctuation (WTF) 87
6.5. Conceptual modelling of the Hout River Catchment aquifer 96

6.5.1 Structural control on groundwater flow patterns 98
6.5.2 Groundwater quality characterisation 98
6.5.3 Groundwater recharge rates and mean residence time 99
CHAPTER 7 : CONCLUSION AND RECOMMENDATIONS 102
REFERENCES 104
Appendix A: GRIP borehole data 113
Appendix B: Mineral (Iron) Map of South Africa. Source: CGS 116
Appendix C: Estimated groundwater abstractions per year per farm from the WARMS data (Ebrahim et al, 2016) 117
Appendix D: Lithology data used to construct a cross-section 121
Appendix E: Data used for conceptual modelling (Data Source: GRIP and NGA) 123

List of figures

Figure 2.1: Three main components of groundwater studies (adapted from Maidment and Hopper, 2005 in Yang et al., 2010).....6
Figure 2.2: Bedrock aquifer layers and their hydraulic properties (Source: Chilton and Foster, 1995).....9
Figure 2.3: Groundwater recharge components in semi-arid environment (Source: Lloyd, 1986).....12
Figure 2.4: Fault anatomy (Source: Bense et al., 2013).....15
Figure 2.5: Vertical Fault (barrier fault) displacing an aquifer (Source: Bense et al., 2013). .16
Figure 3.1: The locality of the Hout River Catchment. 20
Figure 3.2: Long-term rainfall of the Mara (A) and Mogwadi (B) rainfall stations (Data Source: South African Weather Service (SAWS)).....22
Figure 4.1: Regional geology of the study area (Source: Chinoda et al., 2009).....25
Figure 4.2: A) Folded basement Goudplaats Gneiss. B) Highly weathered Hout River Gneiss with an intrusive dolerite dyke.....27
Figure 4.3: Geological map of the Hout River Catchment (Data Source: Council of Geosciences (SA).....30
Figure 4.4: Highly weathered dolerite dyke along the Hout River channel. 33
Figure 4.5: Aeromagnetic map of the Hout River Catchment. Data obtained from the Council of Geoscience (SA).....34
Figure 4.6: Structural map of the Hout River Catchment (Data source: Council of Geoscience (SA)).....36
Figure 4.7: Groundwater level trends of the monitoring boreholes against long-term annual rainfalls within the Hout River Catchment. 38
Figure 5.1: Sampling stations within the Hout River Catchment. (Source: CGS). 40
Figure 6.1: Aeromagnetic map with superimposed geological structures of the Hout River Catchment. 56
Figure 6.2: Groundwater flow patterns.....58
Figure 6.3: Hout River Catchment stable isotopes in rainfall, borehole, river and dam and springs. The LMWL is given by $\delta D=6.7\delta^{18}O +7.2$ ‰ and GMWL by $\delta D=8\delta^{18}O + 10$ ‰ (Craig, 1961).....68
Figure 6.4: D-excess and ^{18}O plots for rainfall, borehole and spring samples within the HRC. 68

Figure 6.5: Depth against ^{18}O for Boreholes (D1 to D8) located within the Mogwadi and eastern-outside the catchment. 69
Figure 6.6: A plot of ^{3}H and ^{14}C for the groundwater samples for pre-1952 and post-1952 recharge. 74
Figure 6.7: A plot of ^{13}C and ^{14}C from the groundwater samples within the HRC. 78
Figure 6.8: Box and Whisker plot of rainfall Oxygen isotopes within the southern, central and northern region of the catchment. 80
Figure 6.9: ^{14}C concentration distribution within the Hout River Catchment. 81
Figure 6.10: A) Rainfall pattern from 2005 to 2016 from the Mogwadi Rainfall Station. B) Rainfall pattern from 1940 to 2013 from the Lekgraal Rainfall Station. C) Rainfall pattern from the Mara PP Rainfall Station. 89
Figure 6.11: A) Hydrograph of averaged groundwater levels from the borehole (A7N0641) from 2008 to 2016 and rainfall record from the Mogwadi rainfall station. B) Hydrograph of averaged groundwater levels from the borehole (A7N0635) from 2006 to 2016 and rainfall record from the Mogwadi rainfall station (data source: SAWS). 90
Figure 6.12: Groundwater recharge rates from boreholes (a) A7N0641 and (b) A7N0635 with rainfall within the Hout River Catchment. 95
Figure 6.13: Surface delineation of the area within the catchment used for cross-section construction. 97
Figure 6.14: Hydrostratigraphic units of the HRC. 100
Figure 6.15: Conceptual model of the Hout River Catchment (groundwater age was determined from the tritium and C-14 results). 101

List of Tables

Table 2.1: Estimated groundwater abstractions from the Hout River catchment for the past 9 years (Ebrahim et al, 2016). 17
Table 3.1: Groundwater use estimation in the Hout River Catchment (Ebrahim et al., 2018). 23
Table 4.1: Stratigraphic column of the Southern Marginal Zone of the LMB. 31
Table 5.1: Magnetic susceptibilities of magnetic iron oxides (Source: Reeves, 2005). 42
Table 5.2: Accepted standards range of physicochemical parameters according to the World Health Organization (W.H.O) (2008, 2009) and DWAF (1996a, b, c). 46
Table 5.3: Samples used for stable isotopes analyses. 48
Table 5.4: Semi-quantitative derived MRT from groundwater tritium values (Sources: Clark and Fritz, 1997 and Weaver et al., 1999). 51
Table 6.1: Physicochemical parameters of groundwater and spring samples within the Hout River Catchment. 63
Table 6.2: Environmental isotope of the Hout River Catchment (November 2016 to March 2017). 70
Table 6.3: Radiogenic isotopes from groundwater, spring and river samples in the HRC..... 75
Table 6.4: Reference evapotranspiration calculation of the year 2015 using the FAO-54 Method (Allen et al., 1998). 83
Table 6.5: Monthly crop evapotranspiration of the year 2015. 86
Table 6.6: Catchment water balance for the year 2015. 86
Table 6.7: Recharge and discharge estimating from boreholes located within gneiss, dolerite, soil and granite rocks in the Hout River catchment. 93

Abbreviations

DIC	- Dissolve Inorganic Carbon
DWAF	- Department of Water Affairs and Forestry
GMWL	- Global Meteoric Water Line
GRIP	- Groundwater Resource Information Project
HRSZ	- Hout River Shear Zone
LMWL	- Local Meteoric Water Line
MRT	- Mean Residence Time
MAP	- Mean Annual Precipitation
SMZ	- Southern Marginal Zone
D_x	- Deformation event
M_x	- Metamorphic event
r	- Correlation Coefficient
WTF	- Water Table Fluctuation Method
NGA	- National Groundwater Archives
SAWS	- South African Weather Services
ARC-ISCW	- Agricultural Research Council- Institute, Climate and Water
IWMI	- International Water Management Institute
VSMOW	- Vienna Standard Mean Ocean Water
TDS	- Total Dissolved Solids
EC	- Electrical Conductivity

Units of Measurements

m.a.m.s.l. l	- Meters above Mean Sea Level
TU	- Tritium Units
Mg/l	- milligrams per litre
µS/cm	- Micro Siemens per centimetre
%	- percentage
nT	- Nanotesla
BP	- Before Present
pMC	- Percent Modern Carbon
NTU	- Nephelometric Turbidity Units
+mV	- Redox potential
m	-meters
M m^3	- million cubic meters

CHAPTER 1 : INTRODUCTION

1.1. Background

The study that deals with the development of a workable conceptual hydrogeological model is focused in the Hout River Catchment (HRC) and includes the town of Mogwadi (Dendron) as a reference in the Limpopo Province. Development of a conceptual model in semi-arid environment requires a holistic understanding of aquifer dynamics. This is to ensure sustainable groundwater management particularly in regions where groundwater is the main source of water supply. Like the study area, groundwater has been the sole source of water for commercial agricultural activities since 1950s (Verster, 2003). Commercial potato farming in the area extends from Mogwadi to Vivo towards the northern part of the catchment (Pietersen et al., 2011). Moreover, groundwater is also used for domestic purposes and livestock watering within the catchment. Over the years, increased water demand as a result of expansion in irrigated areas led to groundwater overexploitation threatening groundwater resource depletion and conflicts amongst the users. In some areas, groundwater levels declined to depths of 50 m by lowering productivity and profit in commercial farming. This problem prompted implementation of groundwater monitoring programmes, which included monitoring of water levels and abstracted volumes, adapting centre pivots irrigation methods, shifting from low value crops such as maize to high value crops (potatoes). However, groundwater levels continue to decline, and more boreholes are abandoned.

The HRC is one of the sub-catchments of the larger Sand River Catchment and overlays the Houdenbrak basement aquifer (Pietersen et al., 2011). The aquifer occurs within the basement crystalline rocks of granitic gneiss known as the Goudplaats-Hout River gneisses with characteristic low permeability and porosity. Tectonic and geomorphological evolutions consequently increased permeability and hydraulic conductivity of these rocks subsequently forming a composite aquifer of a weathered zone and underlying fractured crystalline bedrock. The fractured zone reaches a depth of 120 m in the Mogwadi area increasing groundwater flow and occurrence (Jolly, 1986). In certain boreholes around this area, blow yields of over 40 l/s were recorded (Pietersen et al., 2011).

Results from the previous researches contributed towards an understanding of the groundwater dynamics within the Limpopo Plateau. Holland (2011) explored different regional aspects (geology, weathered zone thickness, structural lineaments, topography, hydrology and geomorphology) to try to understand how each parameter influences aquifer transmissivity in different areas and ultimately borehole yields. The report showed that high transmissivity values are associated with contact aureoles, pegmatites, topographical lows and areas proximal to lineaments. There was no distinct correlation between weathered zone thickness and the transmissivity. Different recharge techniques were also applied to understand groundwater recharge and the residence time within the aquifer (Bredenkamp et al., 1995; Mandiwana, 2004; Holland, 2011; Ebrahim et al., 2016). Bredenkamp et al. (1995) applied the CMB method that gave recharge amount of 0.7-8.0 % of the mean annual precipitation (MAP) (440 mm/a) for the Mogwadi aquifer. A similar recharge value of 0.5 % of MAP was obtained by Holland (2011) using the CMB method. Furthermore, Ebrahim et al. (2016) developed a numerical modelling for the Hout River Catchment to understand irrigation changes and groundwater flow dynamics using a 3D numerical groundwater flow model (MODFLOW 2005 combined with Farm Process Package). The model used similar conceptual model approach as this study although other variables viz. DEM analyses are not considered in this study. The model estimated annual recharge between 2.5-10 mm, which is similar to the range of values found in previous studies. For irrigation, the model gave pumping values within the range of 6.0-7.7 M m^3/a between 2008-2012 simulation period.

1.2. Problem statement

Development of conceptual hydrogeological model in the basement crystalline aquifer of the HRC was motivated by the problem of overexploitation of groundwater over many years. Crystalline aquifer terrains in semi-arid environments are replenished during episodic events of heavy rainfalls and floods (Van Wyk, 2010). In the HRC, groundwater abstractions have been exceeding recharge for many years (Jolly, 1986; Masiyandima et al., 2002 and Verster, 2003). As such, conceptual modelling integrating structural analyses, stable (^{18}O and ^{3}H) and radiogenic (^{14}C and ^{3}H) isotopes, WTF and water balance methods will help conceptually characterise the hydrogeological system towards sustainable management of the aquifer.

1.3. Research questions

This problem ultimately raised questions as to:

- Where is the source of this groundwater and how much is being recharged from the annual rainfall?
- After recharge, how is it moving and for how long has it been circulating within the aquifer?
- What is the water quality of the groundwater in the area?

1.4. Aims and objectives

The aim of this study is to develop conceptually feasible hydrogeological model. The conceptual model will help as a simplified representation of groundwater recharge sources, recharge rates, structural control on groundwater flow and occurrence as well as groundwater quality. The research questions towards conceptual modelling for the aquifer in the HRC will be addressed through the following objectives:

- Reviewing of literature on the aquifer geology, structural setting and groundwater recharge processes specific to crystalline aquifers.
- Analyse structures and identify correlation with groundwater flow and occurrence.
- Analyse physico-chemical parameters.
- Estimate groundwater recharge rates using water balance calculation and Water Table Fluctuation (WTF).
- Apply environmental isotopes (^{18}O, ^{2}H, ^{3}H, ^{13}C and ^{14}C) to identify sources of recharge, groundwater interconnection and groundwater residence time.
- Develop a conceptual model for the study area.

CHAPTER 2 : LITERATURE REVIEW

2.1. Groundwater conceptualisation in basement aquifer

Conceptual modelling in hydrogeology is the development of conceptually simplified representation of a complex and variable hydrogeological process interacting in a hydrogeological system (Anderson and Woessener, 1992). The main purpose of conceptual model development is to solve specific challenges entangled in a complex hydrogeological system (Anderson and Woessener, 1992). These challenges could involve the need to understand the origin and quantity of groundwater, its flow and occurrence, and how it has been influenced by geological as well as anthropogenic factors over the years. Based on the purpose of the conceptual model, conceptual modelling could be used to predict the future outcomes, recreate past hydrogeological environments and interpret changes and behaviours in a hydrogeological system (Anderson and Woessener, 1992). The purpose of modelling should give directions on the type of data that needs to be collected which should also closely represent the real hydrogeological system under study. Subsequently, the conceptual model could be used to develop a numerical model (Yang et al., 2010). Credibility of a numerical model will dependent on the proximity of the conceptual model to the actual site conditions (Maidment and Hopper, 2005). The more conceptual model reflects field conditions, the more accurate will be the numerical model (Anderson and Woessener, 1992).

Development of a conceptual model is preceded by data collection, which will be guided by the purpose of modelling and then succeeded by numerical modelling (Fig 2.1). Data in development of a conceptual model should generally include groundwater levels, geological and geomorphological data, climatic, soil, hydrology, hydrochemistry data and anthropogenic influences. The more data is acquired the more actual conditions are represented, thus simplifying the complex conditions. However, it is not possible to represent all the detailed components of a hydrogeological system being studied; hence a close representation suffices (Fetter, 2001).

After data collection, three main components of conceptual model should be analysed. The first, which is a boundary condition, is used to constrain the focus of the study and very useful for the development of numerical models (Yang et al., 2010). It is delineated based on groundwater divides, hydrogeological features and impermeable rocks identified in geological,

topographical and potentiometric maps of the study area (Anderson and Woessener, 1992). It is important to note that groundwater divide does not always coincide with the watershed. Subsequently, modelling requires identification of hydro-stratigraphic units which are defined as zone of similar hydraulic properties that are grouped into aquifers or aquitards according to how easy they allow groundwater flow and occurrence (Kresic and Mikszewski, 2013). Connectivity of pore spaces and fractures determine whether the unit will be an aquifer or an aquitard collectively forming hydrofacies in a local scale and make hydro-stratigraphic units in a regional scale (Anderson and Woessener, 1992). Hydraulic properties are determined using pumping test analysis (Wilson, 2005).

The representation of the conceptual model involves fence diagrams, cross sections and tables whereby numerous softwares are used to analyse, organise, synthesize and represent conceptual behaviour of a hydrogeological system (Anderson and Woessener, 1992).

In the Limpopo Province, Holland (2011) conceptualised the crystalline basement aquifers using variations in transmissivity values influenced by different regional aspects (topography, geomorphology, geology, structures, weathering thickness, neo-tectonic stress and hydrogeology). These regional factors were found to have influenced borehole productivity. High productivity locations were in areas where boreholes have been sited closer to drainage systems, on the bed rocks and closer to structures. It was also shown that structures (NE and ENE) perpendicular to the neo-tectonic stresses direction (NW) are associated with high transmissivity values.

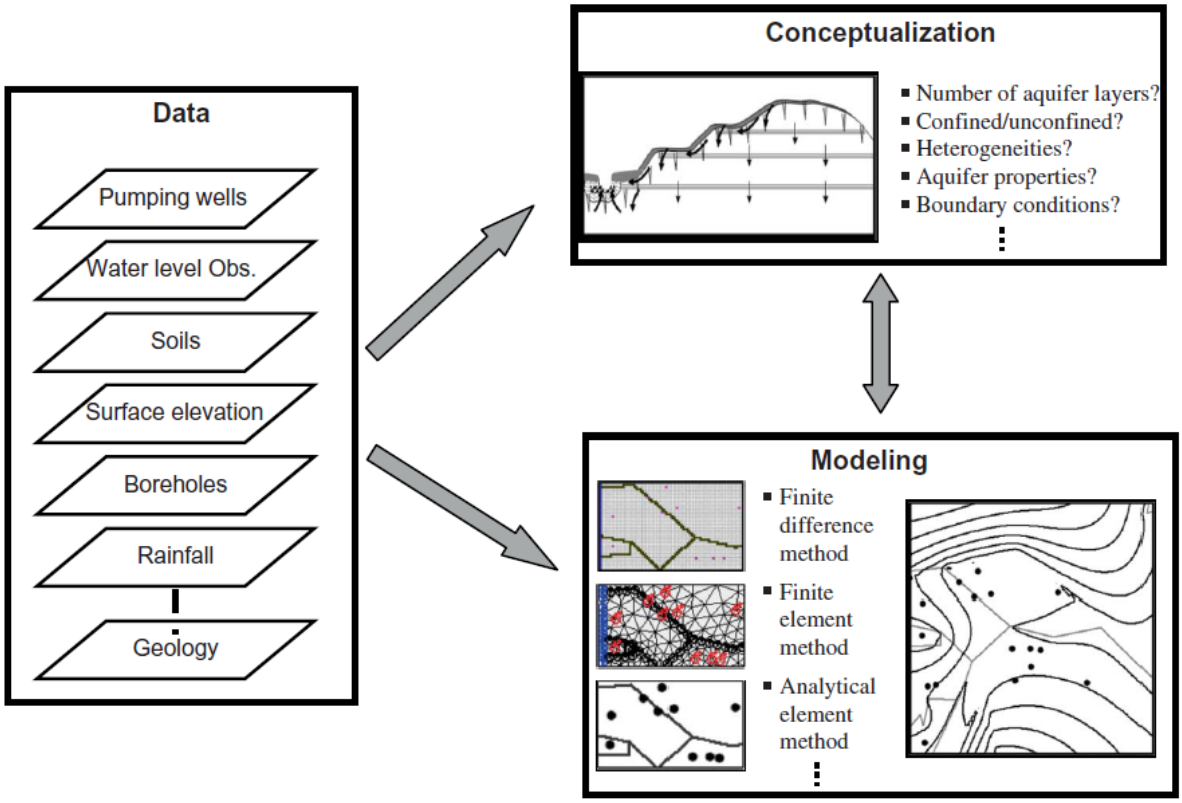


Figure 2.1: Three main components of groundwater studies (adapted from Maidment and Hopper, 2005 in Yang et al., 2010).

2.2. Hydrogeology of the basement crystalline aquifer

2.2.1. Crystalline rock aquifer occurrence

The basement crystalline aquifers are formed in fractured igneous and metamorphic rocks of the Precambrian age with intrinsic low permeability and porosity (Wright, 1992; Guftason and Krasny, 1994). They are overlain by weathered overburden, which is thick in tropical environments and thin in semi-arid environments (Wright, 1992). Their occurrence in South Africa range from the Archaean cratons, mobile belts and an orogenic granite intrusions (Holland, 2011). In the study area, these aquifers are formed in fractured granite gneiss known as the Goudplaats-Hout River gneisses of the Limpopo Mobile Belt (LMB).

The conceptualisation of hydrogeological units in crystalline aquifers has been consistent from the 1980s where studies identified two principal hydrogeological layers forming a composite aquifer (Clark, 1985; Jones, 1985; Acworth, 1987; Wright, 1992). These kinds of aquifers form after regional weathering and fracturing in crystalline rocks. They consist of the upper weathered zone and the lower fractured zone (Wright, 1992) (Fig 2.2). The weathered zone in which the upper unconfined aquifer forms, consists of a collapsed zone and saprolite profile (Jones, 1985). The underlying profile is represented by the fractured rock (sap-rock) with high groundwater storage capacity (Jones, 1985; Wright, 1992). Beneath the sap-rock, fresh (un-weathered) fractured bedrock occurs as a base of the entire profile with negligible groundwater occurrence unless a deep-seated fracture system exists. Within the study area, the composite aquifer in the Mogwadi area is said to be hydraulically connected (Pietersen et al., 2011).

Detailed descriptions of these hydrogeological profiles are given below.

2.2.1.1. The weathered zone

This zone consists of a superficial collapsed zone underlain by saprolite horizon in variable thickness, typically in the range of 30 and 50 m in the humid regions and lesser thickness within the semi-arid conditions (Wright, 1992). On the Limpopo Plateau, the thickness of the regolith is in the range of 15-50 m (Pietersen et al., 2011). The thickness of the weathered zone, which determines the hydraulic parameters of this zone depends on the bedrock mineralogy, petrography, geophormology, deformational events, chemistry and climate (Guftason and Krasny, 1994). The collapsed zone or residual soil is formed by bioturbation and leaching of the saprolite zone (Chilton and Foster, 1995). This zone consists of transported materials (Jones, 1985) and is underlain by stone lines, calcretes and laterites (Chilton and Foster, 1995). The vadose zone mostly comprises the collapsed zone and plays an important role during recharge (Chilton and Foster, 1995).

The saprolite horizon is dived into two portions which resulted from a prolonged in-situ chemical weathering (Houston and Lewis, 1988). The upper portion consists of clay and sand materials due to frequent water table fluctuations leading to extreme weathering (Dewandel et al., 2010). The lower portion has weathered minerals of primary to intermediate nature (Chilton and Foster, 1995). Porosity is generally high, but permeability is low due to clay minerals

concentration (Acworth, 1987; Houston and Lewis, 1988). The groundwater storage capacity is higher along the lower part of the saprolite making it the main upper aquifer horizon; here, weathering has selectively decomposed some of the minerals forming gravels and thus increasing porosity (Jones, 1985). The contact between the saprolite and the underlying saprock is sharp within coarse-grained crystalline rocks and gradational within banded or fine-grained rocks (Chilton and Foster, 1995).

2.2.1.2. Fractured rock (Saprock)

The fractured rock horizon forms the middle horizon of the basement crystalline aquifer profile (Chilton and Foster, 1995). It consists of fractures of variable orientations (Wright, 1992). The formation of these fracture systems could be ascribed to either cooling stresses after magma emplacement (Houston and Lewis, 1988) and/or decompression related to weathering and erosion under litho-static conditions (Wright, 1992; Chilton and Foster, 1995). Although it has been proven difficult to assign these fractures to a specific mechanism of formation, fractures that resulted from decompression activities have been identified to have common sub-horizontal orientations (Wright, 1992). These fractures are said to dominate up to a depth of 40 to 50 m (Chilton and Foster, 1995). Similar depth of decompression fractures occurrence has been recorded during pumping test activity in the Victoria Province of the Zimbabwe region (Houston and Lewis, 1988). In contracts, fractures that resulted from tectonic activities have common sub-vertical orientations and extend to deeper depth as compared to the decompression fractures (Wright, 1992). These fractures decrease with depth consequently allowing less groundwater flow and occurrence. Saprock zone is the most drilled horizon with high storage capacity (Holland, 2011). In the Mogwadi area, this zone reaches a depth of about 120 m (Jolly, 1986).

2.2.1.3. Fresh (un-weathered) Bedrock

It forms the basement layer with deep tectonic fractures without weathered materials (Gustafson and Krasny, 1994). The regional fractures are entirely tectonic in origin, hence characterised by sub-vertical orientations and often in zonal concentrations (Chilton and Foster,

1995). Tectonic fractures allowing groundwater flow are of tensile and shear nature; the flow of groundwater is controlled by the interconnectedness and frequency of these fractures (Chilton and Foster, 1995).

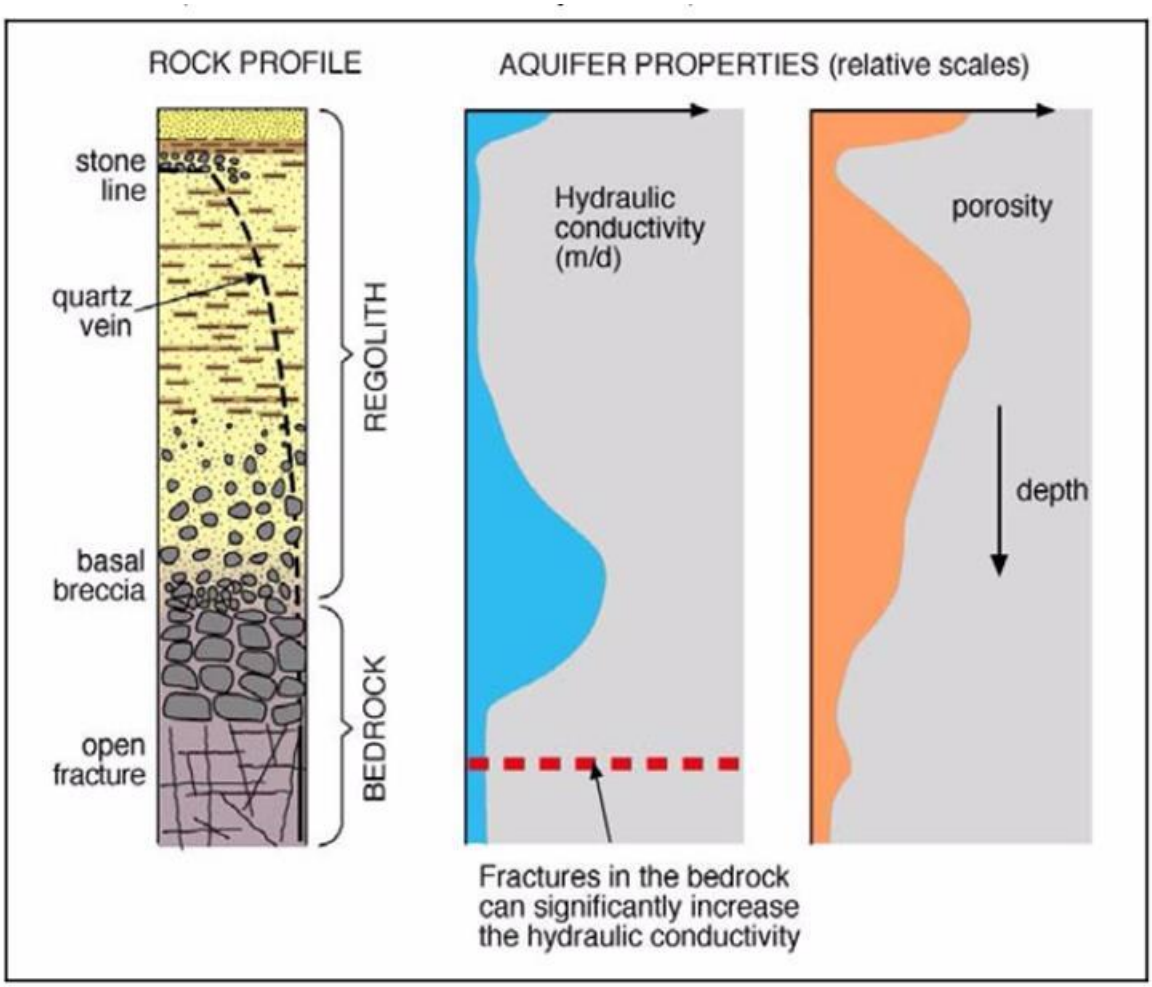


Figure 2.2: Bedrock aquifer layers and their hydraulic properties (Source: Chilton and Foster, 1995).

2.2.2. Basement aquifer recharge

Groundwater recharge is generally defined as the downward movement of water through an unsaturated zone into the water table (Lloyd, 1986; De Vries and Simmer, 2002; Scanlon et al., 2002). It is expressed as a percentage of mean annual rainfall or as mm per year (Xu and

Beekman, 2003). Natural groundwater recharge occurs through direct, indirect and localised mechanisms (Lerner et al., 1990). Direct (diffuse) recharge occurs when water arrives at the water table in excess of soil moisture deficits and evapotranspiration (Lerner et al., 1990). Indirect recharge occurs through beds of surface water bodies, while localised recharge mainly occurring through fractures and depression cracks. In semi-arid environment, the most common recharge mechanisms for total aquifer replenishment are indirect and localised recharge (Simmers, 1998; de Vries and Simmers, 2002). Direct recharge becomes important in this region for aquifer replenishment only during heavy rainfall or flood events (Van Wyk, 2010).

A normal annual rainfall is unlikely to have significant water returns to the aquifer due to potential evapotranspiration, which is always higher than the mean annual rainfall, meaning a lot of rainfall gets evaporated back to the atmosphere before reaching the aquifer (Xu and Beekman, 2003). It has been shown that a mean annual rainfall of less than 400 mm yields a negligible recharge through direct flow in semi-(arid) environments (Bredenkamp et al., 1995). However, there are other factors that control recharge, which need to be considered in addition to the amount of rainfall. These include intensity of rainfall, geological setting, geomorphology (topography, vegetation and soil) setting, weathering processes and degree of fracturing (Scanlon et al., 2002). Considering flow mechanisms and factors influencing recharge helps to choose a reliable and suitable recharge estimation method (Fig 2.3) (Lloyd, 1986; Simmers, 1998). Like in the case of recharge study of the Southern Africa, Abiye (2016) showed that different methods yield large recharge variations which may compromise sustainable management of groundwater resources.

Structures and weathered zone properties similarly play an important role in basement aquifer recharge (Learner et al., 1990). Discontinuities makes recharge estimation complicated, thus it is essential to use multiple recharge estimation techniques in basement aquifers to reduce uncertainty (Simmers, 1998).

There are different groundwater estimation techniques, which require a clear understanding of the purpose of recharge estimation before these recharge estimation methods could be applied. Xu and Beekman (2003) outlined different techniques applicable to the southern African semi-arid environments. Out of these recharge techniques, Cumulative Rainfall Departure (CRD), Chloride Mass Balance (CMB), Water Table Fluctuation (WTF), Groundwater Modelling, Saturated Volume Fluctuation (SVF) and Extended model for aquifer Recharge and moisture Transport through unsaturated Hard-rock (EARTH) are most reliable (Xu and Beekman, 2003).

Abiye (2016) showed that most reliable recharge estimation methods that will give more accurate results are those that consider aquifer properties such as WTF, CMB and SVF methods.

Limitations may be encountered on some trustworthy methods like CMB and ^{3}H if more careful measures are not considered (Xu and Beekman, 2003). These methods are sensitive to flow mechanism in the vadose zone, as such, flow mechanism in this zone should be identified prior to their application. In contrast, WTF method applicable to the unconfined zones is not affected by the flow mechanism. The application of this method requires that precipitation is attributed to the water level rises, thus only effective when there is vertical recharge (Healy and Cook, 2002). However, it is difficult to attribute the water levels changes to precipitation when evapotranspiration, atmospheric pressure and entrapped air also lead to water level changes (Healy and Cook, 2002).

Groundwater recharge studies also cover the knowledge of mean residence time (MRT) of groundwater within the aquifer. Although there are wide range of groundwater dating methods, ^{14}C and ^{3}H isotopes are mostly applied (Beyer et al., 2014). ^{14}C dates older groundwater reaching to maximum age of 50 000 years, while ^{3}H isotope dates groundwater of much younger age (< 50 years) (Clark and Fritz, 1997). The use of ^{3}H isotope to date mean residence time (MRT) of groundwater was first explored in the 1950s (Bergman and Libby, 1957). In various parts of the Limpopo Province, Holland (2011), Verhagen et al. (2009) applied ^{3}H and ^{14}C methods for groundwater dating. Their observations show that groundwater in this region has been mixed whereby they vary in age from modern to sub-modern. In the Hout River Catchment no ^{3}H and ^{14}C study isotopes have been done.

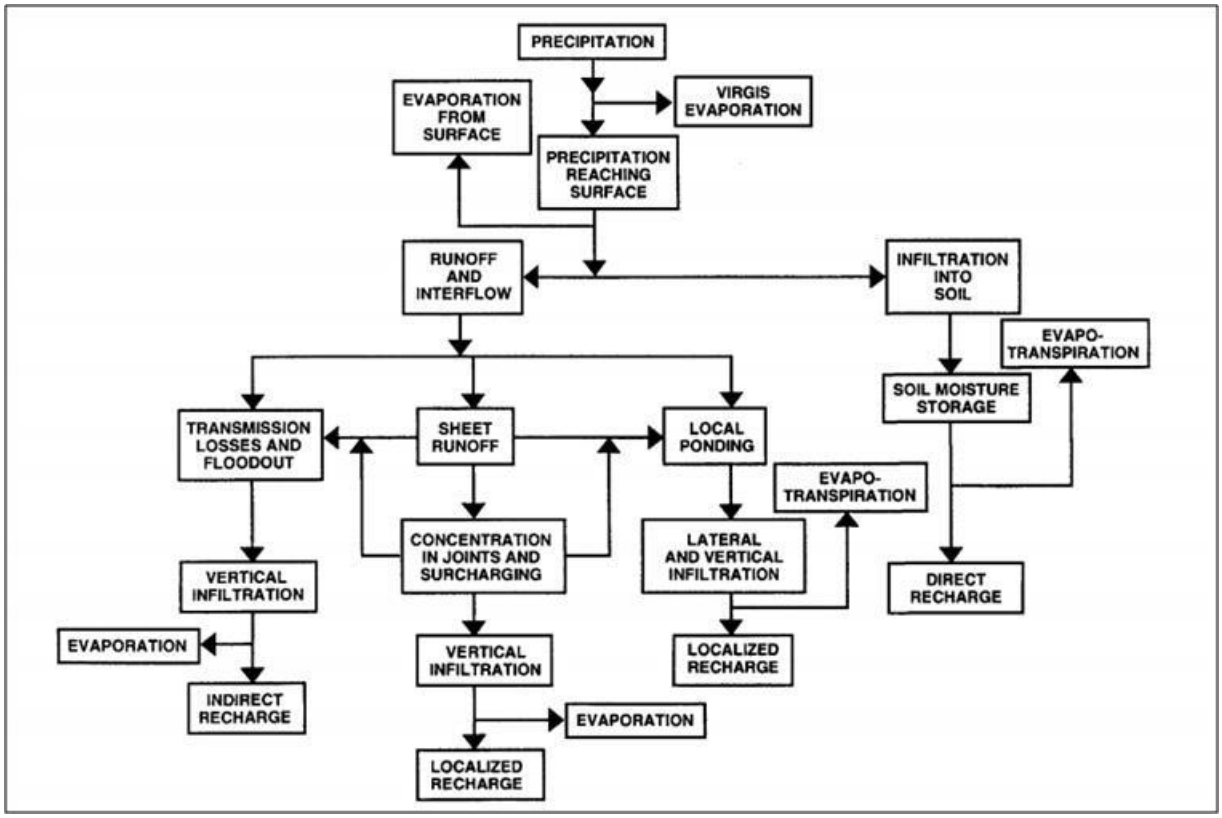


Figure 2.3: Groundwater recharge components in semi-arid environment (Source: Lloyd, 1986).

In the study area, previous recharge work gave recharge percentages of 0.7 to 8 % of the mean annual precipitation around the Mogwadi area (Bredenkamp et al., 1996). Masiyandima et al. (2002) also estimated values in the range of 2-5% of 400 mm MAP. Frequently used recharge method involves CBM whereby recharge was estimated at 0.5% (Holland, 2011). All these results confirm that very little amount of rainfall in this area forms part of recharge into the aquifer.

2.2.3. Groundwater flow and occurrence

The flow and occurrence of groundwater within basement aquifer is influenced by hydraulic properties of the overlying weathered zone (regolith) and the underlying fractured zone. The former has low permeability and high porosity and acts as a reservoir for the underlying high permeable and low porous bedrock (Wright, 1992). The model of groundwater flow within a

weathered-fractured aquifer assumes a homogeneous porous media and purely fractured media (Cook, 2003). The fluid flow in a porous media is explained through the Darcy's law of fluid flow (Cook, 2003).

2.2.3.1 Groundwater flow within the weathered aquifer

As indicated in the previous sections, the weathered zone is made up of 3 sub-zones of variable hydraulic properties. In the collapsed/soil zone, permeability, porosity and specific yield are greatly reduced because of decomposed secondary minerals (Wright, 1992) subsequently reducing the aquifer's hydraulic conductivity. Groundwater flow in this aquifer will either flow in gaps between sand grains if the aquifer is homogenous or flow through preferential zones if the aquifer has a heterogenous nature (Cook, 2003). Like the collapsed zone, the upper saprolite comprises of clay minerals which reduces permeability of this layer (Chilton and Foster, 1995). The lower part of the saprolite has increased porosity and low permeability which increases storage coefficient of this zone (Jones, 1985). Environments where weathering did not produce mica minerals, the area will be characterised by increased permeability like an unconsolidated sediment increasing hydraulic conductivity (Clark, 1985).

In addition to the groundwater flowing through gaps between grains, groundwater flow in the weathered zone also flow along decompression fractures. Southern Africa has undergone five geomorphological cycle that resulted into episodic events of erosion and weathering leading to different events of decompression fracturing (Matthys et al., 2009). These fractures are also potential groundwater flow paths. In this zone, groundwater flow is modelled through fractured porous media whereby groundwater flow through preferential paths with the aquifer matrix storing some water when porosity exists (Cook, 2003).

2.2.3.2. Groundwater flow within the crystalline aquifer

Occurrence of groundwater in the crystalline rocks is determined by the density, aperture and interconnectedness of fractures (Chilton and Foster, 1995). These structures include fractures, shear zones, joints and foliations (Matthys et al., 2009). Groundwater flow through fracture formed by tectonic events is related to stress regimes that may have imposed closing and re-opening of these fractures during different tectonic events. In most cases, groundwater flow in fractured aquifer is modelled through a purely fractured media which assumes planar and parallel fractures with no aquifer matrix (Cook, 2003). Presently in the LMB, the maximum

principal horizontal stresses are in the NW-SE direction and compression stresses along the NE-SW directions (Witthüser et al., 2011). In this case, the structures perpendicular to maximum stress (σ_1) axes have undergone dilation and have high potential to allow groundwater flow and structures parallel to the σ_1 axes have been largely closed. However, Witthüer et al. (2011) indicated that in normal condition structures parallel to the (σ_1) are expected to open. It was further shown that the structures striking NE-SW formed during the Ventersdorp Rifting event with extension in the NW-SE direction, which means that there was re-activation of the structures by subsequent events increasing fractures aperture and connectivity. In the Limpopo Province Matthys et al. (2009) and Holland. (2011), proposed five models on groundwater occurrence within the crystalline aquifer viz. Hout River Shear Zone (HRSZ), closed fractures parallel to the neo-compression stresses, open structures parallel to the extension stresses, geological contacts and decompression fractures in weathered aquifers.

Faults also play an important role in groundwater occurrence in the study area particularly when the HRSZ has been identified to comprise strike slip and reverse faults. Groundwater occurrence associated with fault structures are controlled by the fault's anatomy (Fig 2. 4). A fault zone that forms in the brittle-ductile zones forms a core, damage zone and also a drag zone (ductile). Fault's core is less permeable but increases in the damage zone (Bense et al., 2013). However, the permeability is also anisotropic in the damage zone.

The orientations of fault also influence the flow of groundwater. A vertical fault similar to the identified faults within the study area will act as a barrier if the flow of groundwater is perpendicular to the strike of the fault. In contrast, the flow that is parallel to the strike of the fault will act as a conduit and allow groundwater flow (Fig 2.5) (Bense et al., 2013). In general, faults that are gently dipping are normally associated with high permeability (Bense et al., 2013). The effect of an overburden over a fault zone on groundwater flow and occurrence will be determined by the type of fault, geological and geomorphological evolution and the hydraulic properties of the overburden after faulting. The fault zones occurring within

unlithified sedimentary rocks lead to different hydraulic head or fluid pressure on the hangingwall and footwall of the fault zone (Bense and van Balen, 2004).

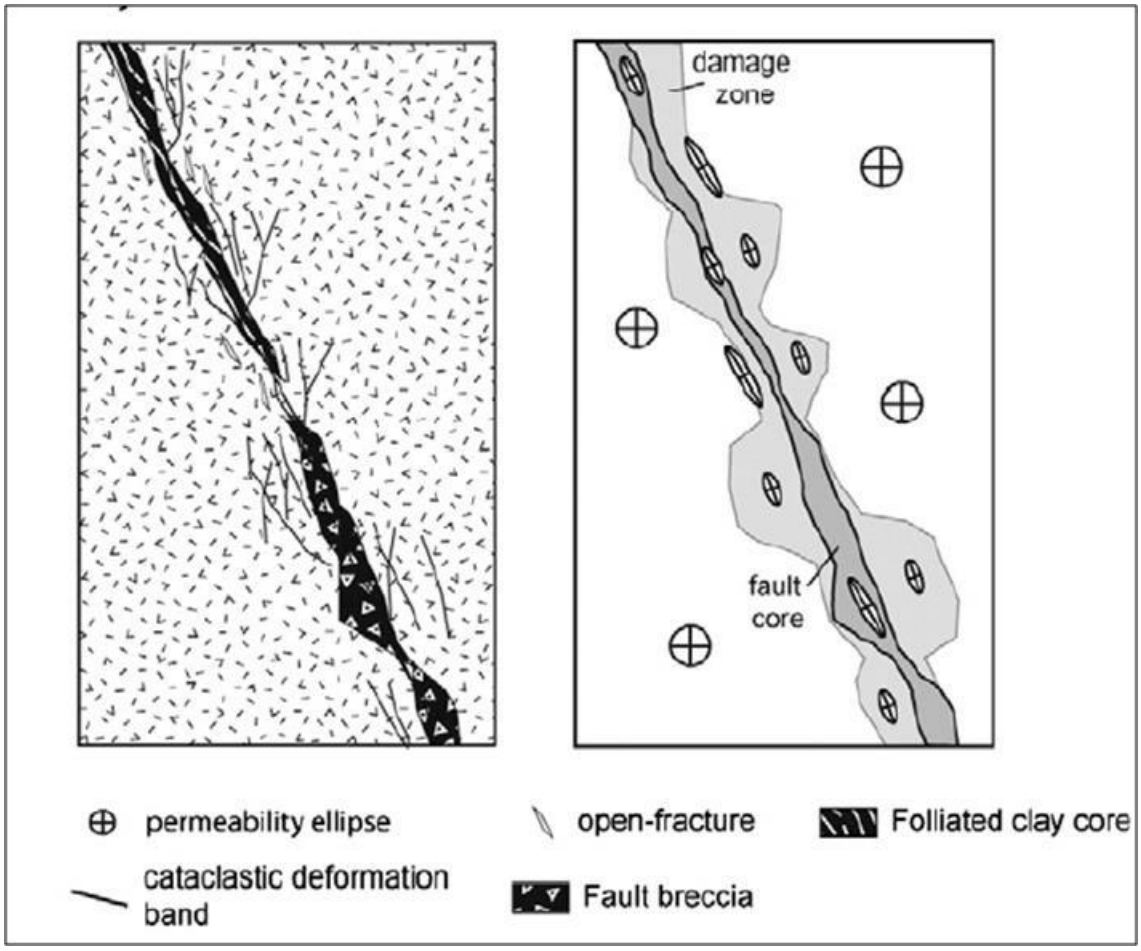


Figure 2.4: Fault anatomy (Source: Bense et al., 2013).

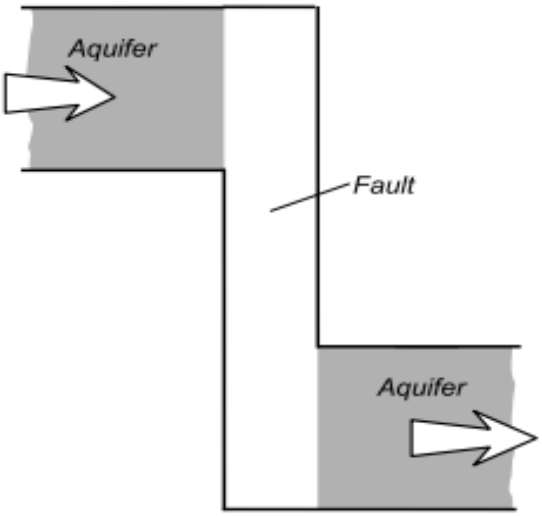


Figure 2.5: Vertical Fault (barrier fault) displacing an aquifer (Source: Bense et al., 2013).

Dykes also control the occurrence of groundwater within an aquifer. Orientation and also thickness of the dykes determine if they act as a barrier or allow groundwater flow (Bromley et al., 1994). Based on groundwater levels and pumping test data, Bromley et al. (1994) found that thickness greater than 10 m behaves as barriers and those less than 10 m in thickness act as conduits for groundwater flow. This suggest high hydraulic conductivity and degree of fracturing of dykes less than 10 m thickness, hence allowing groundwater flow.

2.2.4. Groundwater quality in semi-arid environments

Long groundwater circulation and low recharge rates significantly increases salinity in the semi-arid environment (Clark, 1985). As a result, most water in this region becomes unpalatable “hard water” due to increased dissolved solids of Ca and Mg constituent after long periods of water-rock interaction and agricultural activities (Clark, 1985). In the absence of Ca and Mg, groundwater salinity will be increased as a result of other ions such as Na and Cl (DWA,1996). Groundwater in crystalline aquifers is prone to contamination and pollution since regolith is thinner with fractured zones of high transmissivities allowing fast movements of pollutants and contaminant to flow into the aquifer (Holland, 2011). Quality of groundwater

is evaluated through chemical, physical and microbiological parameters (Mandiwana, 2004). These parameters indicate whether water is suitable for use and measured against different acceptable standards given in DWA (1996) and WHO (2008; 2009; 2011).

2.3. Groundwater abstractions history

Recordings of volume of groundwater abstractions and related irrigated area in the Mogwadi area dates back to 1968s. According to Jolly (1986), groundwater was extracted as the irrigated area increased each year except for the year 1974, where high rainfall events led to less groundwater abstractions. In the 1968, an area of 1319 ha was irrigated using 9.3 million cubic meters. The abstractions decreased to 8.5 million m^2 in the 1974, while the irrigated area increased to 1474 ha. The groundwater abstraction value further increased in 1986 to 21 Mm^3, which irrigated 3579 ha. Recently, a crop consumptive use model has been used to estimate groundwater abstractions for a period of 9 years as is shown in Table 2.1. This groundwater abstraction was obtained from areas delineated as irrigated crops area using Landsat Normalized Difference Vegetation Index (NDVI) and crop water requirements (Ebrahim et al., 2016). The model was calibrated based on groundwater level data observed between 2008 and 2012 and used to validate data in the period of period 2013 to 2015. They found that the hydrogeological system is characterised by delicate human-natural system which relies on a small yet highly variable component of the water balance making it more vulnerable to anthropogenic and climate changes.

Table 2.1: Estimated groundwater abstractions from the Hout River catchment for the past 9 years (Ebrahim et al, 2016).

Year	Estimated abstractions (M m^3/year)
2007	30.034
2008	29.883
2009	29.811
2010	29.596
2011	29.495
2012	29.495
2013	27.975

2014	27.569
2015	27.501

2.4. Geophysical application in hydrogeology

Application of geophysics in hydrogeology to characterise aquifers has been lumped into a section in hydrogeology studies of hydro-geophysics. The potential of geophysics applications in characterisation of aquifer properties and process is increasing due to large spatial data that can be acquired at ease (Rubin et al., 1999). Normal techniques used to understand hydrological properties of a hydrogeological system are limited in spatial distribution where else geophysical methods cover large ground area with high resolution (Rubin et al., 1999). Additionally, geophysical methods are also less invasive (Rubin et al., 1999). As indicated in Butler (2005), a simple wellbore method is unable to identify spatial distribution of aquifer characteristics.

According to Rubin et al. (1999), the most used geophysical techniques in hydrogeology are electrical, seismicity, magnetics and gravity methods. These methods have different applications in hydrogeology, which helps in better characterisation of a hydrogeological system.

In crystalline aquifers, structures are one of the integral parts of the hydrological system and influence groundwater flow within the aquifer. According to Balsubramanian (2007), magnetic methods are commonly used to delineate the features affecting groundwater flow such as intrusive, geological contacts, bedrock lineation and dykes. Additionally, magnetic methods like aeromagnetic data are best used in the interpretation of structures with magnetic nature as well as faults and lineaments. Aeromagnetic survey applications are easy to use because of fewer corrections that need to be done on them (Moghaddam et al., 2015). According to Reeves (2005), mafic dykes retain residual magnetism which formed when magma was rapidly cooled after emplacement. Other magnetic signatures associated with dykes occur along contact aureole which also gives pronounced magnetic anomalies (Reeves, 2005). According to Sakala et al. (2014), some of the NE structures indicate strike slip faults tracing the trail of the Hout River Shear Zone.

Previous aeromagnetic study that was done within the study area have shown that magnetic lineaments have formed patterns representing different tectonic events (Holland, 2011). Most detailed aeromagnetic survey in groundwater investigation within the Limpopo River Basin was that of Holland (2011). Sakala et al. (2014), further used the same method to analyse structures within the Hout River Catchment. Their work showed that lineaments largely interpreted as dykes were emplaced under extensional forces due to parallel pattern. They also indicated that considerable extension of these structures as they appear in aeromagnetic maps is evidence of emplacement of dykes along pre-existing weak zones under extensional forces.

CHAPTER 3 : DESCRIPTION OF THE STUDY AREA

3.1. Location

The study area is within the Hout River Catchment (HRC), which is located north of Polokwane on the Limpopo Plateau (Fig 3.1). This area is dominated by commercial farming that largely depends on groundwater (Masiyandima et al., 2002; Verster, 2003). Mogwadi area, previously known as Dendron, is one of the old towns located approximately on the centre of the catchment and surrounded by potato farms (Fig 3.1). The HRC is a sub-catchment of the larger Sand River within the Limpopo River Basin. It is divided into three quaternary catchments which are A71E, A71F and A71G making an area of 2478 km^2 in total.

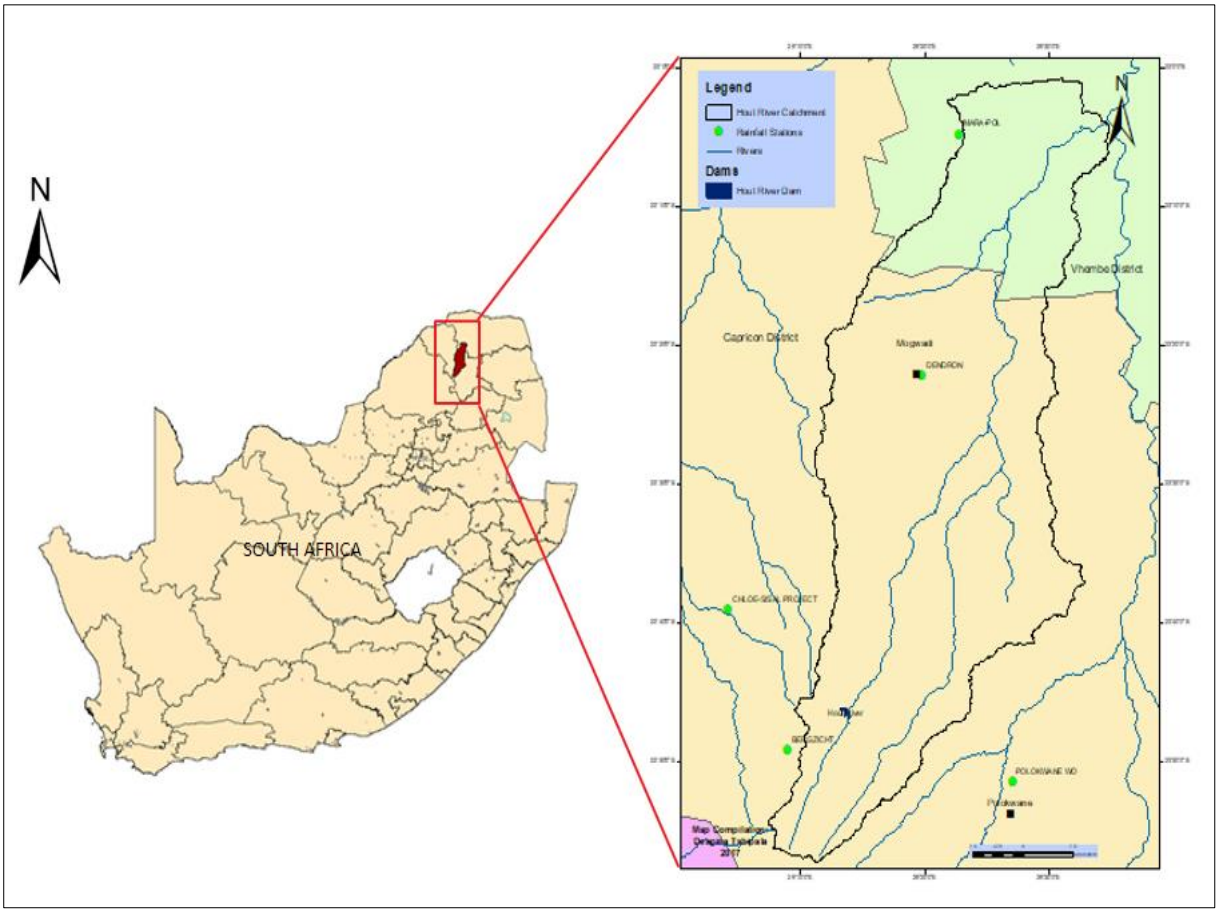
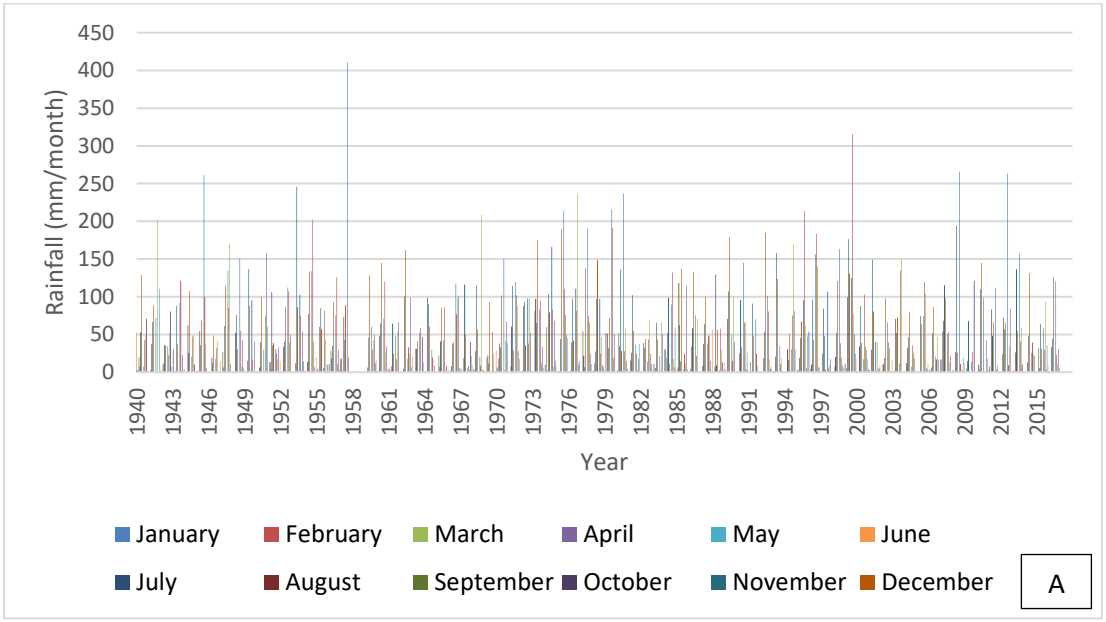


Figure 3.1: The locality of the Hout River Catchment.

3.2. Climate

The HRC is characterised by semi-arid subtropical climate. The mean rainfall ranges from 200 mm/yr towards the south and increases to 1200 mm/yr towards the Soutpansberg Mountains in the north due to an orographic effect (DWA, 2004). Generally, there is a decreasing trend in rainfall from the south towards the north. In the Mogwadi area, mean annual rainfall in the year 2002 was approximately 400 mm with rainy seasons starting in November until March/April (Masiyandima et al., 2002). However, over the years with increasing aridity, each year shows a decrease in rainfall to date (Fig 3.2a and b). Major flood events that might have replenished aquifers in this area and the entire country were in 1934, 1958, 1976, 1986, 1996 and 2000 and major drought in the year 1995 (Verster, 2017). The Mara area rainfall plot shows high rainfall value coinciding with the flood events in 1958 and 2000 (Figure 3.2a).

Mean annual temperatures reach a maximum of 30º in January and minimum annual temperatures reach 4º in July (DWA, 2004). About 95 % of precipitation is lost through evaporation due to potential evapotranspiration that is always greater than precipitation (Masiyandima et al., 2002).



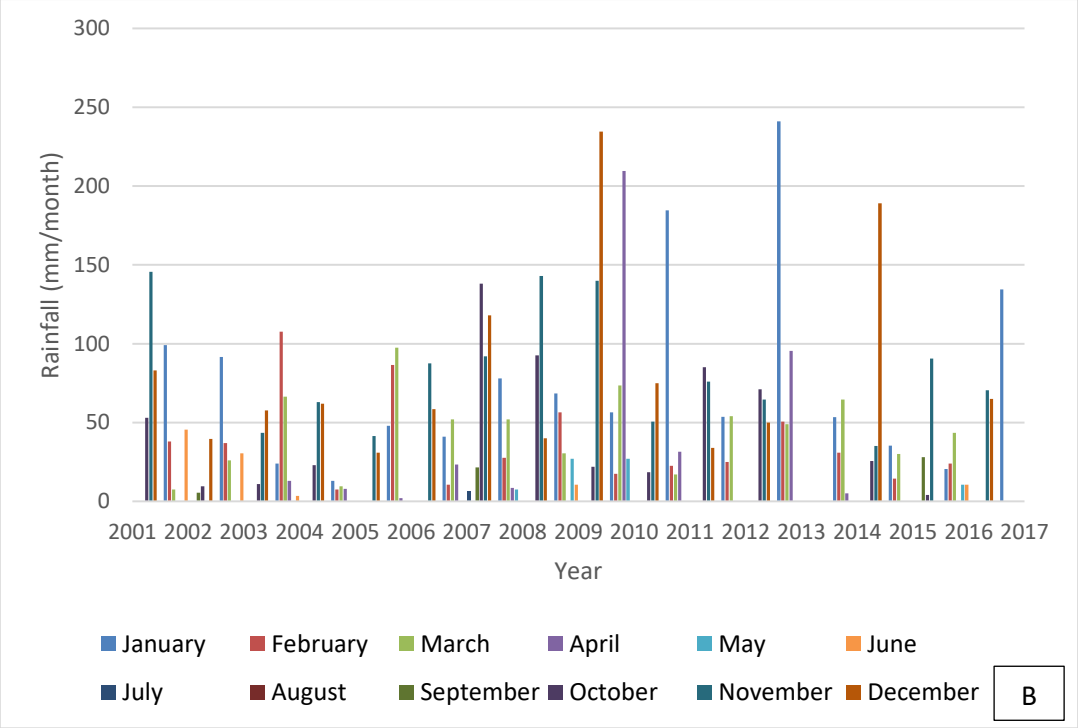


Figure 3.2: Long-term rainfall of the Mara (A) and Mogwadi (B) rainfall stations (Data Source: South African Weather Service (SAWS)).

3.3. Geomorphology and drainage system

The study area is characterised by variable landscapes dominated by old erosional surfaces and sporadic granitic outcrops. Elevations range from 1400 m.a.m.s.l near Polokwane and decreases to 400 m.a.m.s.l towards the confluence where Sand River traverses the Soutpansberg Mountains to join the Limpopo River (DWAF, 2003). To the north, the catchment is bound by Soutpansberg Mountains with elevation of about 1400 m.a.m.s.l (DWA, 2004). The area is covered by old erosional surface with alluvium sands occurring along the trajectories of the river channels.

Headwaters of the HRC are located about southwest of Polokwane and drains towards the northeast. Like other tributaries of the Sand River, Hout River has incised through erosional surfaces and the underlying crystalline rocks with less defined channels due to low elevations towards the northern part of the catchment. These rivers are ephemeral and largely flow during rainy seasons with Hout Dam built along the southern part of the catchment (Verster, 2003).

3.4. Land Use

The main land use within the catchment is represented by the commercial farms that dominated in the area around Mogwadi town stretching towards the northern portion of the catchment Main crops are potatoes, pumpkin, maize, oats, wheat and cotton (Masiyandima et al., 2002). There are also livestock farming as well as sporadic subsistence farming within the surrounding villages. For these activities, groundwater is the sole source of water (Verster, 2003). Towards the southern part of the catchment, the area is dominated by rural settlements that rely on both groundwater and Hout Dam for water supply.

3.5. Groundwater Use

Groundwater is mainly used for irrigation, and also used for livestock watering and domestic use (Verster, 2003). Groundwater is largely used for potatoes' irrigation and less on maize (Masiyandima et al., 2002). According to Jolly (1986), volume of groundwater that was abstracted for 3579 ha reached 20.8 x 10^6 m^3 and 1 x 10^6 m^3 for stock watering and domestic use in the year 1985/6. In 2004, about 50 farms were operational around the Mogwadi area but approximately 150 farms used groundwater for livestock watering (Mandiwana, 2004). Ebrahim et al. (2018) simulated groundwater abstraction for irrigation over from 7 years at an average of 6.2 Mm^3/a (Table 3.1).

Table 3.1: Groundwater use estimation in the Hout River Catchment (Ebrahim et al., 2018).

Ground water use	2008/2009	2009/2010	2010/2011	2011/2012	2012/2013	2013/2014	2014/2015	Mean	Standard Dev
Irrigation pumping (Mm^3/a)	6.2	5.5	6.8	6.4	4.5	6.7	7.5	6.2	1.0

CHAPTER 4 : GEOLOGICAL SETTING

4.1. The Limpopo Mobile Belt

The Hout River Catchment is located within the Southern Marginal Zone (SMZ) of the Limpopo Mobile Belt (LMB). The LMB formed when the Kaapvaal and Zimbabwe Craton collided ~2.7 Ga ago (van Reenen et al., 1992). It is subdivided into three tectonostratigraphic zones, which are the SMZ, Central Zone (CZ) and Northern Marginal Zone (NMZ) trending ENE (Fig 4.1) (van Reenen et al., 1990; Chinoda et al., 2009). Shear zones trending parallel to the three tectonostratigraphic zones dissect and separate them from the adjacent cratons (Chinoda et al., 2009). To the south, the Hout River Shear Zone (HRSZ) separates granite and greenstone rocks of the Kaapvaal Craton from the high-grade granulite facies of the SMZ (van Reneen et al., 1990). Towards the north, the Northern Shear Zone separates the Zimbabwe Craton from the granulite rocks of the NMZ (Van Reenen et al., 1990). After peak metamorphism into the granulite facies, these rocks underwent retrogression consequently forming the upper amphibolite facies localised in certain areas (Van Reenen et al., 1992). An orthoamphibole isograd trending E-W occurs along the hanging-wall of both the SMZ and the NMZ (van Reenen et al., 1992).

4.1.2. The Southern Marginal Zone

The SMZ is bounded to the south by the HRSZ and to the north by the Sunnyside-Palala Shear Zone (Chinoda et al., 2009). Goudplaats-Hout River Gneisses (Baviaanskloof Gneisses) of the tonalitic and trondjemitic compositions are the basement rocks of this zone (Van Biljon and Legg, 1983; Anhaeusser, 1992). Greenstone dismembered remnants are sporadically infolded within these basement rocks (Anhaeusser, 1992). According to Smit et al. (1992), the SMZ went through four stages of deformation, which formed major structural fabrics trending NE-SW and Neoarchean granite intrusions of varying ages. Larger granite intrusions are of post-D_2 (second deformation) event, showing intrusive relation with the D_2 event fabrics (Smit et al., 1992). There are two metamorphic sub-regions within the SMZ separated by a retrograde isograd, which formed north of the HRSZ during the last stage of metamorphism (M_3) at T=600-620^{o}C and 6 Kbar (Smit et al., 1992). It separates high grade facies towards the north

from the retrogressed rocks to the south. The peak metamorphism (M_1) at T=800-850 ^oC and P=8.5 Kbar coincide with the last stages of D_1 (first deformation) event followed by isothermal decompression (M_2) at T=800^oC; P=8 and 5-6 Kbar (van Reenen et al., 1987).

4.1.2.1. According to Smit et al. (1992), there are four deformation events in the HRSZ:

- The initial D_1 event led to the formation of crustal wedges, foliation and isoclinal folds within the granite-greenstone rocks.
- D_2 event is associated with the formation of major shear zones separating the three LMB terrenes. This event led to formation of the HRSZ lineament along the southern boundary of the SMZ.
- D_3 event is related to shearing within the major LMB terrenes, which created variable. structural domains like the Petronella and Matok Shear zones within the SMZ.
- D_4 event led to the re-activation of the pre-existing shear zones in a strike-slip movement which are discordant to the older shear zones and other structures within the SMZ.

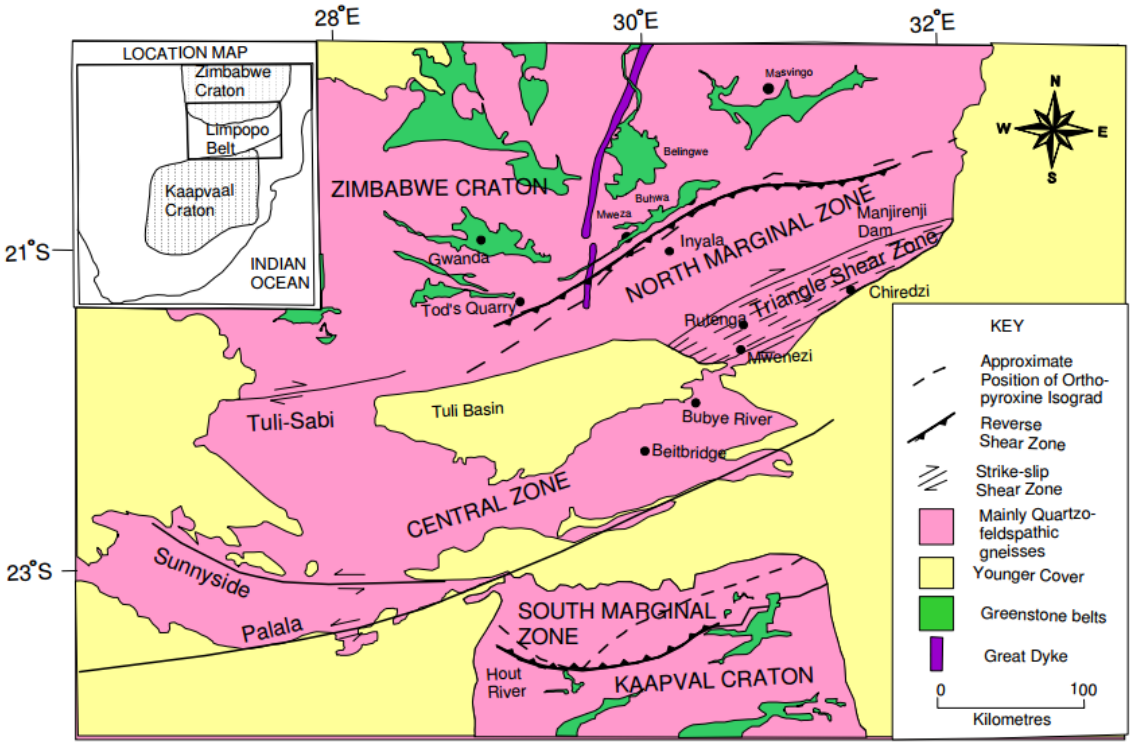


Figure 4.1: Regional geology of the study area (Source: Chinoda et al., 2009).

4.2. Local Geology

4.2.1. Paleoarchean Gneiss (3500-3000 Ma)

The stratigraphic succession described below has been given in Table 4.1.

The basement rocks of the Goudplaats-Hout River Gneisses are the oldest rocks in the study area and poorly exposed due to the overlying younger successions (Holland, 2011). The Goudplaats Gneiss is dark grey, fine grained and largely deformed by ductile deformation (Fig 4.2a) as compared to the younger Hout River Gneiss. The Hout River Gneiss is pinkish-grey in colour, pegmatoidal and highly fractured and weathered (Fig 4.2b). Degree of migmatization within the Goudplaats Gneiss and the Hout River Gneiss is of equal proportion (Robb et al., 2006). In the study area, these rocks are bounded to the north by the Soutpansberg volcano-sedimentary rocks (Holland, 2011).



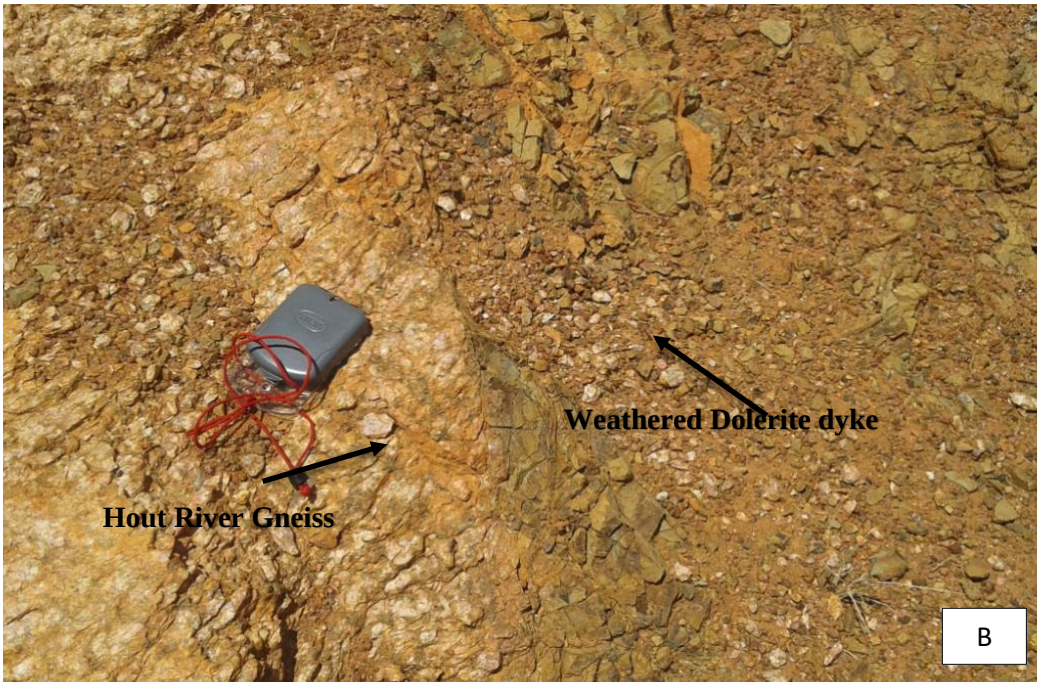


Figure 4.2: A) Folded basement Goudplaats Gneiss. B) Highly weathered Hout River Gneiss with an intrusive dolerite dyke.

4.2.2. Greenstone Belts (2.8-2.7 Ga) and supracrustal (2.67 Ga)

The Mothiba Formation and Zandriespoort Formation are the only formations of the Pietersburg Group found within the study area. Mothiba Formation is made up of ultramafic rocks with minor amphibole quarzitic schist and banded iron formation (BIF) (de Wit et al. 1992). Zandriespoort Formation is younger than Mothiba Formation and is made up of mafic metalava which is interlayered with magnetic quartzite (de Wit et al., 1992).

The supracrustal Bandelierkop Formation is made up of mafic, felsic, ultramafic and pelitic gneisses metamorphosed at granulite facies (Table 4.1) (van Biljon and Legg, 1983). Older ultramafic rocks of peridotite, dunite and pyroxenite compositions are widely scattered as pod-like bodies overlain by a mafic member, which is fairly foliated and shows concordant and discordant association with intruded leucocratic granites (van Biljon and Legg, 1983). The younger pelitic member is highly foliated and associated with banded iron-formation (Anhaeusser, 1992). Similar to the basement gneisses, these rocks have suffered anatexis and migmatization (van Biljon and Legg, 1983). Greenstone remnants together with supracrustals

occur as sporadic infolded keels within the Goudplaats-Hout River gneisses in the study area (Anhaeusser, 1992).

4.2.3. Neoarchean Intrusions (2800-2500 Ma)

Elevated granite batholiths raised above the low-lying erosional surface occur in the study area. They are non-orogenic, unfoliated and massive granite plutons that were emplaced post D_1 and D_2 events (Smit et al., 1992). Within the HRC, the largest plutons are the Moletsi Granite situated south of the HRC and Mashashane Suite towards the southern edge of the catchment boundary (Fig 4.3). The Hungomond Granite is the smallest and occurs north of the HRC. The Moletsi Granite was emplaced in three phases with the oldest phase with tonalitic composition occurring as inclusions within younger course grained pinkish-grey phases and core bodies (Robb et al., 2006). All phases were characterised by blue opalescent quartz (Robb et al., 2006). The Mashashane Granite Suite was also emplaced in three phases forming the earliest Uitvlugt Granite then the Lunsklip Granite, and the youngest Uitloop Granite (Robb et al., 2006). The composition varies from tonalitic composition in Uitvlugt Granite to syenogranite in the Lunsklip Granite and alkali-granite in the Uitloop Granite rocks (Robb et al., 2006). The Lunsklip Granite is the most extensive and situated in the southern edge of the study area (Fig 4.3). It is pinkish and medium-coarse grained to porphyritic with dominant biotite and hornblende minerals (Robb et al., 2006).

Other intrusions of significance closer to the study area are the Matok Granite, Matlala and elongated Turfloop Granite and the Dulvelskloof leucogranite with the latter two intrusions related to the Pietersburg and Giyani Greenstone Belts, respectively (Fig 4.3). The Matok Granite is located to the east of the catchment and shows fabric cuttings of D_3 shear zones (Smit et al., 1992). Matlala Granite occurs to the southwest of the HRC in various phases (Fig 4.3).

4.2.4. The Soutpansberg Group (1.85 Ga)

The Soutpansberg Group rocks mainly occur within the Soutpansberg Mountains, which forms the northern boundary of the study area. These rocks outcrop in a linear ENE trend stretching

from Vivo in the west to Punda Maria towards the east and gently dip towards the north (Bumby et al., 2002). It forms a succession of marine and continental clastic sedimentary deposits that were derived from erosion of mountains formed during the Limpopo Orogeny (Barker et al., 2006). The volcanic rocks are intercalated with these sedimentary rocks to form two main successions subdivided into a lower and upper lithostratigraphy separated by an unconformity (Geng et al., 2014). The whole rock Pb dating within basalts of the Sibasa Formation gave an age of the Soutpansberg Group of 1.85 Ga (Cheney et al., 1990).

Tshifhefhe Formation forms the base of the lower stratigraphy and is only developed towards the eastern side of the Soutpansberg basin (Bumby et al., 2002). This formation comprises of chloritised and epidotised greywacke, shale and rounded to angular conglomerate clasts (Geng et al, 2014). Conglomerate clasts are locally derived granitoid gneiss with quartz veins (Geng et al., 2014). The Sibasa Formation conformably overlies the Tshifhefhe Formation and mainly made up of tholeiitic basalts (amygdaloidal and epidotised) and pyroclastic lenses that are interbedded with clastic sediments towards the upper contact of the formation (Barker et al., 2006). The overlying Fundudzi Formation is mainly developed along the eastern side of the basin and comprises of areneous and argillaceous rocks interbedded with basalts and pyroclasts (Barker et al., 2006). Wyllie's Port Formation unconformably overlies the Fundudzi Formation and forms the base of the upper lithostratigraphy (Geng et al., 2014). It consists of reddish-pink quartzite mixed with minor pebble washes and locally interbedded with volcanic rocks. Musekwa and Nzhelele Formations forms the upper successions of the Soutpansberg Group, respectively (Geng et al., 2014). Musekwa Formation thickness ranges between 400 to 500m and comprises basaltic rocks intercalated with minor pyroclastic and clastic sediments (Geng et al., 2014). Nzhelele Formation is made up of volcanic rocks which are intercalated with argillaceous in the middle to areneous rocks towards the top of the formation's contact (Barker et al., 2006).

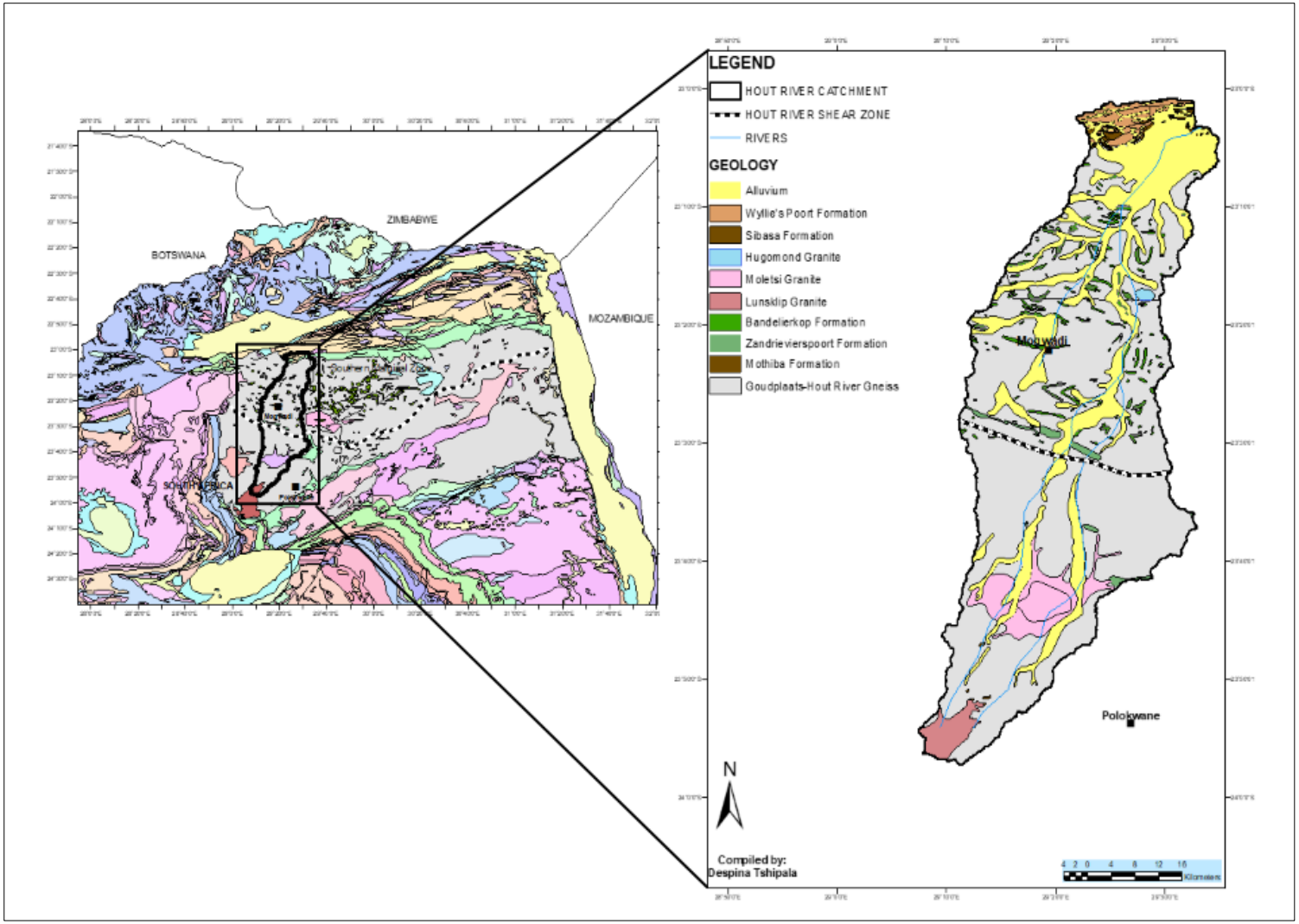


Figure 4.3: Geological map of the Hout River Catchment (Data Source: Council of Geosciences (SA).

Table 4.1: Stratigraphic column of the Southern Marginal Zone of the LMB.

		LITHOLOGIES
SOUTPANSBERG GROUP (1850 Ma) (a)	Nzhelele Formation	Volcanic rocks intercalated with argillaceous and areneous rocks
	Musekwa Formation	Basaltic rocks intercalated with minor pyroclastic and clastic sediments
	Wyllie's Formation	Reddish-pink quartzite with minor pebble washes and interbedded with volcanics
	Fundudzi Formation	Areneous and argillaceous rocks interbedded with basalts and pyroclastic
	Sibasa Formation	Tholeiitic basalts and pyroclastic lenses with clastics sediments
	Tshifhefhe Formation	Chloritised and epidotised greywacke, shale and conglomerate clasts of granitoid gneiss
Hugomond Granite (2656±2 Ma) (b)		Coarse grained, biotite bearing granite with tourmaline pegmatite veins
Moletsi Granite		Pinkish-grey phases with tonalitic inclusions
MASHASHANE GRANITE	Uiltloop Granite (2687 ±2 Ma) (c)	Pinkish and medium coarse grained with biotite and hornblende
	Lunsklip Granite	Alkali-granite
	Uvtylugt Granite	Tonalitic granite
BANDELIRKOP FORMATION (2670 Ma) (d)	Pelitic Member	Purplish brown gneiss composed of biotite, quartz, garnet, cordierite and hypersthene with sporadic banded iron formation
	Mafic Member	Dark grey to black fine-crystalline rocks composed of clino and ortho-pyroxenes, plagioclase and hornblende
	Ultramafic Member	Serpentinised peridotite and pyroxenite

PIETERSBURG GROUP (2700-2800 Ma) (e)	Zandrivierspoort Formation	Mafic metalava interlayered with magnetic quartzite
	Mothiba Formation	Ultramafic rocks with minor amphibole quarzitic schist and Banded Iron Formation
BAVIANSKLOOF GNEISS (Goudplaats and Hout River Gneiss) (3500-3000 Ma) (f)		Grey, migmatised tonalitic to trondhjemitic banded gneiss consisting of plagioclase, quartz, hornblende and biotite

Reference:(a) Cheney et al. (1990), (b) Robb et al. (2006), (c) Robb et al. (2006), (d) Anhaeusser (1992), (e) de Wit et al. (1992), (f) Anhaeusser (1992).

4.3. Structural setting

4.3.1. Dykes and lineaments

Regionally, dyke swarms (Fig 4.5) and other lineaments within the LMB represent progressive and different tectonic stages of changing principal stress directions. Dyke's orientation is indicative of paleo-stress directions along extensional stresses, which resulted into the zones of weakness in the rocks (Stettler et al., 1989). However, the present-day trajectories overprint other pre-existing variable stress directions in the region. Stettler et al. (1989) observed different orientations and magnetic properties of these lineaments along the north-eastern portion of the Kaapvaal Craton. They used these properties to divide the region into 6 domains. The A, C and E domains are predominately orientated NE-SW and B, D and F being randomly orientated. The study area falls within the A and B domains of this classification.

According to Uken and Watkeys (1997), pre-Karoo dykes within the north-eastern Kaapvaal Craton and LMB were emplaced from the Archaean to Mesozoic ages. The main trends are in the NW, NE and E-W directions with repeated emplacements along the same trajectories over the geological time (Letts et al., 2011). Dykes trending NW are the oldest and related to the Pongola rifting event that occurred 3.0 Ga ago (Uken and Watkeys, 1997). In the study area and the entire southern part of the LMB, the dominant type is the mafic dykes trending NE,

which could coincide with the 2.7 Ga Ventersdorp rifting event. This period involved crustal extension along the NW-SE direction such that zones of weakness were created perpendicular to this orientation, thus allowing dykes emplacement (Stettler et al., 1992). However, crustal extension in the southern Africa is currently along the NW-SE direction and compression along the NE-SW direction (Bird et al., 2006). The youngest dykes that might have been emplaced during the neo-tectonic stress regimes are orientated in the NE-SW direction. The NE-SW trends are also associated with the Karoo dykes dominating the regions southeast of the LMB. The Karoo dykes are related to the Karoo magma emplacement and were dated approximately at 1.80 Ga (Letts et al., 2011).



Figure 4.4: Highly weathered dolerite dyke along the Hout River channel.

4.3.2. Faults

Based on the structural data obtained from the Council of Geoscience, faults occur along the northern catchment boundary, in the Soutpansberg Mountains. The aeromagnetic map shows areas of high magnetic anomalies along the Soutpansberg Mountains and mafic dykes predominately trending NE (Fig 4.6). Aeromagnetic mapping of the catchment has shown that there are strike slip and reverse faults within the HRSZ (Sakala et al., 2014). Other previous

work indicated that mapped faults are striking NNW-SSE and E-W directions (Holland, 2011). The aeromagnetic map below shows area of high magnetic anomalies tracing the NE-SW trending dolerite dykes, greenstone belt and along the Soutpansberg Mountains (Figure 4.6). Areas of low magnetic intensity approximately -280 nT shows areas with magnetic concentrations, which possibly show less resistant and weathered zones within the country rocks.

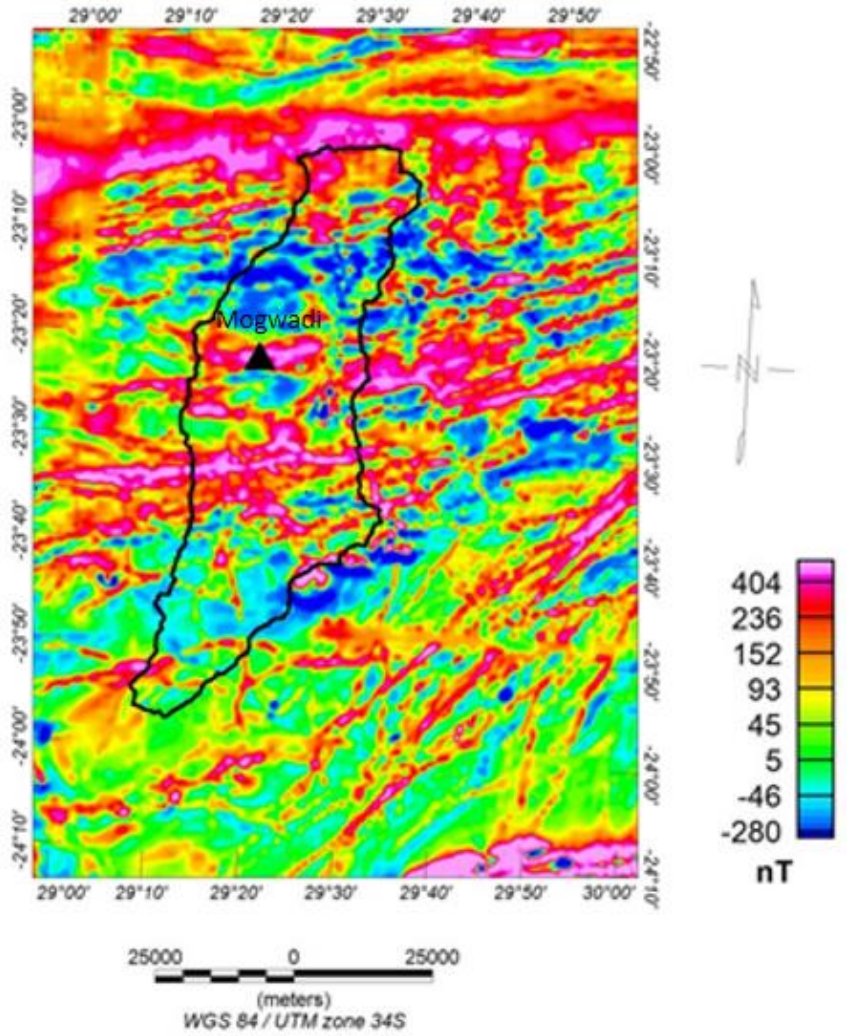


Figure 4.5: Aeromagnetic map of the Hout River Catchment. Data obtained from the Council of Geoscience (SA).

4.3.3. Hout River Shear Zone

The HRSZ cut across the HRC in an east-west direction separating the granulite facies of the SMZ to the north from the granite-greenstone rocks of the Kaapvaal Craton to the south (Fig 4.7). The rehydrated granulites in the hanging wall separate the high grade granulites rocks on the footwall further north by an orthoamphibole isograd (Smit et al., 1992). The HRSZ is a linear feature stretching 250 km with 4 km width in some places across the Limpopo Plateau and the Litaba Lowveld (Holland, 2011). It comprises of thrust and steep dipping reverse faults as well as strike slip faults linked to the reverse faults. Reverse faults formed lateral and frontal ramps through, which the granitiods of the SMZ were thrust onto the Kaapvaal Craton (Smit et al., 1992). The timing of the thrust is contemporaneous to the peak metamorphism (M_1) obtained from Pb/Pb step leaching dating of synkinematic garnet, which gave a metamorphic age of 2691±20 Ma (Kreissig et al., 2001). Thrusting of the SMZ rocks on to the Kaapvaal Craton coincides with the D_2 event, which led to a 15 km vertical displacement of rocks along the fault's line (van Reenen et al., 1990).

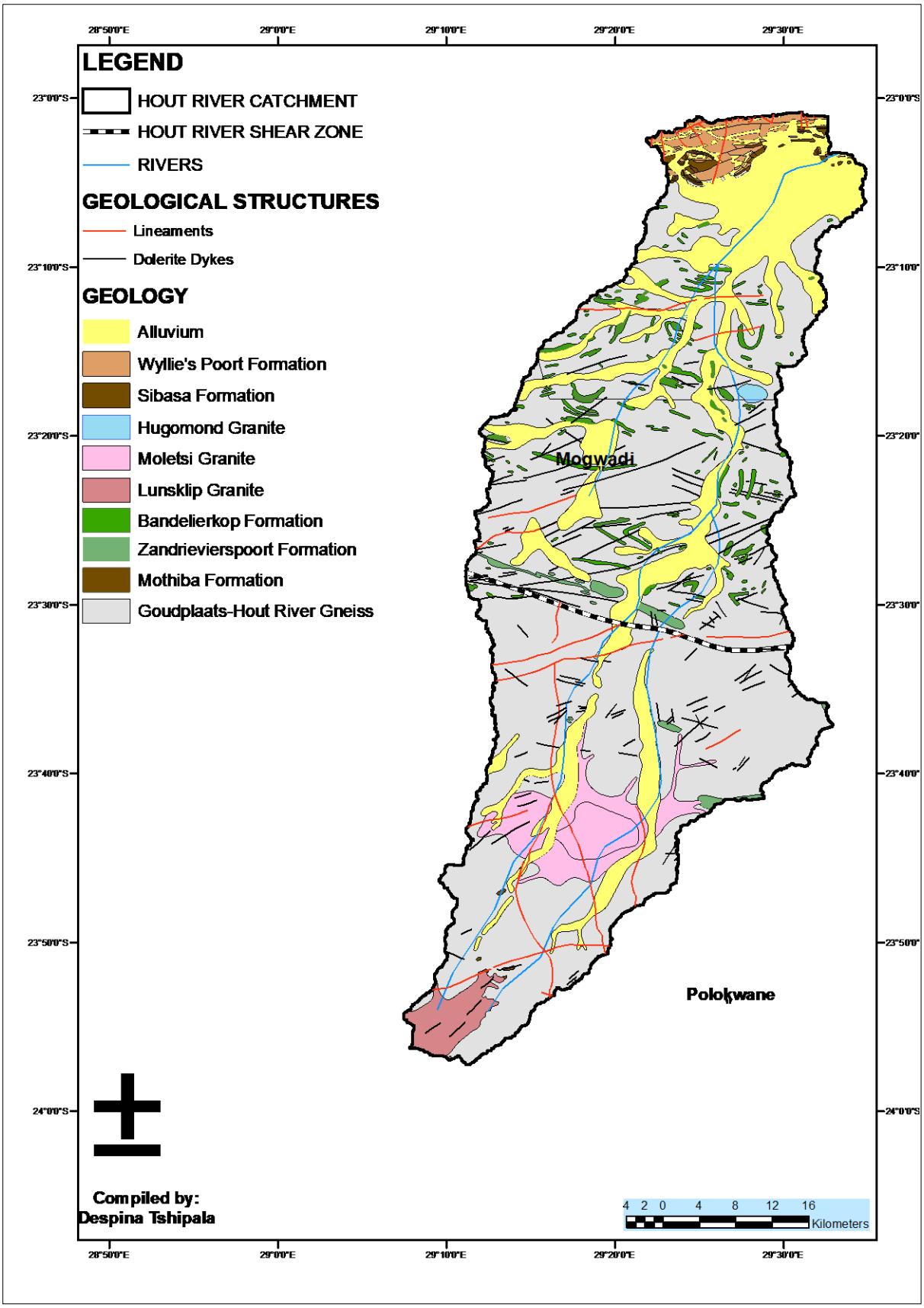


Figure 4.6: Structural map of the Hout River Catchment (Data source: Council of Geoscience (SA)).

4.4 Hydrogeological Setting of the Hout River Catchment

According to Pietersen et al. (2011) three distinct aquifers exist within the Limpopo Plateau namely: the composite aquifer, deep fractured aquifer and the alluvial aquifer. The composite aquifer is characteristic of the Houdenbrak aquifer with the weathered thin zone underlain by fractured basement rocks (Jolly, 1986). Deep fractured aquifer consists of connected fractures containing un-reworded matrix. The alluvial aquifer resulted from a reworked weathered material that formed laterally narrow and shallow water reservoirs along river channels (Pietersen et al., 2011). Secondary porosity forming mechanisms (weathering, faulting, fracturing and intrusives) control groundwater occurrence within these basement rocks. The identified aquifer within the catchment has been in the government monitoring programme under the Water Act 1956 and is known as the Houdenbrak aquifer (Pietersen et al., 2011). It has an extent of 1600 km^2 stretching from few km south of the Mogwadi town towards the Vivo area along Soutpansberg Mountains (Masiyandima et al., 2002).

The weathered zone of the Houdenbrak aquifer has a variable depth within the range of 15-50 m (Pietersen et al., 2011). The fractured bedrock of granitic gneiss is much thicker reaching a depth of about 120 m around the Mogwadi area (Jolly, 1986). The two zones of the composite aquifer in the catchment are in hydraulic connection such that the upper weathered unit with low permeability and high porosity acts as a reservoir that feeds the lower fractured rock with high permeability and lower porosity (Jolly, 1986). Furthermore, the composite aquifer is said to be confined and partially confined in certain locations (Pietersen et al., 2011). According to Jolly (1986) the storage coefficient of the upper and lower units of the composite aquifer are 0.01 and 0.0025, respectively. However, due to low permeability of the weathered zone, low borehole yields were recorded with values averaging to about 1 l/s (Pietersen et al., 2011). The borehole yields increase when the boreholes penetrate the lower fractured zone that have a blow yield of 40 l/s. Recharge in this aquifer accounts for about 3.8 % of the annual mean rainfall (Dziembowski, 1976). This value is consistent with subsequent recharge estimated values in the range of 2-5 % of the annual rainfall (Masiyandima et al., 2002). The connectivity of fractures and nature of the granites ensure high transmissivity and hydraulic conductivity. The transmissivities from the Groundwater Resource Information Project (GRIP) database indicated between 4 m^2/d and 40 m^2/d with high values around the Mogwadi area (Holland, 2011). The rainfall plot with groundwater levels of borehole located in the northern part of the

catchment shows insignificant influence of the rainfall variations to groundwater level changes (Fig 4.8). The highest groundwater level for the analysed period of 5 years was at 63.922 m.b.g.l. which seem to be responding to the rainfall amount of 335.05 mm (Fig. 4.8). This gives a hydraulic head of 1.13 m. From these observations, it is apparent that rainfall occurring in this area is insignificantly contributing to the groundwater recharge of the aquifer.

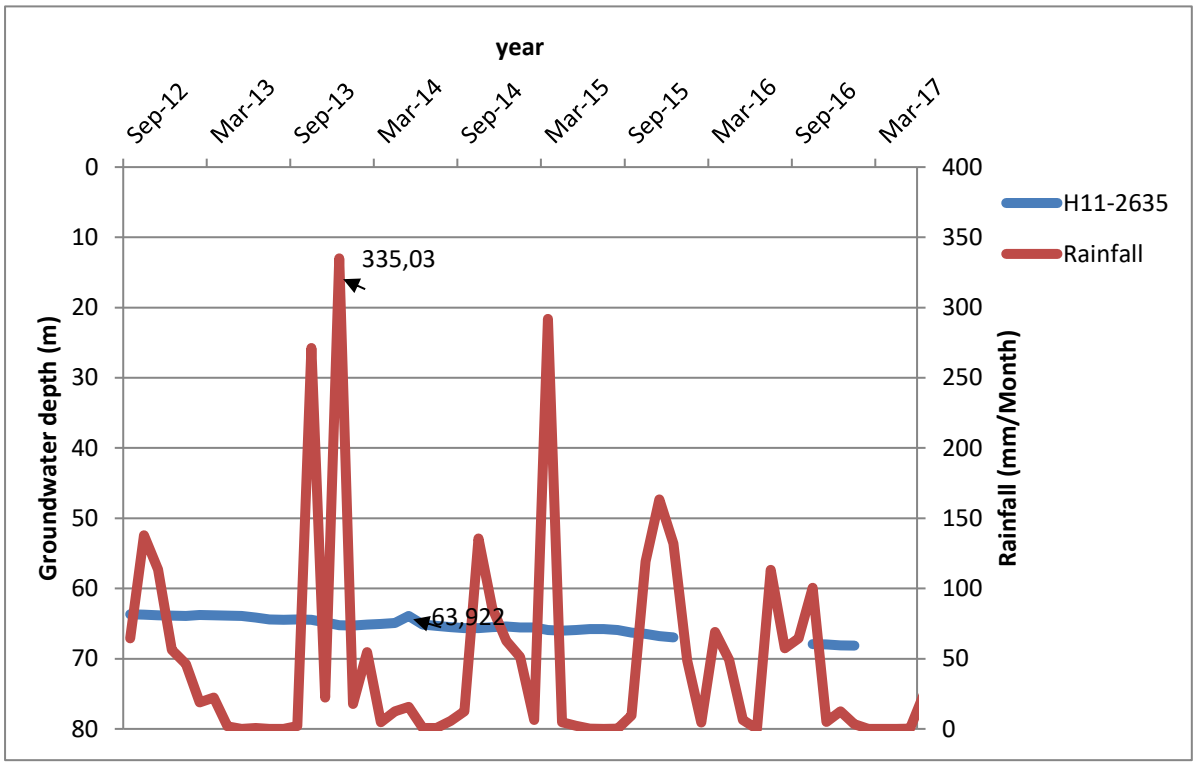


Figure 4.7: Groundwater level trends of the monitoring boreholes against long-term annual rainfalls within the Hout River Catchment.

CHAPTER 5 : METHODOLOGY

The approach to the conceptualisation of the hydrogeological system in the Hout River Catchment involved a detailed review and interpretation of the hydrogeological, geological, aeromagnetic data and structural characteristics of the area. To compute a conceptual model, recharge was estimated using water balance calculation and Water Table Fluctuation (WTF). Physico-chemical variables and environmental isotopes were used to understand chemical and physical properties and mean residence time of the groundwater.

Data collection for this study started by a field trip to the Hout River Catchment area in Oct-Nov 2016 and March 2017 where rainfall, groundwater, river and spring samples were collected from different locations shown in Fig 5.1. In each sampling location, GPS coordinates were recorded. At each station, water samples were collected for ^{2}H and ^{18}O stable isotopes, few samples were collected for ^{14}C, ^{13}C, and ^{3}H analyses. The rainfall samples represent rainfall events from the 6th of November 2016 until the 5th of March 2017. Observation borehole data i.e. groundwater levels and lithology were obtained from the National Groundwater Archives (NGA) and Groundwater Resource Information Project (GRIP). Meteorological data was obtained from the Agricultural Research Council-Institute of Soil, Climate and Water (ISCW) and South African Weather Service (SAWS). Geological, aeromagnetic data and structural information were obtained from the Council of Geoscience.

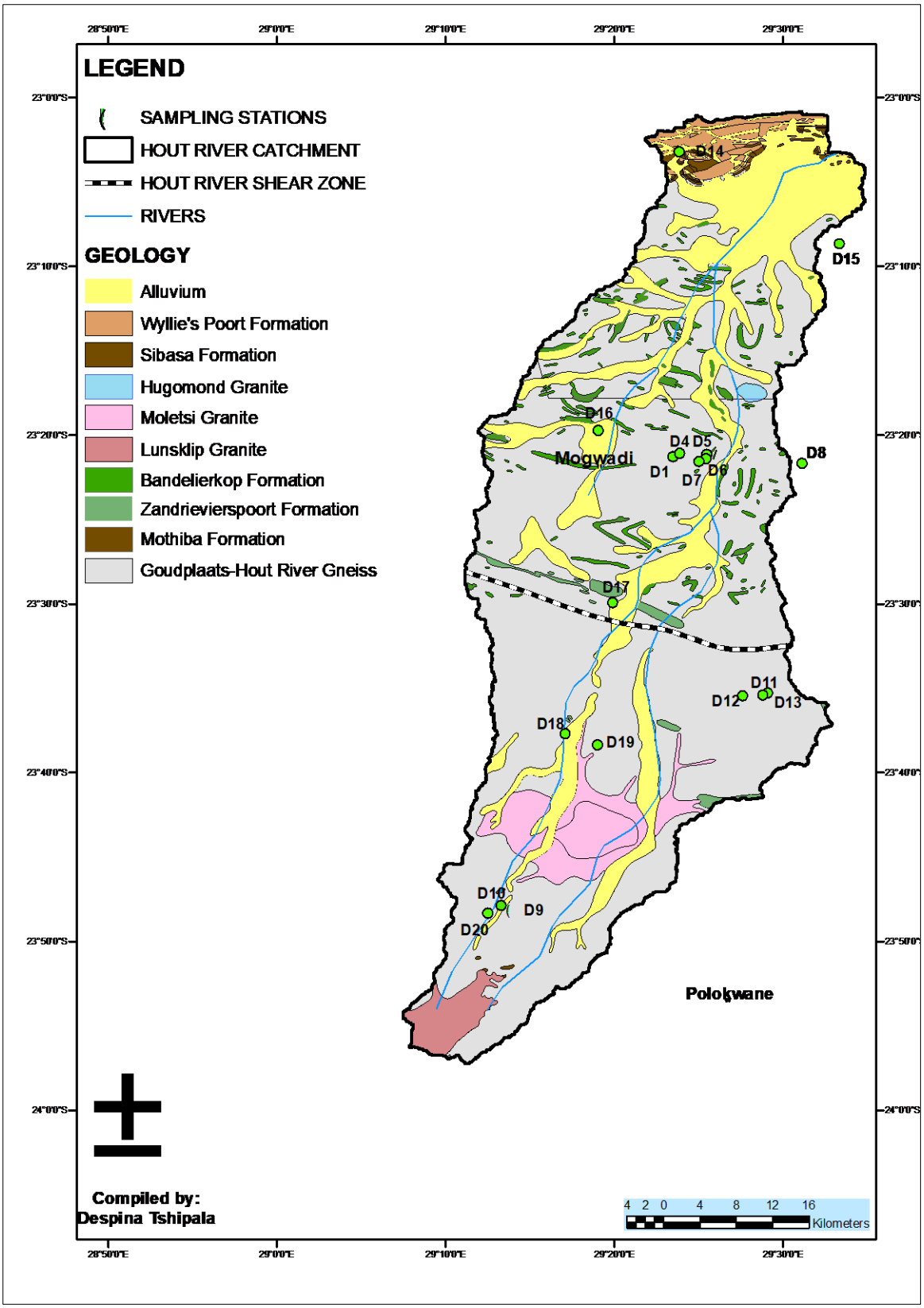


Figure 5.1: Sampling stations within the Hout River Catchment. (Source: CGS).

5.1 Structures and Groundwater analyses

5.1.1 Aeromagnetic and structural data

The use of aeromagnetic data has been favoured for many years for critical identification of geological structures, mineral exploration with high affordability as well less need for data corrections. Magnetic minerals or rocks are detected in magnetic surveys depending on different concentration of the magnetic materials. Group of minerals that are magnetic are classified under Fe-Ti-O group, with magnetite being the most magnetic mineral and has a susceptibility value of 15 (Table 5.1). Pyrrhotite found within sulphides and metasedimentary ore deposits have some form of magnetism although with lesser susceptibility as compared to magnetite. The mostly detected minerals in aeromagnetic surveys are classified under ferromagnetic minerals and have magnetic moments occurring in opposite direction but do not completely cancel each other because of minor difference (Reeves, 2005). Magnetic field is measured in nanotesla (nT) which is equal to 10^{-9} Tesla (Reeves, 2005).

Mafic dykes and sills exhibit strong residual magnetism, which formed during fast cooling of magma (Reeves, 2005). However, some dykes do not show magnetic signatures and have lower susceptibility. Other areas related to dyke's intrusion of high susceptibility are along the contact areole horizons (Reeves, 2005).

The aeromagnetic data in the form of a grid used in this study was obtained from the Council of Geoscience (CGS) South Africa. The grid was processed using Geosoft software (Oasis Montag model 9.2.3) to produce an aeromagnetic map for the study area.

During the field work, few structural measurements were taken from rocks exposed along the road cuttings and river channels. Limitation to representative structural measurements resulted from less exposed country rocks and structures since the area is largely covered by old erosional surface. As a result, only 2 measurements were taken during the sampling exercise. A strike and dip for these dykes were taken using a campus clinometer. These measurements were used to confirm the structural characterisation of the study area which already exist in the body of literature. The coordinates for these sampling stations are as follows:

1) Dolerite dykes along a river: -23,73816; 29,26145
2) Dolerite along a road cutting: -23,71148; 29,31850

Table 5.1: Magnetic susceptibilities of magnetic iron oxides (Source: Reeves, 2005).

Magnetic minerals/ore	Susceptibility
Pure magnetite	15
Magnetite Ore	0.07-14
Ilmenite ore	0.3-4
Pyrrhotite	0.001-0.1
Hematite ore	0.004-0.01
Pyrite	0.0001-0.005

5.1.2 Groundwater level analyses

Groundwater levels obtained from the GRIP database was used to construct a groundwater level map with the raw data in Appendix A. The data was converted into a csv format and then processed using Surfer 15 software program. A 3D surfacing contour map with contours showing the distribution of groundwater levels was produced with an interval of 5 m.

5.2. Catchment Water Balance Calculation

The water balance calculation forms the elementary steps used to solve hydrogeological system problems. It generally works on the premises that input into the hydrology system is equal to output plus/minus storage represented as:

Input =Output ±ΔS

The water balance for the HRC is given by:

$$P_i - (ET + Wg + R_{off}) = \pm \Delta S$$

Where Pi is precipitation, ET is evapotranspiration, Wg is groundwater abstraction, R_{off} is runoff and ± ΔS is change in storage of the aquifer.

5.2.1. Runoff

Runoff is the integral part of water balance estimation. It is defined as the part of rainfall that runoff on the ground-surface (Tripathi and Singh, 1998). It depends on rainfall, soil types, surface water bodies within the catchment, the catchment slopes and vegetation.

The latest Hout River Catchment runoff was estimated in 2015 by Ebrahim et al. (2018). The method of estimation was based on the Precipitation Runoff Modelling System (PRMS) method and was calibrated with streamflow measured from the gauging station A7H010, which is at the outlet of the Sand Catchment because there is no river gauging station in the Hout catchment. This method gave an average value of 2.44 mm/a between the year 2014 and 2015. This runoff value is going to be used for water balance estimation in this study.

5.2.2. Evapotranspiration

Evapotranspiration defines the simultaneous process of evaporation and transpiration from the surface water bodies, soil water and vegetation (Zotarelli et al., 2010). It is estimated as reference evapotranspiration (ETo) which could be measured using the FAO Penman-Montheith method. It requires climatic data that involves temperature, relative humidity, wind speed and radiation, which could be obtained from the local rainfall station (Allen et al., 1998). ETo is used to obtained crop evapotranspiration (ETc) when crop coefficient (Kc) is considered (Allen et al., 1998). ETc is used to account for different crop types that may occur within the interest of the study.

$$ETo = \frac{0.408\Delta(Rn - G) + \gamma \frac{900}{T + 273}\mu 2(es - ea)}{\Delta + \gamma(1 + 0.34\mu 2)}$$

Where:

ETo= reference evapotranspiration

Rn = net radiation at the crop surface

G = soil heat flux density

T = mean daily air temperature at 2 m height

u2 = wind speed at 2 m height

es = saturation vapour pressure

ea = actual vapour pressure

es -ea = saturation vapour pressure deficit

Δ = slope of the vapour pressure curve

γ= psychrometric constant

The climatic data for the evapotranspiration calculations was obtained from the Mara PP weather station located at -23.11725 and 29.55624.

5.3. Water Table Fluctuation (WTF) Method

Groundwater recharge estimation using WTF method considers groundwater level fluctuations within an unconfined aquifer to result from water reaching the water-table (Healy and Cook, 2002; Scanlon et al., 2002). Recharge is a function of specific yield and groundwater level changes over a period of time (Scanlon et al., 2002). For this method, the only considered cause of groundwater fluctuation is precipitation and not climate change or anthropogenic activities (pumping, land use, induced infiltration or irrigation (Healy and Cook, 2002). Climate and land use changes is considered in net recharge estimation when there is long term groundwater level fluctuation data. This is to ensure that groundwater fluctuation is only due to rainfall recharging the area. It works best if that rainfall is in the form of a storm and not of low intensity, since the latter yields steady state recharge conditions (Healy and Cook, 2002). The method is only applicable to an unconfined aquifer of shallow water tables with sharp rise and decline of groundwater levels over a short-term period (Scanlon et al., 2002).

Recharge estimation using WTF is calculated from the following equation:

$$R = Sy\frac{\Delta h}{\Delta t}$$

Where S_y is specific yield and Δh is the change in groundwater levels and Δt as the change in time upon which groundwater level changes. The equation works on the assumption that recharge water is stored after reaching saturated zone and when all other water balance parameters are zero (Healy and Cook, 2002). The challenges in using the method involve

difficulty in estimating specific yield (Varni et al., 2013) and identifying the cause of groundwater fluctuation (Scanlon et al., 2002). However, the readily available groundwater level data, its simplicity and less influenced by flow mechanism within the unsaturated zone makes the method mostly preferred compared to other methods that uses groundwater level and rainfall variations to assess recharge (Healy and Cook, 2002). It is with the same reasons that this method was chosen for this study to estimate groundwater recharge.

The WTF method was applied on boreholes that are situated within the soil zone, gneiss, dolerite and granite; these boreholes are A7N0635, A7N0641, A7N0661, and A7N06658, respectively. In these boreholes, groundwater levels over the years have been analysed and compared to groundwater recharge as well as abstractions for the similar year. The monthly recharge and discharge estimates using WTF method was then computed and averaged into yearly recharge and discharge for the selected boreholes.

5.4. Physicochemical variables analyses

To evaluate water quality in the study area, temperature (T), pH, Oxidation-Reduction Potential (ORP), Electrical Conductivity (EC), Total Dissolved Solids (TDS) and Dissolved Oxygen (DO) were measured in the field during sampling. These variables were measured at each site using Mm40, Mm26+ and OXi-45p meters. The electrodes were calibrated using standardized buffer solutions.

Temperature of water affects all other physico-chemical variables and needs to be monitored whenever other variables are being measured. The measure of pH will determine whether a particular water species is acidic or alkaline. This is controlled by the concentration of hydrogen ions ($^{+}$H) in water (DWAF, 1996a). If conditions favour high concentration of $^{+}$H, then the pH will be less than 7 consequently forming an acidic environment. The opposite will be true if low production of $^{+}$H is favoured, and an alkaline species of water will be formed.

TDS and EC are directly related such that an increase in the former results in the increase of the latter (WHO, 2009). As such, EC could be used to estimate TDS, since it is much easier to calculate as compared to TDS. TDS measures total dissolved solids (e.g. calcium, potassium, sodium, magnesium, sulphates and bicarbonates) that come from water-rock interaction and minor organic materials from decomposition of plants and effluent materials (WHO, 2008).

Groundwater will lose its potability if TDS becomes greater than 1000 mg/l consequently giving rise to salty taste and forming what is referred to as "hard water" if the main constituents of the dissolved solids are Ca and Mg (WHO, 2008) (Table 5.2). EC of a water sample measures the ability of water to allow an electrical current flow through it (DWAF, 1996a). It depends on different ionised species (salts) dissolved in water which aid the flow of an electrical current.

Dissolved Oxygen (DO) is the amount of oxygen dissolved in a water parcel. Oxygen solubility increases with atmospheric pressure and decreases when salinity and water temperature rise as described by Henry's Law (Rose and Long, 1988). It controls solubility of trace metals and bacterial metabolism (Weaver et al., 2007). Bacterial metabolism consumes oxygen to oxidise carbon, ammonium, and sulphide such that resulting environment is anoxic (Weaver et al., 2007). Similar to DO, redox potential also controls occurrence of metal ions (O_2, NO_3^-, SO_4^2, CH_4 and H_2S) and metabolism of organic compounds (Weaver et al., 2007). This is due to the fact that their reactions are catalysed by micro-organisms. Redox potential determines the oxidising and reduction potential of a species related to a reference (DWAF, 1996a).

Table 5.2: Accepted standards range of physicochemical parameters according to the World Health Organization (W.H.O) (2008, 2009) and DWAF (1996a, b, c).

Physicochemical parameters	Units	WHO (2008, 2009)	DWAF (1996a) Domestic use	DWAF (1996b) Irrigation	DWAF (1996c) Livestock watering
pH	-	6.5-9.2	6-9	6.5-8.4	-
T	$^{\circ}C$	<37.2	-	-	-
ORP	+mV	-	-	-	-
EC	µS/cm	180-500	-	0-400	0-1540
TDS	mg/l	<600	0-450	0-260	0-1000(a) 0-2000 (b) 0-3000 (c)
Turbidity	NTU	<5	0-1	-	-

DO	%	-	-	-	-

a) Dairy, poultry and pigs

b) Cattle and horses

c) Sheep

5.5. Environmental isotopes analyses

5.5.1. Stable isotopes ($\delta^{18}O$ and $\delta^{2}H$)

For stable isotope analyses, 26 rainfall, 17 groundwater, 1 river water, 1 dam water and 1 spring samples were collected (Table 5.3). In each station, water samples were collected in 10 ml bottles for analyses.

Stable isotopes of ^{18}O and ^{2}H were analysed at the University of the Witwatersrand, South Africa using the Liquid Water Isotope Analyser-model 45-EP. The precision for the machine is approximately 1‰ for $\delta^{2}H$ and 0.2‰ for $\delta^{18}O$ in liquid water samples of up to 1000 mg/L dissolved salt concentration. The analysis was done against five standards of different known isotopic signatures.

The relationship between the standard and the isotopic ratios is expressed as:

$$\delta^{18}O\ (‰) = \left[\frac{\left(\frac{\delta 18_O}{\delta 16_O}\right)_{Sample}}{\left(\frac{\delta 18_O}{\delta 16_O}\right)_{Standard}} - 1\right] \times 1000$$

Where $\delta^{18}O/\delta^{16}O$ is the ratio of most abundant isotopes in the water molecules for the sample water and the standard. The standard is called the Vienna Standard Meteoric Ocean Water (VSMOW) (Craig, 1961). Sampled water will either be enriched or depleted with respect to this standard.

Stable isotopes ($\delta^{18}O$ and $\delta^{2}H$) are conservative in nature and have been used to trace flow paths and sources of rainfall and groundwater within a hydrogeological system. Variations in atomic mass of elements results into different reaction rates causing fractionation (Clack and Fitz, 1997). In precipitation, fractionation is due to evaporation, rainfall amount, temperature, altitude and latitude effects (Dansgaard, 1964). After recharge, stable isotopes will be depleted

due to water-rock interaction and prolonged groundwater circulations in the aquifer (Clack and Fitz, 1997).

Stable isotopes are normally compared to local and global meteoric water lines. Local Meteoric water Line (LMWL) is found from a best line fit of locally derived rainfall samples. Global Meteoric Water Line (GMWL) has been derived from global analyses of δ^{18}O and δ^{2}H in natural waters from meteoric stations around the world (Craig, 1961). The best line fit (GMWL) for these samples is expressed as:

$\delta D = 8^{18}O+10‰$

Where, the slope and intercept (deuterium=d) of the straight line are 8 ‰ and 10 ‰, respectively. The variations in a moisture source conditions and different paths of the moisture until the precipitation site results into deuterium excess (d-excess) (Clark and Fritz, 1997). While δ^{18}O and δ^{2}H are correlated to the local surface temperatures, D-excess reflect conditions of the moisture source which involves humidity, sea surface and air temperatures (Dansgaard, 1964). D-excess is calculated from the Pretoria LWML equation, which is as follows:

$D_{excess} = \delta D - 6.7\delta^{18}O$

The slope of the straight line will be changed according to the LMWL slope, which reflects local conditions as compared to that of GMWL that represents global precipitation stable isotope conditions.

Table 5.3**:** Samples used for stable isotopes analyses.

Code	**Source**	**Latitudes**	**Longitude**	**Location**
RN1	Rain	-23.7681	29.2259	Hout River Dam
RN2	Rain	-23.7681	29.2259	Hout River Dam
RN3	Rain	-23.7681	29.2259	Hout River Dam
RN4	Rain	-23.6838	29.09244	Moletji
RN5	Rain	-23.6838	29.09244	Moletji
RN6	Rain	-23.6838	29.09244	Moletji
RN7	Rain	-23.7318	29.30774	Koloti

RN8	Rain	-23.7318	29.30774	Koloti
RN9	Rain	-23.3697	29.32233	Mogwadi
RN10	Rain	-23.3697	29.32233	Mogwadi
RN11	Rain	-23.3697	29.32233	Mogwadi
RN112	Rain	-23.3697	29.32233	Mogwadi
RN13	Rain	-23.3697	29.32233	Mogwadi
RN14	Rain	-23.3697	29.32233	Mogwadi
RN15	Rain	-23.3697	29.32233	Mogwadi
RN16	Rain	-22.9063	29.61918	Water Poort
RN17	Rain	-22.9063	29.61918	Water Poort
RN18	Rain	-22.9063	29.61918	Water Poort
RN19	Rain	-22.9063	29.61918	Water Poort
RN20	Rain	-22.9063	29.61918	Water Poort
RN21	Rain	-22.9063	29.61918	Water Poort
RN22	Rain	-22.9063	29.61918	Water Poort
RN23	Rain	-23.8944	29.43483	Polokwane Rain 1
RN24	Rain	-23.8944	29.43483	Polokwane Rain 2
D1	Borehole	-23.3552	29.39173	Wimpie farm- Mogwadi
D2	Borehole			Wimpie Farm- Mogwadi
D3	Borehole	-24.6521	25.92857	Wimpie Farm-Mogwadi
D4	Borehole	-23.3518	29.39822	Wimpier Farm- Mogwadi
D5	Borehole	-23.3529	29.42515	Wimpier Farm- Mogwadi
D6	Borehole	-23.3571	29.42419	Wimpier Farm- Mogwadi
D7	Borehole	-23.3599	29.41747	Wimpier Farm- Mogwadi
D8	Borehole	-23.3616	29.51921	Legraal Farm
D9	River	-23.798	29.23362	Hout River Down Stream
D10	Dam	-23.7982	29.22188	Hout River Up stream
D11	Borehole	-23.2956	28.05641	Leeuwfontein farm
D12	Borehole	-23.5915	29.46064	Leeuwfontein farm
D13	Borehole	-23.5886	29.48516	Leeuwfontein farm
D15	Borehole	-23.1449	29.55613	Mara Research Station
D16	Borehole	-23.3292	29.31769	West of Mogwadi

D17	Borehole	-23.4994	29.33227	De Loskop farm- Mid West
D18	Borehole	-23.6287	29.28533	Southern part of Hout Dam
D19	Borehole	-23.6487	29.31703	Southern part of Hout Dam
D20	Borehole	-23.8059	29.20866	Northern part of Hout Dam
D14	Spring	-23.054	29.39789	Mara- Soutpansberg Mountain Springs

5.5.2. Radiogenic isotopes (^{14}C and ^{3}H) and stable carbon isotope (^{13}C)

5.5.2.1 Tritium (^{3}H) in rainfall, spring and groundwater samples

To obtain mean residence time (MRT) for modern groundwater within the aquifer, ^{3}H groundwater dating method has been applied. A total of 20 samples (17 from groundwater, 2 from a river and 1 from a spring) were collected for ^{3}H analyses. 500 ml polyethylene bottle was used at each sampling station. Samples for tritium were collected in two sampling periods where boreholes D1 to D8 were sampled twice. The detection limit of tritium on enriched samples is 0.2 TU. The samples were analysed at the iThemba Labs, Gauteng.

^{3}H isotope is naturally formed in low concentrations in the upper atmosphere after bombardment of nitrogen by cosmic rays, which subsequently interacts with the atmospheric water molecules to form tritium-laden water molecules expressed as $^{1}H^{3}HO$ (HTO) (Hiscock, 2005). It is also found in the subsurface as a result of spontaneous breakdown of Uranium (U), Thorium (Th) and Lithium (Li) as well as in nuclear reactors (Clark and Fritz, 1997). Prominent anthropogenic production of tritium in the atmosphere occurred during the nuclear bomb testing in 1952 peaking in 1963 (Clark and Fritz, 1997). In the 1960s, tritium concentration in the atmosphere increased to be in the range of 60 to 80 TU in the Southern African (Weaver et al., 1999). However, concentrations have since been decreasing due to radioactive decay and ceased major anthropogenic injections into the atmosphere (Clark and Fritz, 1997). Recent tritium concentration in precipitation is in the range of 3 to 5 TU in the Southern Africa (GNIP-*http://isohis.iaea.org*). Weaver et al. (1999) suggested a value of 5 TU for the atmospheric concentration in the Southern Africa. A rainfall sample taken in Johannesburg during the Dineo Cycle (21 to 22 February 2017) gave a tritium value of 1.4 ±0.3 TU. An average value of 2.8

TU has been recorded in the Taaibosch area, south-east of Mogwadi area (Butler and Verhagen, 2013).

After recharge of tritium-laden precipitation, tritium starts to decay into its daughter isotope (^{3}He) realising β-particles (Clark and Fritz, 1997). Tritium activity is measured in tritium units (TU), which is the same as one ^{3}H atom per 10^{18} hydrogen atoms (Hiscock, 2005) and has a half-life of 12.43 years (Bergman and Libby, 1957). The MRT of groundwater since recharge is determined using the following equation:

$$t = -17.93ln\left[\frac{a_t 3_H}{a_o 3_H}\right]$$

Whereby $a_o 3_H$ is the initial tritium activity and $a_t 3_H$ is the final tritium activity. The equation assumes a closed system and a piston flow mechanism where there is no dispersion along the flow path (Scanlon et al., 2002). However, it is apparent that in reality it is difficult to determine groundwater age since tritium concentrations are not only affected by radioactive decay but also by diffusion in the matrix and mixing with very recent or old groundwater (Weaver et al., 1999). As such, qualitative age dating is essential to constrain MRT of groundwater. In the Southern Africa, Weaver et al. (1999) suggested qualitative tritium values and derived MRT as shown in Table 5.4.

Table 5.4: Semi-quantitative derived MRT from groundwater tritium values (Sources: Clark and Fritz, 1997 and Weaver et al., 1999).

Tritium values (TU)	MRT	Tritium values (TU) (Clack and Fritz, 1997)	Tritium values (TU) Weaver et al., 1999
<0.5	Groundwater recharged before 1952	<0.8	<0.5
0.5-5	Recharged before and after 1952 (Mixed groundwater)	0.8-4	0.5-5
5	Groundwater recharged after 1952	>4	5

5.5.2.2. Radiogenic carbon (^{14}C) and stable carbon (^{13}C) isotopes

^{14}C and ^{13}C have been analysed in groundwater samples in order to identify the occurrence of old groundwater and the effect of hydro-geochemical processes on groundwater. Only 10 samples of groundwater from boreholes were analysed for ^{14}C and ^{13}C isotopes from different sampling locations within the catchment. Sample preparation for the precipitate ($BaCO_3$) involved collection of 50 L groundwater sample then addition of NaOH to increase pH, phenolphthalein indicator and lastly $BaCl_3$. This solution was then left for about three hours consequently forming a white precipitate. The formed precipitate subsequently was stored in 500 ml polyethylene bottles at each sampling location. Precipitate samples were analysed at the iThemba Labs, Gauteng.

^{14}C is naturally formed in the upper atmosphere during interaction of nitrogen with the cosmic rays whereby concentration of one radiocarbon is equal to 10^{12} atoms of the stable carbon (Clark and Fritz, 1997). Anthropogenic production of ^{14}C is related to the nuclear bomb testing in the 1950s to 1960s, similar to anthropogenic production of tritium (Clark and Fritz, 1997). Upon entering the atmosphere, it is subsequently oxidized into carbon dioxide and becomes part of precipitation with initial carbon activity value of 100 pMC. Vogel (1970) suggested that 85% of 100 pMC should be adopted as an initial activity value. Verhagen et al. (2009) further suggested the use of 80 and 95% as the initial carbom-14 activity for Bochum area located west of the Hout River Catchment. Radioactive decay begins after groundwater recharge where ^{14}C proceed to decay releasing β-particles and has a half-life of 5730 years (Clark and Fritz, 1997). Since carbon-14 isotope is not part of a water structure, it can only give MRT of groundwater in terms of Before Present (BP) years and not the actual age of groundwater. Hydro-geochemical reactions such as carbonates dissolution along the flow path add dead carbon that increases the ^{14}C activity which over estimates MRT of groundwater. Using this diluted ^{14}C values will yield uncorrected ages determined using the following equation:

$$t = -8267 ln \frac{A}{A_o}.$$

Where, t is residence time of groundwater between the time of recharge until groundwater abstraction, A_o is the initial ^{14}C activity and A is the final ^{14}C activity measured in percent modern carbon (pMC) units (Clark and Fritz, 1997). To correct diluted ages given by ^{14}C, ^{13}C

is used since is available in different carbonate reservoirs able to determine evolution of carbon within the reservoirs.

CHAPTER 6 : RESULTS AND DISCUSSION

6.1. Structures and Groundwater flow patterns

6.1.1. Magnetic anomalies signatures and superimposed geological structures

Groundwater occurrence and flow are largely influenced by structures hence, it is important to analyse these structures using favourable techniques available. The total aeromagnetic map exhibits positive and negative anomalies. Qualitative analyses of the aeromagnetic and structural data have shown that large positive magnetic anomalies (~404 nT) coincide with granite batholiths, the Soutpansberg Mountains, greenstone remnants and mafic dykes as they appear in the aeromagnetic map showing a general trend of NE-SW (Fig 6.1). The high magnetic signatures along the Soutpansberg Mountains are possibly related to volcanic layers forming the volcano-sedimentary sequence of the Soutpansberg Group. Magnetic anomalies tracing greenstone belts within the study area shows what could possibly be an extended greenstone belt buried beneath younger successions. Furthermore, a mineral map of the area indicates iron deposits along the greenstone remnants (Appendix B), which supports high magnetic anomalies observed within the magnetic map. The areas of negative anomalies showing a general trend of NE-SW have amplitudes in the range of -46 nT to -280 nT (Fig 6.1). These areas of negative anomalies indicate rocks of different compositions and depths to the areas with positive magnetic anomalies and potentially influencing groundwater flow and occurrence differently.

During geological mapping of the study area, highly weathered dolerite dykes with thickness in the range of 7 to 20 m were observed. These dykes were sited in two locations with a strike in the range of 088^{o} to 075^{o} and dip angle of 50^{o} to 55^{o}, respectively. Based on the aeromagnetic and structural maps, dolerite dykes show a dominant parallel and continuous trend of NE, which also agree to the measured dykes for this study (Fig 6.1). Additionally, these dykes seem to be superimposed along the positive magnetic anomalies. Sakala et al. (2014) interpreted the continuous and parallel characteristics of the dykes as an indication of emplacement in an extensional crustal regime along zones of weakness due to earth's crust pulling apart. However, not all superimposed dykes and other lineaments on the aeromagnetic map coincide with high magnetic anomalies indicating that some of these dykes are not magnetic (Fig 6.1). Dolerite

dykes and other lineaments are more concentrated north of the Hout River Shear Zone as compared to the southern part with dominating NE trend. Other apparent orientations of these structures are NW, N and E-W with no prevailing dominant directions south of the HRSZ (Fig 6. 1). Previous study that correlates the dyke trends and borehole productivity showed that high mean transmissivities are related to NE, ENE and WNW trending dykes and lower transmissivity in the NW and NNE trending dykes (Holland, 2011). This means that dykes allowing more groundwater flow and occurrence are those perpendicular to the neo-tectonic principal horizontal stresses and lesser to those parallel due to high degree of fracturing of these dykes observed during field excursion and also groundwater contour maps that shows general groundwater flow along channels parallel to the NE and WNW structures. However, this study did not involve analyses of dyke's thickness and degree of fracturing in detail and no pumping test was carried out, thus it is not apparent which dykes act as barriers or conduits within the catchment.

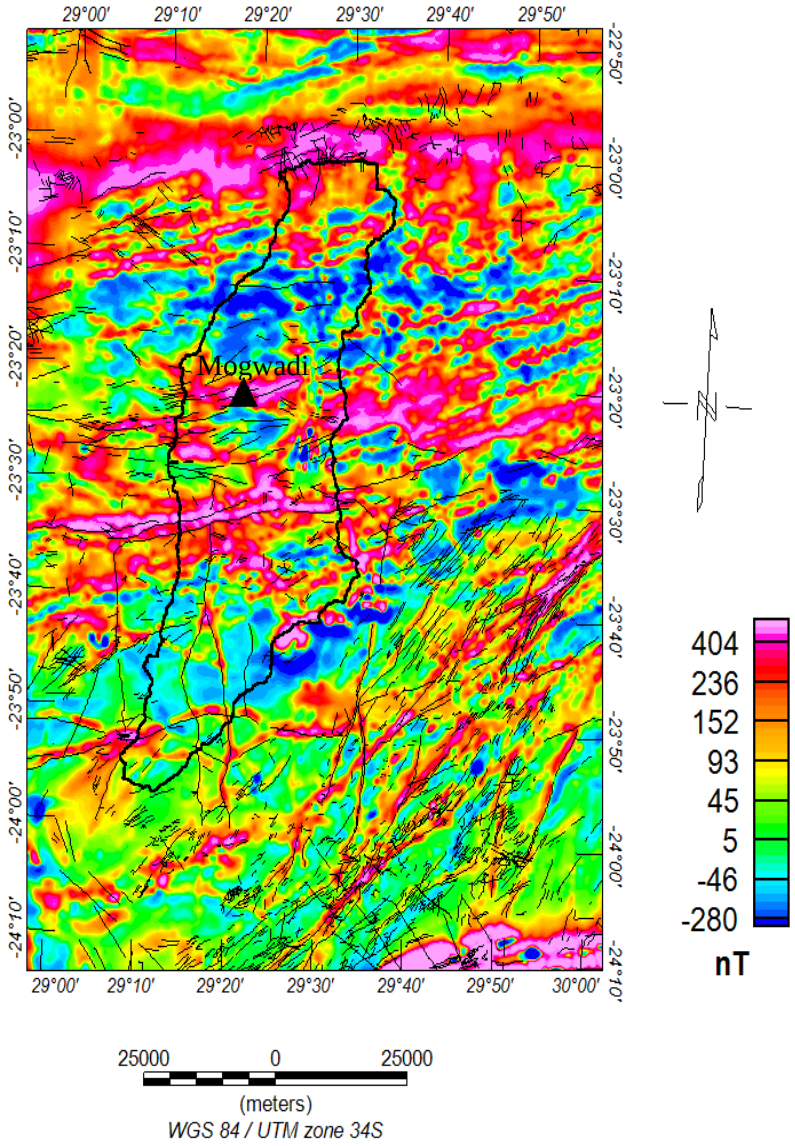


Figure 6.1: Aeromagnetic map with superimposed geological structures of the Hout River Catchment.

6.1.2. The groundwater flow patterns and effects of lineaments on borehole yields

Groundwater levels data from 77 boreholes obtained from the GRIP database were used to construct a groundwater contour map (Fig 6.2). The local groundwater flow direction map of the HRC shows a general trend of groundwater trajectories moving from elevated groundwater levels along positive magnetic anomalies to lower groundwater levels in areas with negative groundwater anomalies. The areas with positive magnetic anomalies seem to represent areas of recharge with high groundwater levels. High groundwater head is also linked to topographical highs within the study area (Fig 6.2). Structures with positive magnetic anomalies have created ridges trending NE where regional groundwater flow seems to be following this pattern; after being recharged from the high topographical areas and areas associated with positive magnetic anomalies, regional groundwater storage and flow seems to occur parallel to positive magnetic ridges (Fig 6.2).

Shallow groundwater levels are in the range between 2 to 5 m.b.g.l. Along the HRSZ, groundwater level is elevated and approximately 13 m.b.g.l. Generally, groundwater levels are higher where structures are densely concentrated and deeper in areas with less structural concentrations. The patterns observed here most likely indicate situations where mafic dykes are acting as pass ways allowing groundwater flow, although this study did not involve field investigation of the structures in detail and their influence on groundwater occurrence, thus depriving detailed information of structural behaviour on groundwater occurrence and flow.

.

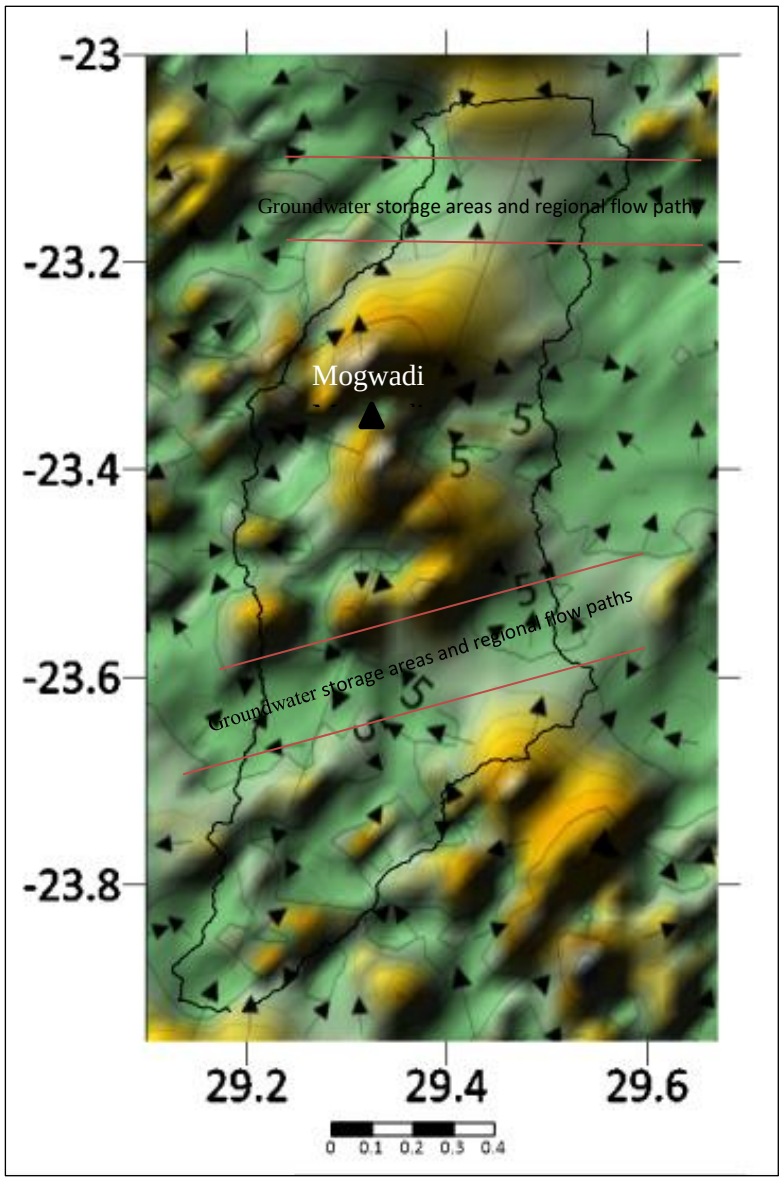


Figure 6.2: Groundwater flow patterns.

6.2. Physico-chemical parameters

Table 6.1 is showing outcomes of physical and chemical parameters measured from groundwater and one spring samples within and outside the study area.

6.2.1. Measured parameters

6.2.1.1. Temperature (T)

The water temperature varies between 23.85 °C and 29.7 ºC with a mean value of 26.21 °C (Table 6.1). These values are within the accepted range for domestic use (WHO, 2009). Cool water is more palatable as compared to warm water (WHO, 2008). The latter favours growth of microorganisms which leads to changes in the water taste, odour, colour and increase in its corrosive abilities.

6.2.1.2. Oxidation-Reduction Potential (ORP)

The range of ORP value in the study area for boreholes is in the range of +149 to +92 mV with a mean value of +118.4 mV (Table 6.1). A spring water has an ORP value of +99 mV. The results show that this water was circulating in an oxidizing environment, which could suggest the presence of an open system or an environment rich with an oxidizing chemical constituent such as iron.

6.2.1.3. pH

The measure of pH determines the acidity and alkalinity of water samples. For groundwater samples, pH gave values in the range of 6.97-7.86 and a mean value of 7.41, which is within the accepted water quality standards. From these results, it is evident that there is insignificant change in water taste, metal ions dissolution and deprotonated compounds that have a potential of causing adverse effects on consumer's health (DWAF, 1996a). However, towards the extremes of this acceptable range some metals may start to dissolve such as aluminium which

dissolves approximately at pH of 6; other metal ions may also dissolve if the solution contains complexing ions. Amphoteric oxides also dissolve when pH passes 8.5 whereby a slight change in the taste of water may be felt (DWAF, 1996a).

The spring (SP1) water sample shows a pH value that is slightly alkaline at a value of 8.84 but is still within the accepted range values according to WHO (2008) and the South African water quality standards (DWAF, 1996a). This indicates that there are no health effects that will be experienced upon the use of this water for domestic use although for irrigation purpose, it might be slightly higher than the accepted limits according to the acceptable South African water quality standards of irrigation (DWAF, 1996b).

6.2.1.4. Dissolved Oxygen (DO)

There are no health constraining concentration limits for the molecular oxygen in water. However, the knowledge of its concentration in water is essential to know the stability of toxic species within the water like the radionuclides, trace metals, organic contaminants and anoxic complexes (Rose and Long, 1988). For groundwater samples, DO is in the range of 13.56-6.7 mg/l and a mean value of 10.56 mg/l. The sample from a spring gave a value of 9.36 mg/l (Table 6.1).

6.2.1.5. Total dissolved solids (TDS) and Electrical Conductivity (EC)

EC and TDS are interdependent (Table 6.2), thus EC is normally used to estimate TDS (DWAF, 1996a). This is because EC is easier to measure and depends on concentration of the ionized particles within the water which in turn forms part of the dissolved solids within the same water sample. For groundwater samples, high TDS and EC values greater than 1000 mg/l are around the Mogwadi area (D1 to D7) and one sample outside the catchment (D16). The EC and TDS ranges for these boreholes are 1035-2180 µS/cm and 1046-1400 mg/l, respectively. From these results, it is evident that TDS and EC in the groundwater samples are not within the accepted limits of water quality for domestic use with the accepted range of 0-450 mg/l (DWAF, 1996a) and 180-500 µS/cm (W.H.O, 2009), respectively. These results also show that neither is this groundwater within the acceptable standards for irrigation and livestock watering. The obtained results are within the same range as those obtained by Mandiwana

(2004) around the Dendron area. The same trend of high TDS and EC, which exceed acceptable range of drinking water was observed in Vegter (2003) and Holland (2011). While EC values seems to be variable throughout the catchment, TDS decreases further towards the southern part of the catchment (Table 6.1). However, borehole D20 shows significantly reduced values of TDS and EC as compared to other groundwater samples, which is indicative of less mineralised groundwater. This could be indicative of mixed groundwater or young groundwater. However, this study did not include analyses of bicarbonate and other geochemical contents thus the obtained results are not conclusive as they stand. Geochemical study in Holland (2011), shows that the southern part of the HRC is dominated by less mineralised groundwater, with low EC and enriched bicarbonate which is indicative of recent recharge groundwater. However, there are also pockets of mixed and old groundwater with increased mineralisation signature and low bicarbonate enrichment.

Mineralisation and considerable dissolved solids in groundwater around the Mogwadi area might be attributed to agricultural activities, low groundwater recharge and prolonged water-rock interaction. Mandiwana (2004) found that groundwater type in this area is that of Ca-Na-Cl-HCO_3 with bicarbonate concentration decreasing towards the northern part of the town. Personal communication with some of the Mogwadi farmers has shown that borehole depths in this area varies from 60 m to 110 m with others having a life span of over 100 years to date. This might suggest occurrence of old groundwater. Additionally, deeply fractured nature of the aquifer around the Mogwadi area as outlined in Jolly (1986) might also be allowing longer residence time. Depending on the type of dissolved solids within the groundwater, humans, livestock and crops could be affected negatively. For an example, geochemical investigation of this groundwater in 2004 and in 2011 involving the study area, have shown that nitrate and fluoride are amongst the dominant constituents of this groundwater (Mandiwana, 2004; Holland, 2011). Furthermore, Holland (2011) observed higher chloride, sodium and nitrate content along some boreholes located within the southern part of the catchment and interpreted as groundwater showing progressed chemical development and hence older groundwater.

7.2.1.5. Turbidity

Turbidity analyses was carried out during the first sampling period in 2016 and only boreholes from the Mogwadi and the Legkraal (outside the catchment) farms were sampled. The range of the turbidity in these samples is from 245 to 133 NTU (Table 6.1). According to the acceptable water quality standards of DWAF (1996a) and WHO (2008), these samples have considerably high turbidity. The acceptable range is less than 5 NTU according to WHO (2008) standards and about 1 NTU based on the DWAF (1996a) domestic use standards. These results show that water in the Mogwadi area have higher suspended materials that either reflect or refract light upon encountering water. It also shows the presence of fine particles within the aquifer, which could also signify the predominant role of weathered zone rather than fractures for the storage of groundwater.

Table 6.1: Physicochemical parameters of groundwater and spring samples within the Hout River Catchment.

Code	Geosite	Latitude	Longitude	Temp (°C)	ORP (+mV)	pH	DO (mg/l)	EC (µS/cm)	TDS (mg/l)	Turbidity (NTU)
D1	Borehole	-23.3529	29.42515	25.2	149	7.5	12.5	1035	1238	218
D2	Borehole	-23.3529	29.42515	25.9	92	6.98	12.22	1050	1300	198
D3	Borehole	-23.3529	29.42515	25.4	94	7.02	12.14	1110	1250	197
D4	Borehole	-23.3529	29.42515	26.8	100	7.00	12.09	1500	1352	245
D5	Borehole	-23.3529	29.42515	26.7	115	7.00	10.3	2180	1400	205
D6	Borehole	-23.3571	29.42419	27.1	112	6.97	11.13	2170	1386	191
D7	Borehole	-23.3599	29.41747	29.7	119	6.94	9.4	1635	1046	133
D8	Borehole	-23.3616	29.51921	27.7	119	7.23	10.2	1384	888	198
D11	Borehole	-23.5915	29.46064	24.5	168	8.33	11.2	1079	694	-
D12	Borehole	-23.5915	29.46064	24.6	139	7.27	12.1	1040	665	-
D13	Borehole	-23.5886	29.48516	26.3	136	7.30	13.56	1120	716	-
D15	Borehole	-23.1449	29.55613	27.3	101	7.47	8.29	1227	785	-
D16	Borehole	-23.3292	29.31769	27.5	121	7.86	9.36	2020	1296	-
D17	Borehole	-23.4994	29.33227	26.1	122	7.70	10.8	1239	793	-
D18	Borehole	-23.6287	29.28533	24.4	112	7.86	9.36	1228	786	-
D19	Borehole	-23.64	29.31703	26.5	103	7.84	10.3	1035	662	-
D20	Borehole	-23.8059	29.20866	23.85	112	7.68	6.7	473	302	-
Mean				26.21	118.47	7.41	10.56	1347.50	904.07	198.125
D14	Spring	-23.054	29.39789	25.6	99	8.84	9.33	49.6	31.9	-

6.3. Environmental isotopes ($\delta^{18}O$, $\delta^{2}H$, ^{3}H, ^{14}C and ^{13}C)

The stable isotope results for $\delta^{18}O$ and $\delta^{2}H$ that are analysed from rainfall, groundwater, Hout River, Hout Dam and spring samples have been presented in Table 6.2. The results were plotted against the Pretoria Local Meteoric Water Line (LMWL) and Global Meteoric Water Line (GMWL) (Fig 6. 3). The Pretoria LMWL has a slope of 6.7‰ and deuterium intercept of 7.2‰.

To understand the sources of rainfall it is important to compare how the slope and intercept (i.e. deuterium) of the LMWL have deviated from that of the GMWL. The slope of the meteoric water line is a function of temperature during secondary evaporation (Clark and Fritz, 1997). The d-excess is a function of relative humidity above the ocean surface which indicates the conditions during formation of vapour (Geyh, 2000). The slope and intercept of the LMWL at value of 6.7‰ is lower than that of the GMWL. According to Wu (2005), LMWL slope less than that of the GMWL is indicative of secondary evaporation and lead to decrease in d-excess. Clark and Fritz (1997) further explained the phenomenon of secondary evaporation as a process where surface water re-evaporates to form vapour that is subsequently re-condensed without interacting with the reservoir in the troposphere. The d-excess of the LMWL at 7.2‰ is lower than that of the GMWL (*d=10*), which further shows that the rainfall originated from a far source possibly from the Indian Ocean. The LMWL's intercept shows that the relative humidity above the ocean surface was higher during the formation of the vapour which formed the local rainfall as compared to what formed the GMWL vapour.

Most of the rainfall is brought about by easterly waves and lows, or tropical–extratropical cloud bands and associated thunderstorms (Van Heerden and Taljaard, 1998; Tyson and Preston-Whyte, 2000). These cloud bands are the most important rainfall-producing weather system over most of southern Africa (Harrison, 1984; Todd and Washington, 1999). According to Van Heerden and Taljaard (1988), rainfall within the Limpopo Province and overall Southern Africa results from easterly winds, low pressure cells, or tropical cloud systems with associated thunderstorms. These cloud systems influence weather patterns over most of Southern Africa regions (Todd and Washington, 1999).

6.3.1. Stable isotopes (^{18}O and ^{2}H) composition

6.3.1.1. Stable isotopes in precipitation

The isotopic composition in rainfall samples has a mean value of $\delta^{2}H$ and $\delta^{18}O$ at -10.1‰ and -2.3‰, respectively. These values include two samples from city of Polokwane located SSE of the catchment (Table 6.2). The mean rainfall value plots along the LMWL as expected. During the sampling period, rainfall amounts in the area ranged from 3.4 mm to 24 mm per day towards the southern portion of the catchment and 70.5 mm to 34.5 mm per day around the Mogwadi area. Towards the northern edge of the catchment, rainfall was in the range of 11.8 mm to 120.4 mm per day. Although low rainfall amount was apparent during the sampling period, most of the samples showed depleted values of oxygen and hydrogen stable isotopes with few samples showing enriched stable isotopes (Fig 6.3). Highly depleted rainfall stable isotopes could be due to either a depleted source that resulted from long circulation air mass and/or elevation variations. D-excess is useful in identifying the source of vapour forming precipitation in an environment (Clark and Fritz, 1997). For these samples, mean d-excess value is low indicating a far source (Table 6.2). As a result, this further attest to the argument that long circulation led to the depleted nature of stable isotopes in this catchment. Elevation variation which drives the "rain-out" effect could also be attributed to the stable isotopes in the region. According to Clark and Fritz (1997), per 100 m rise of the vapour masses, stable isotopes ($\delta^{18}O$ and $\delta^{2}H$) variations is in the range of -0.15‰ to -0.5‰ and -1‰ to -4‰, respectively. The elevations in the catchment are in the range of 1200 to 400 m.a.m.s.l as described in Chapter 3. The effect of seasonal variations cannot be accounted for due to the nature of sampling which only occurred during the summer season.

To further understand the sources of rainfall it is important to compare how the slope and intercept of the LMWL have deviated from that of the GMWL. The slope of the meteoric water line is a function of temperature during secondary evaporation (Clark and Fritz, 1997). The slope of the LMWL at value of +5.69 is lower than that of the GMWL as a result of evaporation losses. The d-excess is a function of relative humidity above the ocean surface which indicates the conditions during formation of vapour (Geyh, 2000).

Stable isotopes results will also determine the environment from which the vapour formed based on the position of the stable isotopes relative to the LMWL and GMWL. Few rainfall

samples plot below the LMWL showing a source of high humid conditions (Fig 6.3). However, most rainfall samples plotted above the LMWL showing the effects of non-equilibrium (secondary) evaporation with low humidity. Clark and Fritz (1997) showed that secondary evaporation occurs when surface water re-evaporates to form vapour that is subsequently re-condensed without interacting with the reservoir in the troposphere.

6.3.1.2. Surface water stable isotopes

The only major river in the catchment is the Hout River. It is normally dry and only flows during rainy seasons. As such, during sampling, one sample from a river and one from the dam were collected. The mean values of $\delta^{18}O$ and $\delta^{2}H$ in these water samples are 0.10‰ and 4.8‰, respectively (Table 6.3). The river sample is plotting along the LMWL, which suggest water directly derived from the local rainfall. The isotopic values of the river sample from the upstream Hout River Dam is more enriched with $\delta^{18}O$ of 2.24 ‰ and $\delta^{2}H$ of 17.7 ‰ as compared to the isotopic values downstream with values $\delta^{18}O$ and $\delta^{2}H$ at -8.07‰ and -2.05‰, respectively (D9). Based on the stable isotopes, there is no apparent interaction between surface water samples and groundwater. D-excess of these samples is lower indicating a regional source of moisture (Fig 6.4).

6.3.1.3. Groundwater stable isotopes

The stable isotopes from the groundwater samples have the mean values of $\delta^{18}O$ and $\delta^{2}H$ at -4.52‰ and -29.0‰, respectively. All the samples are depleted with respect to VSMOW plotted below the LMWL (Fig 6.3). Depleted signature on these samples could be ascribed to evaporation which happened before infiltration and subsequent long term and slow groundwater circulation deep within the aquifer. Their position with relative to the LMWL indicates recharge that occurred during colder climates in high humidity conditions. Isotope data plotting below the LMWL indicates high humidity environments (Clark and Fritz, 1997). These samples also show a smaller range of $\delta^{18}O$ and $\delta^{2}H$ at -3.75‰ to 5.43‰ and -25.1‰ to -35.8‰, respectively. From this clustering, it could suggest that groundwater in this catchment is interconnected through network of fractures or significant regional recharge occurred during

the same event. In addition, the plot of d-excess and ^{18}O shows a lower value (Fig 6. 4), which suggest a regional source of moisture.

A plot of ^{18}O and depth of the boreholes located within the Mogwadi (D1 to D7) and Legkraal (D8) areas was carried out in order to understand the distribution of stable isotopes with depth (Fig 6.5). The stable isotopes data represent a thickness of 50 m within the aquifer and few boreholes shows increase in isotopes depletion with depth. For an example, boreholes D7 and D8 have the deepest static water level (SWL) of groundwater at 100 m.b.g.l and show most depleted stable isotopes (Fig 6.5). In contrast, D4 represent the deepest water levels at 110 m.b.g.l and least depleted ^{18}O at -3.72‰. Furthermore, D1 is one of the shallowest boreholes with water levels at 60 m.b.g.l but amongst the most depleted with respects to ^{18}O at -4.45‰ (Fig 6.5). The aquifer shows what could seem to be mixed groundwater where highly depleted stable isotopes exists at shallows levels and less depleted stable isotopes in greater depths. However, this distribution is not uniform even within short distance of borehole locations, which also suggest compartmentalisation by geological structures.

In other parts of the catchment like the eastern part of the catchment (D11 to D13), stable isotopes are depleted from groundwater that were obtained at average levels of about 100 m.b.g.l. Although no depth was recorded for these boreholes, D15 and D20 are also showing highly depleted stable isotopes along the north-eastern and southern part of the catchment, respectively. This suggest distribution of depleted stable isotopes in compartments within the catchment which could not be extrapolated due to complex stable isotopes variations observed in boreholes in close proximity like the case of the Mogwadi area.

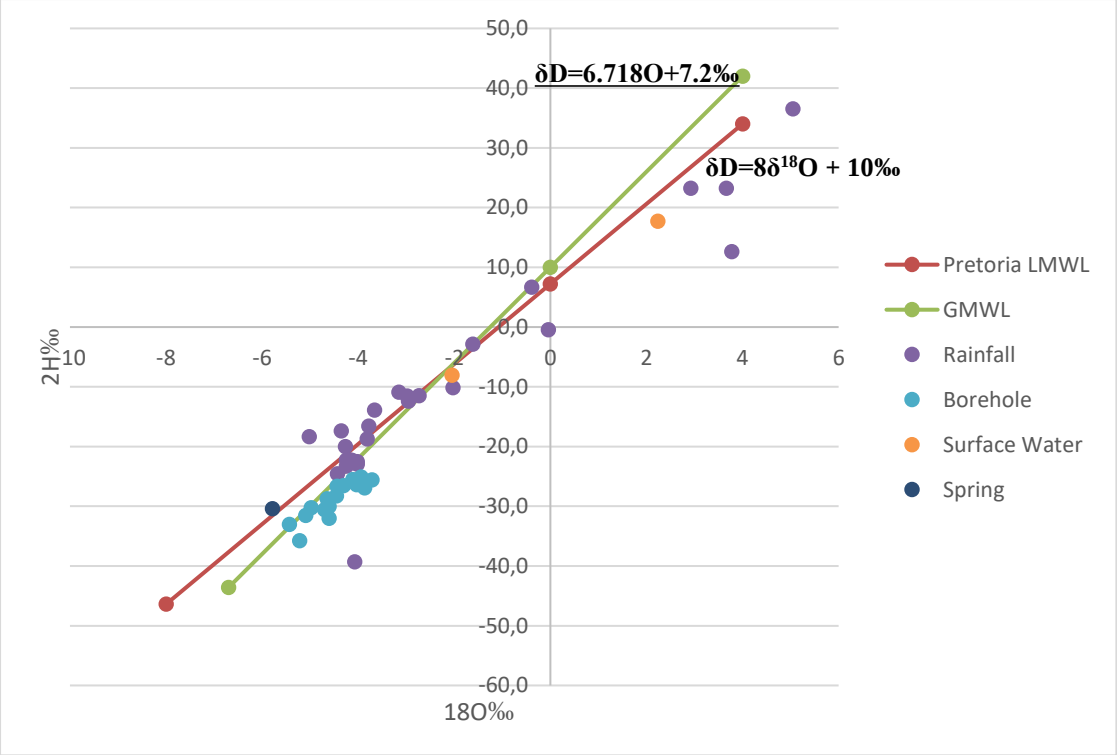


Figure 6.3: Hout River Catchment stable isotopes in rainfall, borehole, river and dam and springs. The LMWL is given by $\delta D=6.7\delta^{18}O+7.2$ ‰ and GMWL by $\delta D=8\delta^{18}O+10$ ‰ (Craig, 1961).

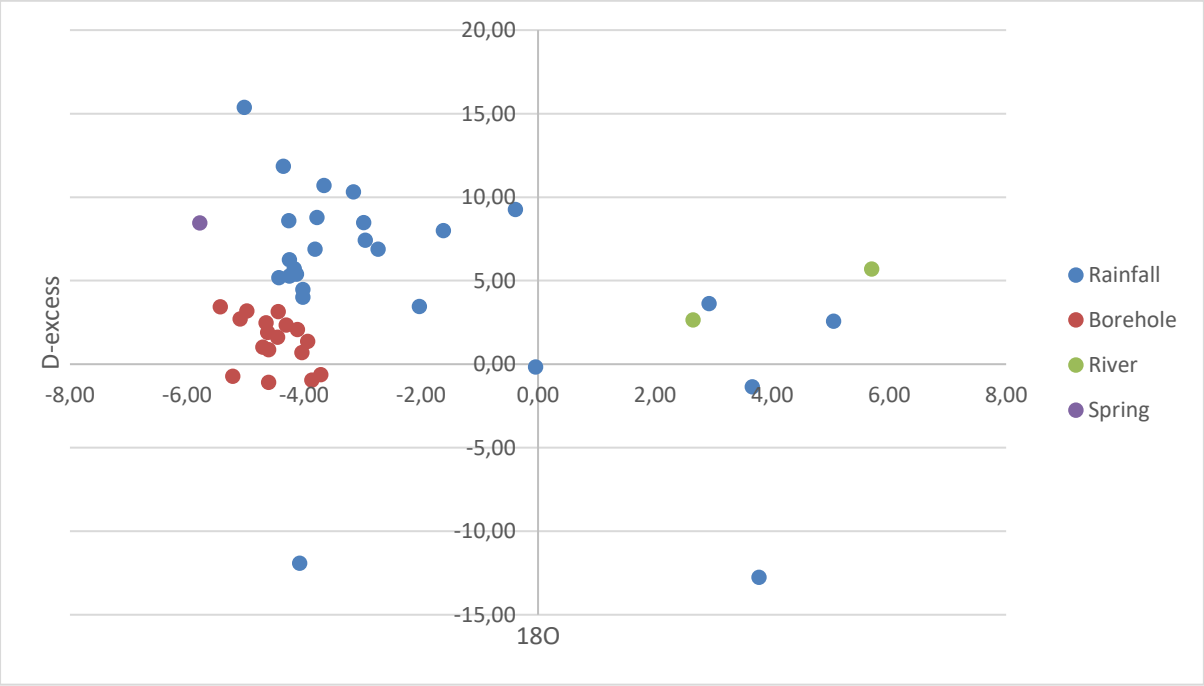


Figure 6.4: D-excess and ^{18}O plots for rainfall, borehole and spring samples within the HRC.

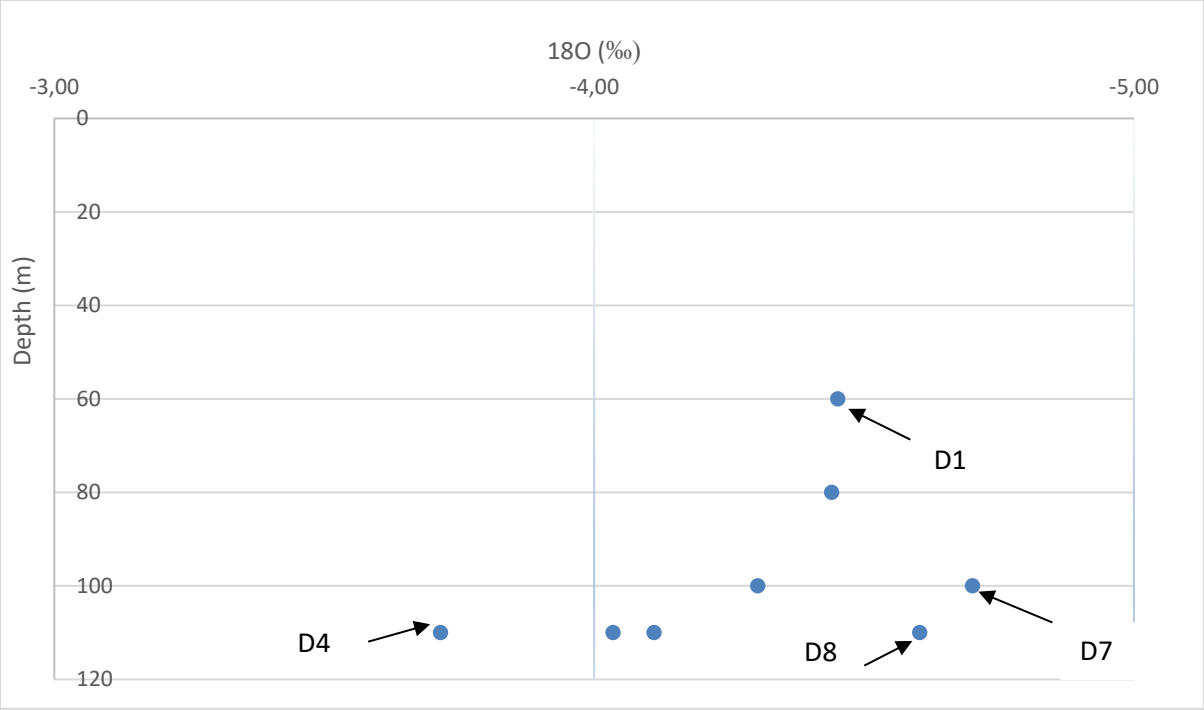


Figure 6.5: Depth against ^{18}O for Boreholes (D1 to D8) located within the Mogwadi and eastern-outside the catchment.

Table 6.2: Environmental isotope of the Hout River Catchment (November 2016 to March 2017).

Code	Source	Latitudes	Longitude	$\delta^{2}H$ (‰)	± ^{2}H StDev (‰)	$\delta^{18}O$ (‰)	± ^{2}H StDev (‰)	D-excess
RN1	Rain	-23.768106	29.2259	-2.9	0.60	-1.62	0.51	7.97
RN2	Rain	-23.768106	29.2259	-18.3	0.31	-5.02	0.19	15.29
RN3	Rain	-23.768106	29.2259	-13.9	1.14	-3.66	0.25	10.63
RN4	Rain	-23.683839	29.092442	-0.4	0.97	-0.04	0.18	-0.17
RN5	Rain	-23.683839	29.092442	-39.3	0.65	-4.08	0.27	-11.99
RN6	Rain	-23.683839	29.092442	-11.6	1.50	-2.98	0.36	8.43
RN	Rain			-10.2	0.80	-2.03	0.20	3.42
RN7	Rain	-23.731775	29.307742	23.3	1.24	2.92	0.39	3.68
RN8	Rain	-23.731775	29.307742	-17.4	0.78	-4.36	0.19	11.78
RN	Rain			12.6	0.70	3.78	0.26	-12.68
RN9	Rain	-23.36965	29.322331	-12.4	2.15	-2.95	0.34	7.38
RN10	Rain	-23.36965	29.322331	-10.9	1.48	-3.16	0.29	10.27
RN11	Rain	-23.36965	29.322331	-11.5	0.69	-2.74	0.14	6.84
RN112	Rain	-23.36965	29.322331	6.7	0.51	-0.39	0.15	9.25
RN13	Rain	-23.36965	29.322331	-16.6	1.04	-3.78	0.21	8.71
RN14	Rain	-23.36965	29.322331	-20.0	3.36	-4.26	0.54	8.52
RN15	Rain	-23.36965	29.322331	-18.7	0.69	-3.81	0.14	6.82

RN16	Rain	-22.906289	29.619178	-22.3	1.00	-4.16	0.30	5.65
RN17	Rain	-22.906289	29.619178	-23.0	1.91	-4.02	0.27	3.94
RN18	Rain	-22.906289	29.619178	-22.3	0.36	-4.25	0.06	6.17
RN19	Rain	-22.906289	29.619178	-24.6	2.86	-4.43	0.52	5.11
RN20	Rain	-22.906289	29.619178	-22.3	0.64	-4.13	0.40	5.31
RN21	Rain	-22.906289	29.619178	-23.3	0.55	-4.25	0.30	5.19
RN22	Rain	-22.906289	29.619178	-22.5	0.26	-4.02	0.09	4.40
RN23	Rain	-23.894436	29.434828	23.2	3.31	3.66	0.38	-1.29
RN24	Rain	-23.894436	29.434828	36.5	1.00	5.05	0.16	2.68
Mean				-10.1	1.2	-2.3	0.3	5.05
D9	River	-23.798003	29.233617	-8.1	0.96	-2.05	0.16	5.67
D10	Dam	-23.798203	29.221881	17.7	1.03	2.24	0.21	2.69
Mean				4.8	1.0	0.1	0.2	4.21
D1	Borehole	-23.35519	29.39173	-28.28	0.60	-4.45	0.31	1.54
D2	Borehole			-26.68	0.98	-4.44	0.24	3.07
D3	Borehole	-24.6521	25.92857	-25.54	0.23	-4.11	0.32	2.00
D4	Borehole	-23.35182	29.39822	-25.59	0.74	-3.72	0.11	-0.69
D5	Borehole	-23.35287	29.42515	-26.40	0.78	-4.03	0.09	0.63
D6	Borehole	-23.35714	29.42419	-26.57	0.65	-4.30	0.29	2.26
D7	Borehole	-23.35988	29.41747	-30.55	1.68	-4.70	0.28	0.95

D8	Borehole	-23.36164	29.51921	-32.01	0.85	-4.60	0.22	-1.17
D11	Borehole	-23.590564	29.48056	-30.26	0.56	-4.98	0.22	3.09
D12	Borehole	-23.59145	29.46064	-31.51	0.82	-5.09	0.20	2.62
D13	Borehole	-23.58864	29.48516	-33.05	0.27	-5.43	0.14	3.34
D15	Borehole	-23.1449	29.55613	-35.78	0.33	-5.22	0.06	-0.81
D16	Borehole	-23.32915	29.31769	-30.06	0.38	-4.60	0.05	0.79
D17	Borehole	-23.49936	29.33227	-25.11	0.58	-3.94	0.21	1.29
D18	Borehole	-23.62874	29.28533	-29.14	1.06	-4.62	0.19	1.82
D19	Borehole	-23.63997	29.31703	-26.92	3.06	-3.86	0.24	-1.03
D20	Borehole	-23.80593	29.20866	-28.74	0.45	-4.65	0.06	2.39
Mean				-28.95	0.83	-4.52	0.19	1.30
D14	Spring	-23.05404	29.39789	-30.4	1.75	-5.78	0.50	8.36

6.3.2. Radiogenic isotopes (^{14}C and ^{3}H) and stable carbon (^{13}C)

To evaluate the MRT of groundwater recharge in the past few decades and more than a century, tritium and radiocarbon samples from river, spring and groundwater were analysed and results are given in Table 6.3. Results show that tritium values of 1.4 and 1.9 TU for water obtained within the Hout River and Dam, respectively. Around the Taaibosch area, tritium value from the rainfall for a period of 5 years (from 2000 to 2005) gave an average value of 2.8 TU (Butler and Verhagen, 2013). Using 2.8 TU as the initial value in the atmosphere and a half-life of 12.43 years, the MRT of the Hout River and Dam are 5.16-12.43 years, respectively indicating that this is recent water (Table 6. 3). The river sample was obtained after an auger drilling of about 1 m below the river surface.

^{3}H values in groundwater samples are in the range of 0.0-2.1 TU (Table 6. 3), which indicates groundwater recharge that occurred pre-1952 and post-1952 periods in accordance with qualitative classification given in Clark and Fritz (1997) whereby it has been shown that tritium concentration of less than 0.8 TU shows groundwater that recharged before 1952. Modern or mixed groundwater has tritium concentration greater than 0.8 TU (Clark and Fritz, 1997).

The calculated MRT for groundwater samples using tritium and radiogenic carbon gave two categories of groundwater. The first category with 100 pMC values of ^{14}C showed MRT of between 5 to 40 years using 2.8 TU and 12.43 years (Table 6.3). The second category showed groundwater samples that gave ^{14}C signatures. These samples showed both sub-modern and modern groundwater. Groundwater samples that were analysed for ^{14}C, attest to both sub-modern and mixed samples. Groundwater samples that were recharged before 1952 based on both tritium and ^{14}C were obtained from the Mogwadi area (D1 and D7), eastern edge of the catchment (D8 and D12) and one sample from the southern edge of the catchment (D18 and D20) (Fig 6. 6). For these samples, ^{3}H has the range of 0 to 0.4 TU with corresponding narrow range of ^{14}C at 84.30 to 93.40 pMC (Table 6. 3). This shows groundwater which was recharged between 500 to 1400 years. In contrast, groundwater samples that were recharged post-1952 have ^{14}C values greater than 100 pMC and their corresponding ^{3}H values greater or equal to 0.8 TU (Fig 6. 6). Such samples represent remnant of anthropogenic ^{14}C (Clark and Fritz, 1997). Groundwater samples showing this group were obtained from boreholes D15 and D16 located north of the Mogwadi area and northeast outside the catchment, respectively. These samples suggest the presence of recent recharge from the Soutpansberg Mountains as

Mountain-front recharge into the aquifer. Recharge for these groundwater samples occurred between 14 to 22 years using rainfall tritium value of 2.8 TU and half-life of 12.43 years.

Going further north of the catchment, a spring emerging from the Soutpansberg Mountains gave tritium value of 2.2 TU (Table 6. 3). Using a half-life of 12.43 and 2.8 TU as the tritium value in the local rainfall, the recharge occurred 4 years ago, which suggests younger groundwater towards the northern boundary of the catchment. This further suggest that recharge zones also occur along the northern part of the catchment.

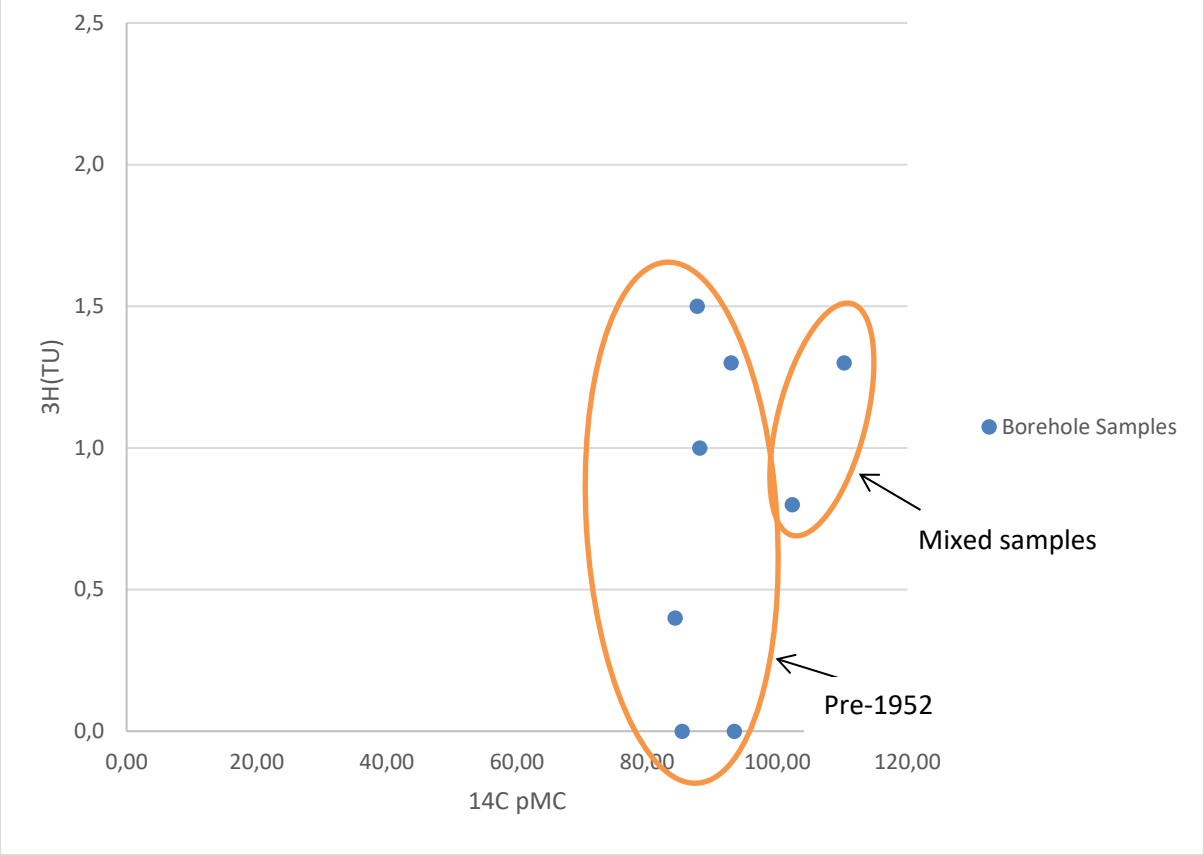


Figure 6.6: A plot of ^{3}H and ^{14}C for the groundwater samples for pre-1952 and post-1952 recharge.

Table 6.3: Radiogenic isotopes from groundwater, spring and river samples in the HRC.

Code	Source	Latitudes	Longitude	Tritium (TU)		MRT	14 C (pMC)		13C (‰)	Corrected ages
D1	Borehole	-23.35519	29.39173	0.50	±0.2	30.89	-	-	-	-
D2	Borehole	-	-	1.50	±0.3	11.19	-	-	-	-
D3	Borehole	-24.6521	25.92857	0.80	±0.2	22.46	-	-	-	-
D4	Borehole	-23.35182	29.39822	1.00	±0.3	18.46	-	-	-	-
D5	Borehole	-23.35287	29.42515	1.40	±0.3	12.43	-	-	-	-
D6	Borehole	-23.35714	29.42419	1.70	±0.3	8.95	-	-	-	-
D7	Borehole	-23.35988	29.41747	0.00	±0.0	ND	85.40	±2.5	-12.63	1304.73
D8	Borehole	-23.36164	29.51921	0.00	±0.0	ND	93.40	±2.6	-11.10	564.46
D9	River	-23.798003	29.23362	1.4	±0.3	12.43	-	-	-	-
D10	Dam	-23.798203	29.22188	2.1	±0.3	5.16	-	-	-	-
D11	Borehole	-23.2956	28.05641	2.10	±0.3	5.16	ND	-	ND	-
D12	Borehole	-23.59145	29.46064	0.40	±0.2	34.89	84.30	±2.5	-11.42	1411.91
D13	Borehole	-23.58864	29.48516	0.30	±0.2	40.05	ND	-	ND	-
D14	Spring	-23.05404	29.39789	2.20	±0.3	4.32	-	-	-	-
D15	Borehole	-23.1449	29.55613	0.80	±0.2	22.46	102.30	±2.6	-13.81	-187.99
D16	Borehole	-23.32915	29.31769	1.30	±0.3	13.76	110.30	±2.7	-9.76	-810.44

D17	Borehole	-23.49936	29.33227	1.30	±0.3	13.76	92.90	±2.6	-11.57	608.84
D18	Borehole	-23.62874	29.28533	1.00	±0.3	18.46	88.10	±2.5	-9.41	1047.41
D19	Borehole	-23.63997	29.31703	0.70	±0.2	24.86	ND	-	ND	-
D20	Borehole	-23.80593	29.20866	1.50	±0.3	11.19	87.70	±2.5	-10.67	1085.03

(-) = Not measured

ND= Not detected

6.3.2.1. Source of carbon and ^{14}C corrections

Different source of carbon ranging from CO_2 in soil, magma, hydrothermal fluids and carbonate minerals exists in nature (Geyh, 2000). These different sources make up the total dissolved carbons (both organic and inorganic) within groundwater giving rise to variable ranges of $\delta^{13}C$. For groundwater samples in this study, $\delta^{13}C$ values gave a narrow range of -9.41‰ to -13.81‰ with an average value of -11.30‰ (Table. 6.3). These results indicate a source of $\delta^{13}C_{DIC}$ that formed in part from carbon fractionation through C_4 plants photosynthetic cycle and carbon reduction processes in metamorphic and igneous rocks. C_4 plants are common in hot ecosystems and have a range of $\delta^{13}C$ between -10 and -16‰ (Clark and Fritz, 1997). Although metamorphic and igneous rocks have a wide range of $\delta^{13}C$ values in the range of -35‰ and 0‰, their presence in the study area means that there is possibly some degree of $\delta^{13}C$ contributed from these rocks.

In different paths along which groundwater flows, carbonate reactions alter ^{14}C concentrations which may give incorrect MRT values for groundwater. ^{13}C is again useful to determine the extent at which hydro-chemical reactions have diluted the ^{14}C concentrations in groundwater. A plot between ^{14}C and $\delta^{13}C$ that shows an increase in the activity of ^{14}C with corresponding decrease in $\delta^{13}C$ is indicative of young groundwater with less dilution by DIC (Clark and Fritz, 1997). One sample obtained from D15 in the northern part of the catchment, shows higher ^{14}C activity at 102.30± 2.6 pMC with decreased value of $\delta^{13}C$ at -13.81‰ indicating younger groundwater with minor dilution by DIC (Fig 6.7). This groundwater is related to the thermonuclear period recharge. In contrast, ^{14}C activity decreases with increase in $\delta^{13}C$ when mean residence time of groundwater is longer (Verhagen et al., 2009). Although not all samples conform to these claims in the study area, some samples for an example D18 and D20 indicate values of ^{14}C and $\delta^{13}C$ at 88.10± 2.5 pMC; -9.41 ‰ and 87.70 ±2.5; -10.67 ‰, respectively (Fig. 6. 7). Collectively, these results suggest that there has been minor dilution of ^{14}C by DIC. Moreover, Verhagen et al. (2009) proposed an initial ^{14}C activity between 80 and 90 pMC near the study area which further suggest less deviation from the initial ^{14}C activity in the atmosphere, meaning this groundwater have been slightly diluted by DIC.

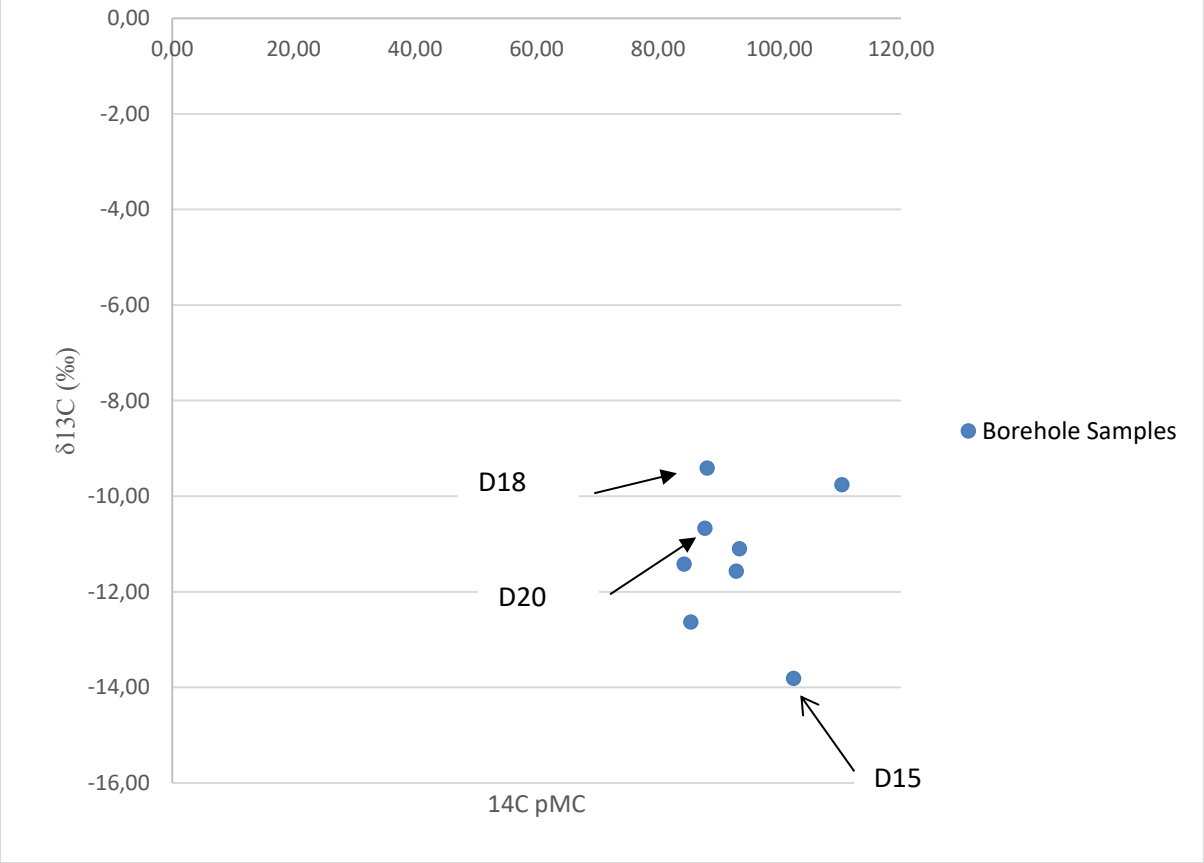


Figure 6.7: A plot of ^{13}C and ^{14}C from the groundwater samples within the HRC.

6 3.3. Characterisation of the Hout River Catchment aquifer

Based on the stable isotopes results, groundwater recharge within the HRC occurred during the humid environments in colder climates, whereby moisture came from a regional source, which could be from the nearest Indian Ocean. The box and whisker plot of rainfall oxygen isotopes based on the three rainfall sampled regions (Figure 6.8). The plot shows that oxygen isotopes from the sampled rain within the central region with smaller range of 3.9‰ is less scattered as compared to those from the southern and northern regions of the catchment. The southern and northern regions have a wide range of stable isotopes with the minimum at -5.12‰ to a maximum of 3.78‰ for southern region and range of -4.43‰ and -5.05‰ in the northern region. The wide range might be due to the shadow effect or the wide distribution of the sampling stations. The data for all the regions falls within the upper quartile (Figure 6.8).

Groundwater recharge responsible for aquifer replenishment is emerging from the north-western, southern and northern part of the catchment. This groundwater seems to be confined within two aquifers that are progressively disconnected towards the south and south-eastern part of the catchment. This is also apparent through the tritium results and ^{14}C distribution map with general trend of decreasing concentrations from the northwest to the south-eastern side of the catchment, which shows less groundwater dilution moving towards southeast (Fig 6.9). The groundwater samples that gave oldest MRT with ^{14}C less than 100 pMC occurred along the eastern, southern and south-eastern part of the catchment (Fig 6.9). This results also suggest compartmentalisation of groundwater. The general trend of groundwater flow seems to be following the structural trends of the neotectonic stress regime which is NW-SE. As such, structures trending NE and ENE could be acting as conduits, thus allowing groundwater to flow.

As groundwater seems to be emerging from the northern, southern and northwest part of the catchment, it shows that groundwater flow in some sections of catchment are in contrast to the surface water flow direction, which is towards the northeast direction. For an example, D16 along the northwest of the catchment has the lowest ^{14}C activity while D18 and D20 located in the headwaters of the catchment have groundwater that recharged more than 1000 years ago. However, these observations might also suggest compartmentalisation of the aquifer. Apart

from recharge during heavy rainfall, groundwater could be recharged from the neighbouring catchments through interconnected fractures which are crosscutting the catchment's boundary. The carbon source is locally derived from the country rocks and C_4 plants within the catchment showing a closed system with limited supply of carbonates.

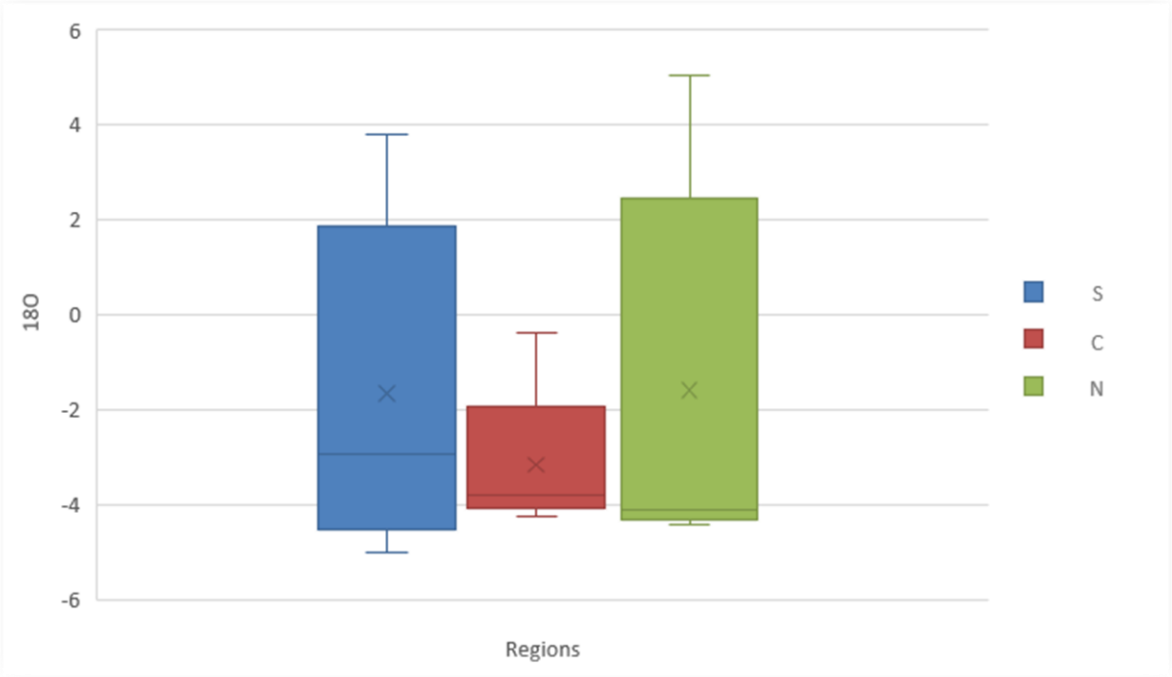


Figure 6.8: Box and Whisker plot of rainfall Oxygen isotopes within the southern (S), central (C) and northern (N) region of the catchment.

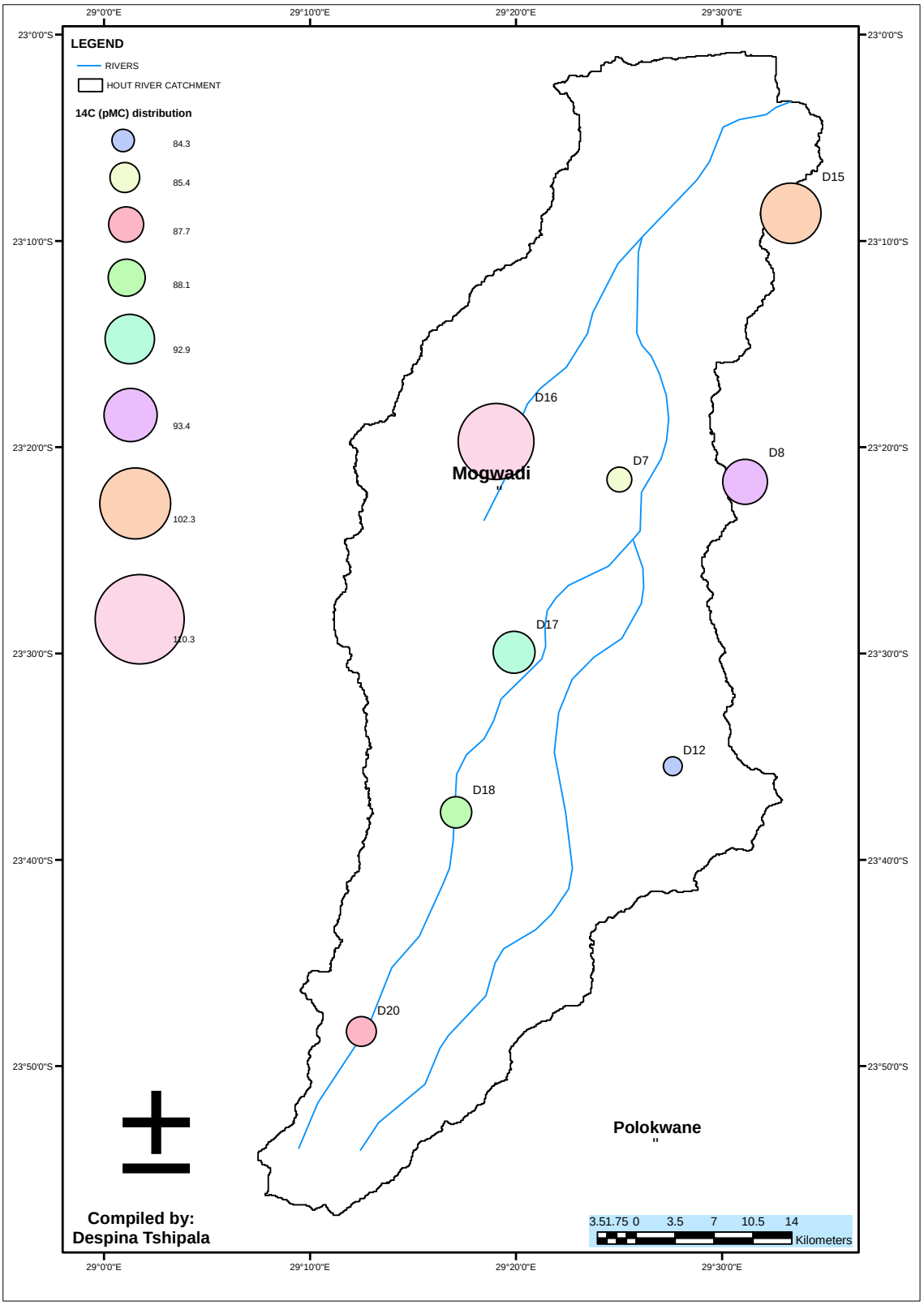


Figure 6.9: ^{14}C concentration distribution within the Hout River Catchment.

6.4. Water balance and recharge

6.4.1. Catchment water balance calculation

Water balance approach is important to estimate water budget of a catchment. For the Hout River Catchment, rainfall, evapotranspiration and estimated groundwater abstraction data for 2015 were obtained. The nature of data which was available, favoured water balance calculation for the year 2015. This involves only recent groundwater abstraction data estimation for the same year, which was obtained from Ebrahim et al. (2016). Rainfall data was obtained from the Mara, Lekgraal and Dendron Rainfall Stations which gave an average annual rainfall of 17.542 mm/year. Although rainfall is the most important component of water balance, it is apparent that in 2015 very minimal rainfall occurred throughout the year. The second most important component of water balance is evapotranspiration and was the highest in January at 166.842 mm/month and lowest in May at 103.563 mm/month. Detailed calculation of crop evapotranspiration is given in Table 6.4 and 6.5. Change in storage has been estimated through mass balance approach and gave a value of -133.78 mm/year. Available groundwater abstractions data were only for annual average estimations, thus for the calculated year, the monthly values were estimated considering the rainfall seasons. The water balance parameters are given in rates unless stated otherwise. Runoff estimation was obtained from Ebrahim et al (2018) and gave an average value of 2.44 mm for the year 2015, which is about 13. 38% of the MAP for that year (Fig 6.6). This result shows minimal amount of runoff which can attributed to the semi-arid conditions whereby out of the little rainfall received, most of it is taken back to the atmosphere and the gentle slope of the catchment favours infiltration as opposed to runoff.

Table 6.4: Reference evapotranspiration calculation of the year 2015 using the FAO-54 Method (Allen et al., 1998).

Year	**2015**											
	January	**February**	**March**	**April**	**May**	**June**	**July**	**August**	**September**	**October**	**November**	**December**
Tmin (°C)	17.13	17.19	15.49	12.65	7.01	2.73	3.12	5.1	10.49	14.01	15.65	19.08
Tmax (°C)	30.25	31.16	30.92	27.76	29.17	24.02	25.51	27.73	27.11	31.89	31.78	33.36
Tmean (°C)	23.69	24.175	23.205	20.205	18.09	13.375	14.315	16.415	18.8	22.95	23.715	26.22
Rs (MJ m-2 d-1)	24.33	22.01	21.16	19.93	15.8	15.53	14.7	18.78	19.24	21.99	20.04	19.33
U2 (m/s)	1.17	0.71	2.54	1.4	0.99	1.66	1.51	1.8	1.16	1.73	1.33	0.93
Δ (kPa ºC-1)	0.137	0.139	0.135	0.122	0.112	0.087	0.092	0.103	0.115	0.134	0.138	0.148
Altitude (m)	890.00	890.00	890.00	890.00	890.00	890.00	890.00	890.00	890.00	890.00	890.00	890.00
P (KPa)	91.213	91.213	91.213	91.213	91.213	91.213	91.213	91.213	91.213	91.213	91.213	91.213
Y (kPa °C-1)	0.061	0.061	0.061	0.061	0.061	0.061	0.061	0.061	0.061	0.061	0.061	0.061
Δ/(Δ+Y)(1+0.34U2)	0.618	0.649	0.545	0.576	0.579	0.479	0.501	0.514	0.577	0.582	0.610	0.649
Y/(Δ+Y)(1+0.34U2)	0.428	0.376	0.577	0.491	0.470	0.642	0.600	0.596	0.481	0.494	0.444	0.383
TT	3.549	2.150	7.718	4.297	3.061	5.217	4.730	5.597	3.578	5.261	4.034	2.797

es (kPa)	2.467	2.512	2.422	2.136	1.928	1.460	1.553	1.763	2.000	2.398	2.470	2.703
RHmax (%)	91	81.18	76.37	85.39	91.83	92.31	84.76	75.68	89.69	92.39	90.64	80.3
RHmin (%)	23.66	18.03	37.27	32.3	25.1	36.83	26.86	39.22	28.89	44.18	26.44	21.89
e(Tmin) (kPa)	1.931	1.937	1.757	1.451	0.823	0.326	0.372	0.603	1.214	1.599	1.774	2.134
e(Tmax) (kPa)	3.242	3.328	3.305	3.003	3.139	2.636	2.783	3.000	2.940	3.397	3.387	3.534
ea (kPa)	1.262	1.086	1.287	1.105	0.772	0.636	0.531	0.817	0.969	1.489	1.252	1.244
dr	1.000	1.000	1.000	1.000	1.000	1.000	1.000	1.000	1.000	1.000	1.000	1.000
δ	-0.401	-0.295	-0.130	0.085	0.272	0.390	0.401	0.303	0.121	-0.088	-0.279	-0.391
ϕ (rad)	-0.403	-0.403	-0.403	-0.403	-0.403	-0.403	-0.403	-0.403	-0.403	-0.403	-0.403	-0.403
ωs	1.744	1.701	1.627	1.534	1.452	1.403	1.389	1.437	1.519	1.608	1.693	1.747
Gsc (MJ m-2 min-1)	0.082	0.082	0.082	0.082	0.082	0.082	0.082	0.082	0.082	0.082	0.082	0.082
sinϕsinδ	0.153	0.114	0.051	-0.033	-0.105	-0.149	-0.153	-0.117	-0.047	0.035	0.108	0.149
cosϕcosδ	0.847	0.880	0.912	0.916	0.886	0.851	0.847	0.878	0.913	0.916	0.884	0.850
Ra (MJ m-2 day-1)	41.423	40.119	37.360	32.511	27.329	23.678	23.323	26.397	31.595	36.523	39.890	41.307
Rso (MJ m-2 day-1)	31.805	30.803	28.685	24.962	20.983	18.180	17.907	20.267	24.259	28.042	30.627	31.715

Rns (MJ m-2 day-1)	18.734	16.948	16.293	15.346	12.166	11.958	11.319	14.461	14.815	16.932	15.431	14.884
α (MJ K-4 m-2 day-1)	0.000	0.000	0.000	0.000	0.000	0.000	0.000	0.000	0.000	0.000	0.000	0.000
0.34-0.14√ea	0.183	0.194	0.181	0.193	0.217	0.228	0.238	0.213	0.202	0.169	0.183	0.184
1.35Rs/Rso-0.35	0.683	0.615	0.646	0.728	0.667	0.803	0.758	0.901	0.721	0.709	0.533	0.473
Rnl	4.764	4.587	4.444	5.118	5.147	6.113	6.096	6.692	5.216	4.544	3.741	3.436
Rn	13.970	12.361	11.849	10.228	7.019	5.846	5.223	7.769	9.599	12.389	11.690	11.448
Rng	5.700	5.043	4.834	4.173	2.864	2.385	2.131	3.170	3.916	5.055	4.769	4.671
ETrad	3.525	3.275	2.634	2.405	1.659	1.142	1.068	1.628	2.258	2.943	2.907	3.034
Etwind	1.830	1.154	5.051	2.174	1.665	2.759	2.902	3.158	1.774	2.363	2.184	1.562
Eto (mm/day)	5.355	4.429	7.686	4.579	3.324	3.901	3.970	4.787	4.032	5.306	5.091	4.596
Eto (mm/month)	166.012	124.014	238.255	137.383	103.048	117.028	123.073	148.389	120.966	159.179	152.741	142.471
Eto (mm/year)	12.032											

Table 6.5: Monthly crop evapotranspiration of the year 2015.

		Jan	Feb	March	April	May	June	July	Aug	Sept	Oct	Nov	Dec
Eto (mm/month)		166.01	124.01	238.26	137.38	103.05	117.03	123.07	148.39	120.97	159.18	152.74	142.47
	Kc	**Etc**											
Cultivated Land	1	166.01	124.01	238.26	137.38	103.05	117.03	123.07	148.39	120.97	159.18	152.74	142.47
Water Bodies	1.27	210.83	157.50	302.58	174.48	130.87	148.63	156.30	188.45	153.63	202.16	193.98	180.94
Plantation	1	166.01	124.01	238.26	137.38	103.05	117.03	123.07	148.39	120.97	159.18	152.74	142.47
grasslands	0.75	124.51	93.01	178.69	103.04	77.29	87.77	92.30	111.29	90.72	119.38	114.56	106.85
Average Etc (mm/month)		166.84	124.63	239.45	138.07	103.56	117.61	123.69	149.13	121.57	159.98	153.51	143.18

Table 6.6: Catchment water balance for the year 2015.

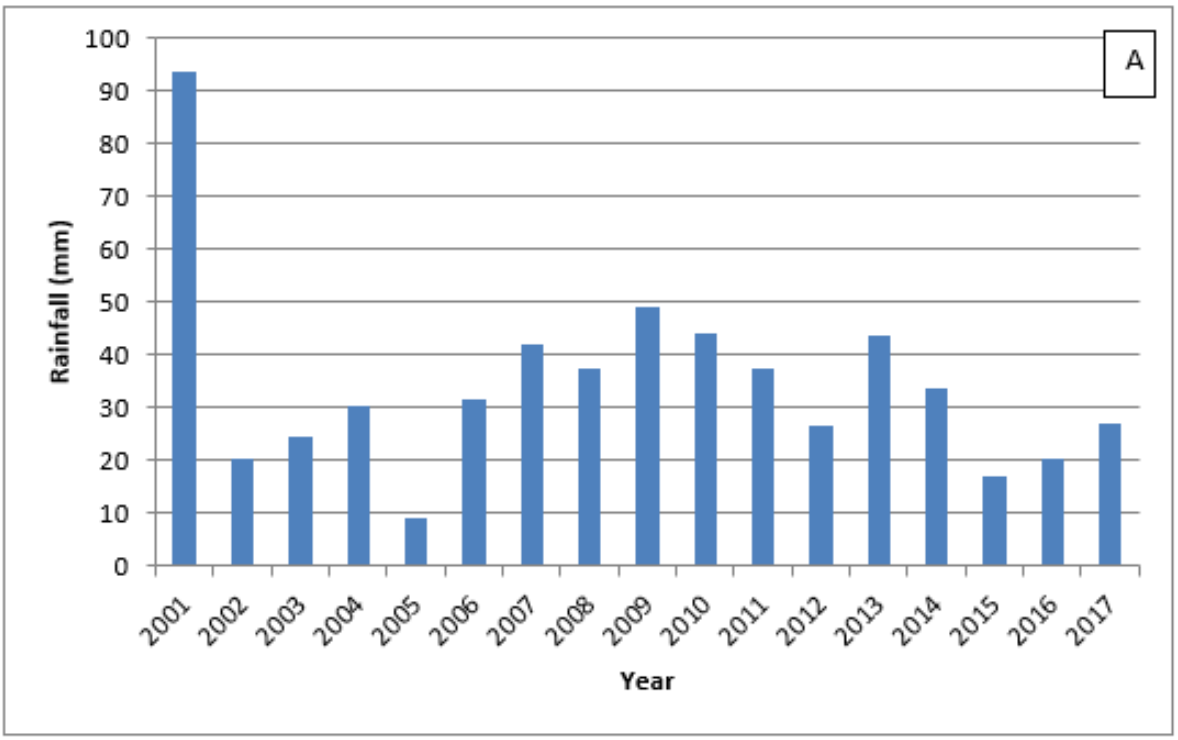
Surface water catchment area (km^2)	**Pi(mm/a)**	**Etc (mm/a)**	**Wg (Mm^3)/a**	**Runoff (mm/a)**	**Change in storage (mm/year)**
2451	18,24	145.10	1,83	2,44	-133,78

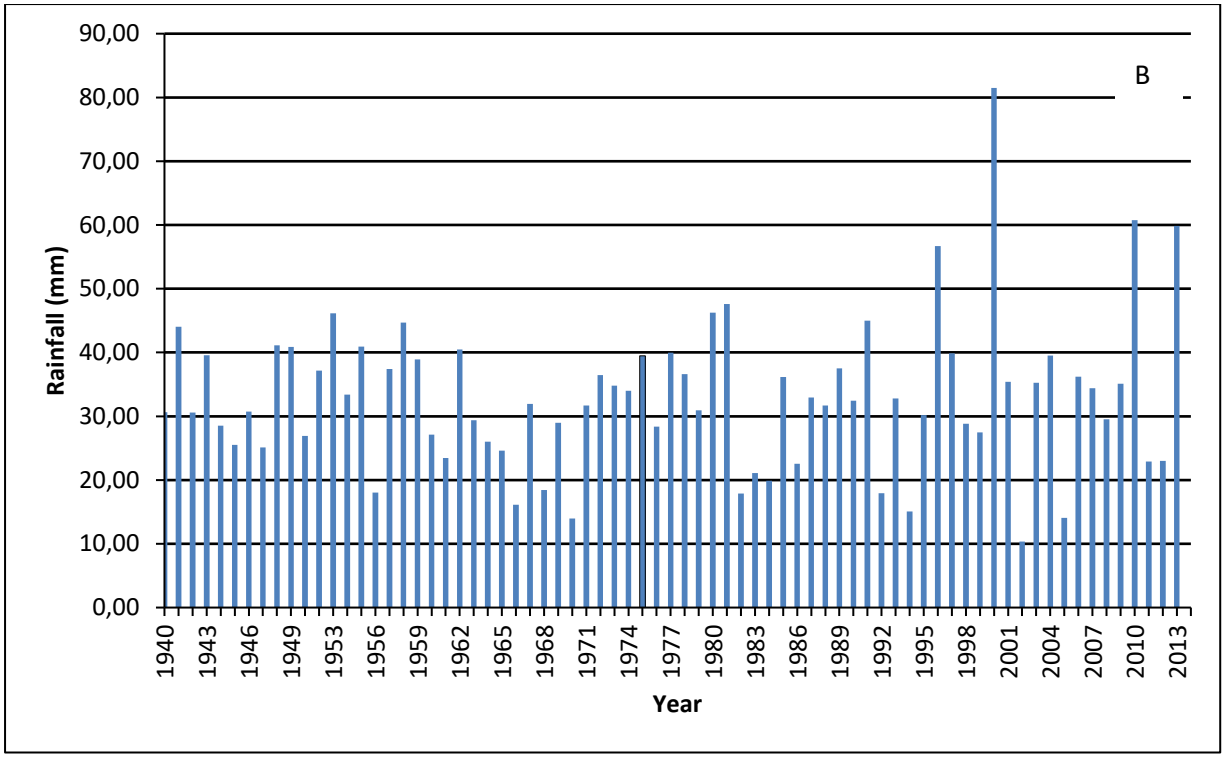
Pi= Precipitation, Etc=Actual Crop Precipitation, Wg=Groundwater abstraction, Runoff= Estimated runoff from the PRMS method (Ebrahim et al., 2018).

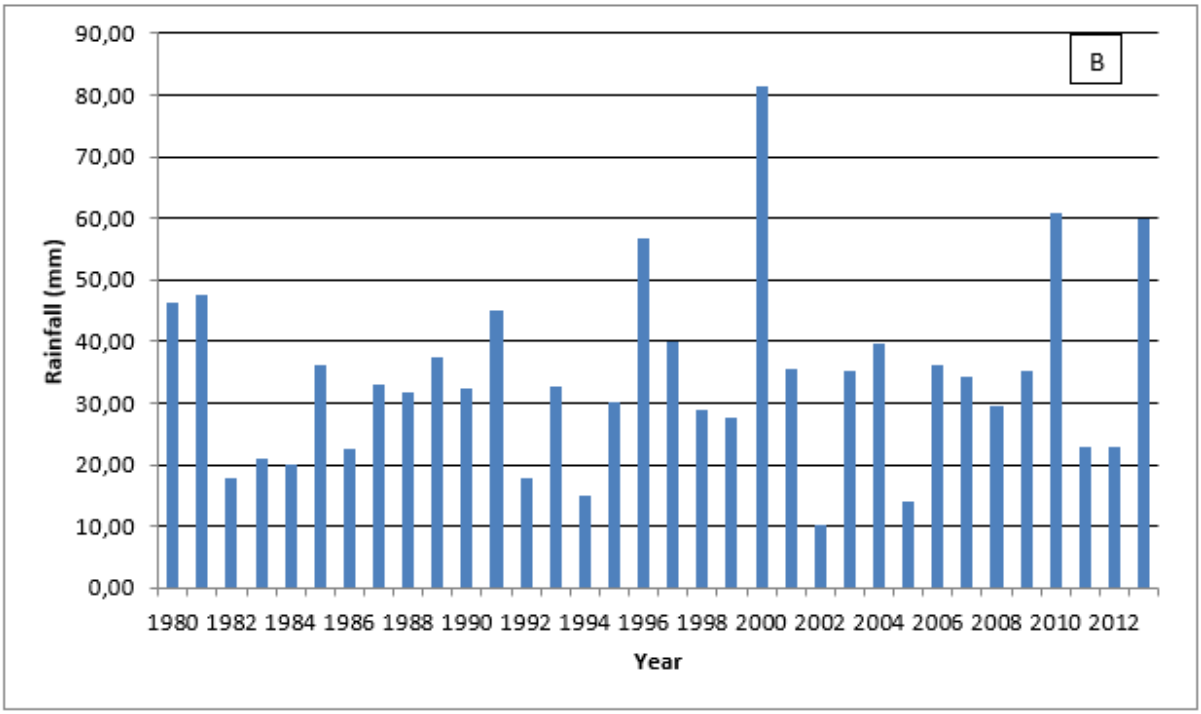
6.4.2. Water Table Fluctuation (WTF)

6.4.2.1. Rainfall trends

Using the WTF method to estimate recharge requires the knowledge of rainfall, groundwater data and specific yield of lithology where boreholes are located. There are several rainfall stations within the catchment and data from these stations were plotted to determine the trends of rainfall over the years within the catchment. From the Mogwadi Rainfall Station, highest rainfall record was in 2012 at 352.04 mm/year and lowest rainfall between 2014 and 2015 (Fig 6.10a). The Lekgraal Rainfall Station has the longest rainfall data with highest rainfall in the year 2000 at 81 mm/year (Fig 6.10b). Mara PP Rainfall Station recorded highest rainfall in 1958 at 215 mm, with the other years being less than 50 mm records (Fig 6.10c).




B
Rainfall (mm)
90,00
80,00
70,00
60,00
50,00
40,00
30,00
20,00
10,00
0,00
1940
1943
1946
1949
1953
1956
1959
1962
1965
1968
1971
1974
1977
1980
1983
1986
1989
1992
1995
1998
2001
2004
2007
2010
2013
Year


B
Rainfall (mm)
90,00
80,00
70,00
60,00
50,00
40,00
30,00
20,00
10,00
0,00
1980 1982 1984 1986 1988 1990 1992 1994 1996 1998 2000 2002 2004 2006 2008 2010 2012
Year

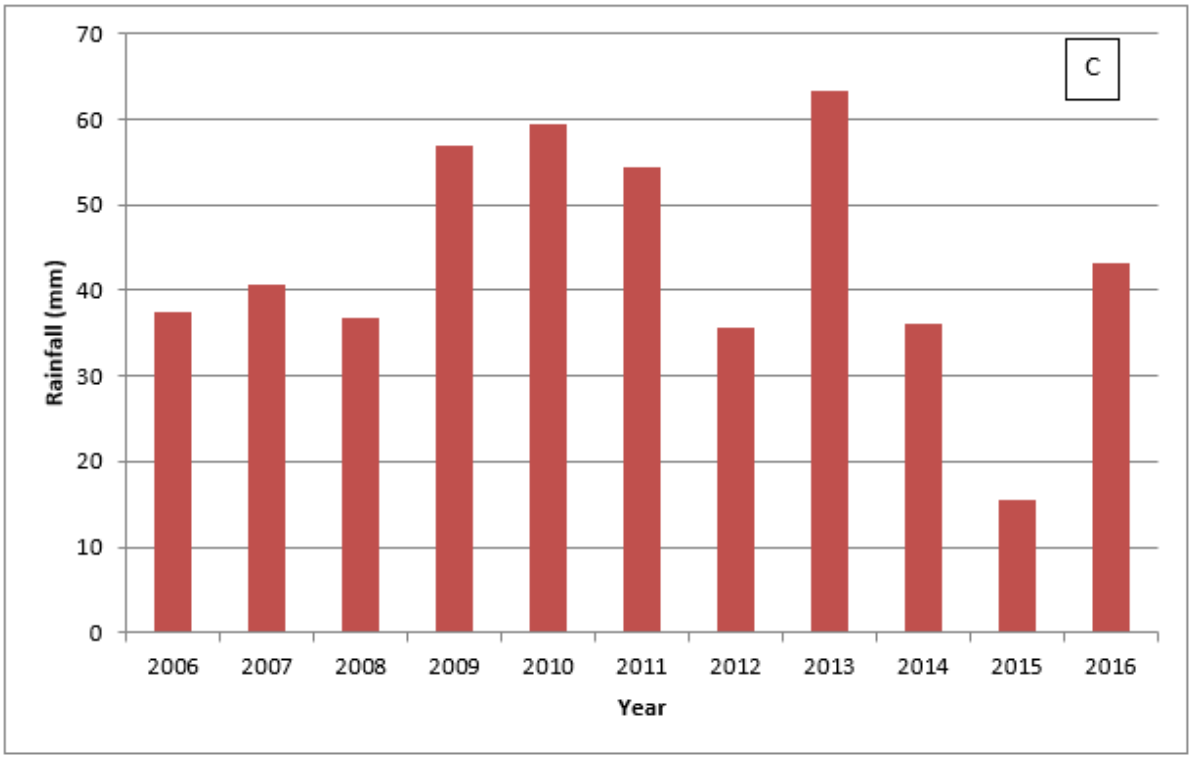


Figure 6.10: A) Rainfall pattern from 2005 to 2016 from the Mogwadi Rainfall Station. B) Rainfall pattern from 1940 to 2013 from the Lekgraal Rainfall Station. C) Rainfall pattern from the Mara PP Rainfall Station.

6.4.2.2. Groundwater levels response to rainfall events

Two groundwater hydrographs for boreholes A7N0641 and A7N0635 were plotted with rainfall data from the closest rainfall station to understand groundwater levels response to rainfall events (Fig 6.11a and b). For the two boreholes, it is apparent that the correlated rainfall data are almost completely not recharging the area for the years analysed. Most rainfall events, for example 2008 to 2009, rainfall amount increased but groundwater levels decreased in borehole A7N0641 (Table 6.7). Similarly, in the borehole A7N0661, groundwater levels seem to have increased with increasing annual rainfall. However, in the borehole A7N0635 groundwater levels increased from 2009 to 2010 when the correlated annual rainfall decreased. Based on the lack of correlation between groundwater levels and local annual rainfall,

boreholes are possibly not influenced by the recorded rainfall or responding to lateral recharge through lateral flow of groundwater since there is no reported artificial recharge in the area.

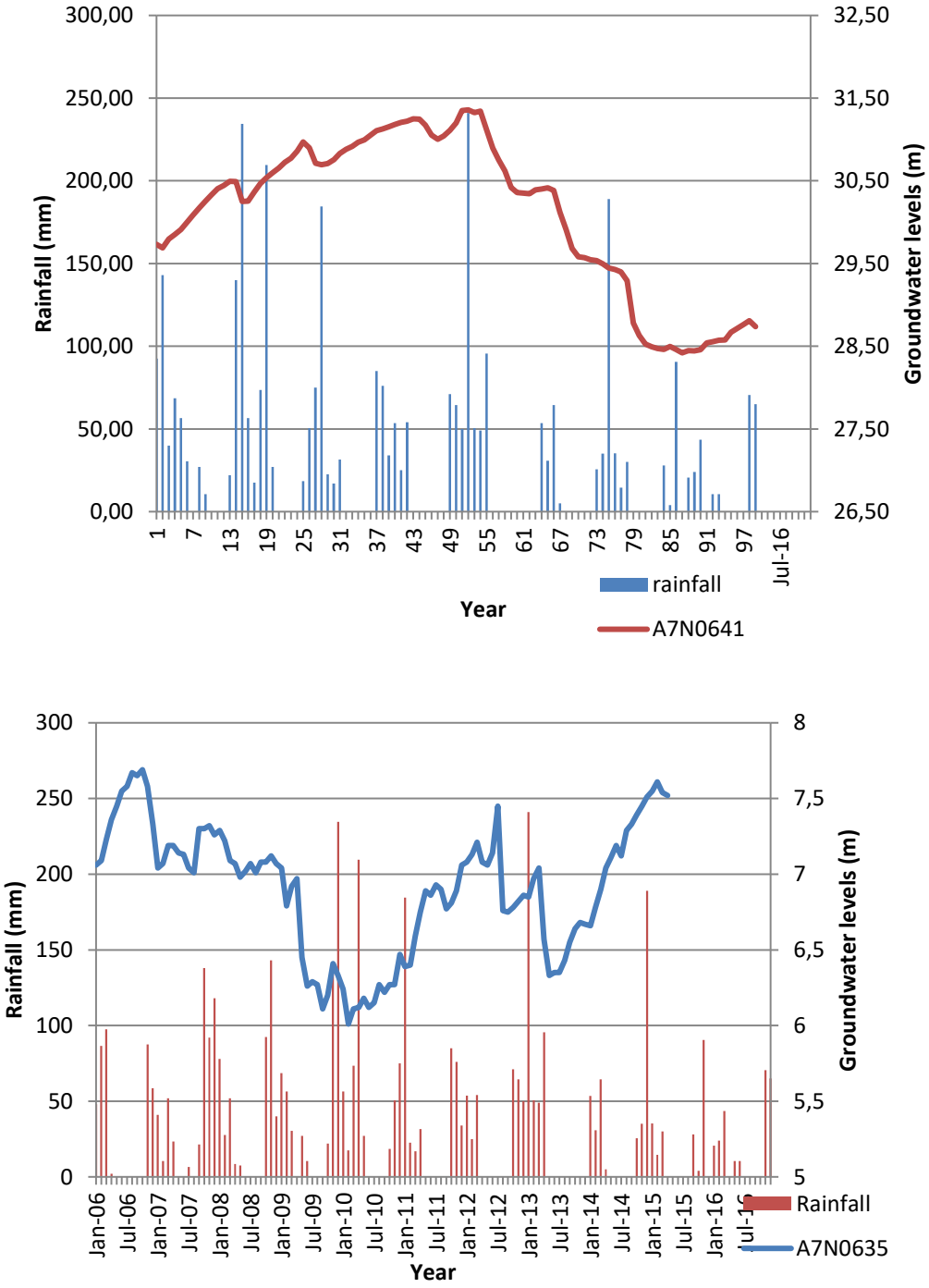


Figure 6.11**:** A) Hydrograph of averaged groundwater levels from the borehole (A7N0641) from 2008 to 2016 and rainfall record from the Mogwadi rainfall station. B) Hydrograph of

averaged groundwater levels from the borehole (A7N0635) from 2006 to 2016 and rainfall record from the Mogwadi rainfall station (data source: SAWS).

6.4.2.3. Groundwater recharge and abstractions rates

WTF method is one of the most reliable recharge estimation methods because it considers aquifer properties. As such, groundwater recharge estimation in this regard involved the use of five boreholes located within gneiss, dolerite and the soil profile to see the influence of different specific yields of these rocks. Borehole intersecting gneiss of specific yield of 0.02 gave groundwater recharge of 1.82 mm/year, which is 5.42% of the Mean Annual Precipitation (MAP) (Table 6.7). Previous recharge estimation within the study area, used the simple rainfall model calculations provided by DWAF (1990) which gave recharge rates similar to the values obtained in this study, which is in the range of 1.76-17.82 mm/year (Mandiwana, 2004) and Masiyandima et al. (2002) found a range between 3-5% of MAP using the same model. This further shows that the catchment is receiving minimal rainwater as recharge. For a period of 9 years, only 4.81 mm of recharge occurred through gneiss lithology, showing very insignificant recharge of the aquifer for a longer time. Moreover, tritium and ^{14}C dating of groundwater closer to this borehole (D12) shows that MRT of 1411.91 years, hence indicating that is old groundwater. Recharge rates through dolerite with specific yield of 0.01 was at 33 mm/year in 2013 and previous investigation of hydraulic properties of the rocks within the Limpopo Plateau has shown that mafic rocks have transmissivity of 20 m^2/d (Holland, 2011). For the soil profile, highest recharge occurred in 2010 at 17.33 mm/year (Table 6.7). These results show wide variation of the recharge due to different aquifer properties for different rocks within the aquifer. There is no correlation between groundwater recharge rates and local rainfall which shows little to insignificant influence of rainfall on recharge (Fig 6.12).

Comparing abstractions rates for the analysed years with highest recharge shows that groundwater abstractions are higher than groundwater replenishment of the aquifer. Estimated average groundwater from 2007 to 2015 was in the range of 27.501 to 30.034 million cubic meters with detailed abstractions provided in Appendix C. The outcomes clearly show that groundwater abstractions far exceed recharge which has been recorder for the past few decades, thus clearly showing groundwater loss from the aquifer. Around the Mogwadi area, production

boreholes yield a range of 10000 to 25000 l/hour which also shows high amount of groundwater abstractions from the aquifer.

Table 6.7: Recharge and discharge estimating from boreholes located within gneiss, dolerite, soil and granite rocks in the Hout River catchment.

Sample ID	Year	Precipitation (mm)	Mean SWL (m)	Mean ΔH (m)	Lithology	Specific yield (Sy)	Recharge or discharge (mm/year)	R or D(%P)
A7N0641	2008	37.40	30.06	-0.06	gneiss	0.02	-1.27	-3.41
	2009	49.10	30.59	-0.03	gneiss	0.02	-0.61	-1.24
	2010	44.00	30.82	-0.01	gneiss	0.02	-0.21	-0.49
	2011	37.50	31.14	-0.01	gneiss	0.02	-0.14	-0.38
	2012	26.50	31.18	-0.04	gneiss	0.02	-0.76	-2.87
	2013	43.60	30.62	0.08	gneiss	0.02	1.60	3.67
	2014	33.60	29.67	0.09	gneiss	0.02	1.82	5.42
	2015	16.90	28.58	0.07	gneiss	0.02	1.39	8.22
	2016	20.40	28.64	-0.03	gneiss	0.02	-0.54	-2.67
A7N0661	2013	43.60	12.28	3.30	dolerite	0.01	33.00	75.69
	2014	33.63	8.98	1.29	dolerite	0.01	12.90	38.36
	2015	16.87	7.69	-1.82	dolerite	0.01	-18.20	-107.91
A7N0635	2006	31.67	7.14	-0.01	soil	0.26	-2.652	-8.37
	2007	41.91	7.44	0	soil	0.26	0.43	1.03
	2008	37.43	7.17	-0.02	soil	0.26	-5.42	-14.47
	2009	49.13	7.09	0.02	soil	0.26	5.42	11.03
	2010	44	6.5	0.07	soil	0.26	17.33	39.39
	2011	37.54	6.2	-0.01	soil	0.26	-3.25	-8.66
	2012	42.13	6.69	-0.07	soil	0.26	-13.99	-33.21

	2013	39.64	6.98	-0.02	soil	0.26	-5.85	-14.76
	2014	33.63	6.96	0.04	soil	0.26	10.7	31.83
	2015	16.87	6.58	-0.04	soil	0.26	-10.18	-60.38
	2016	20.38	7.34	-0.03	soil	0.26	-6.59	-32.33

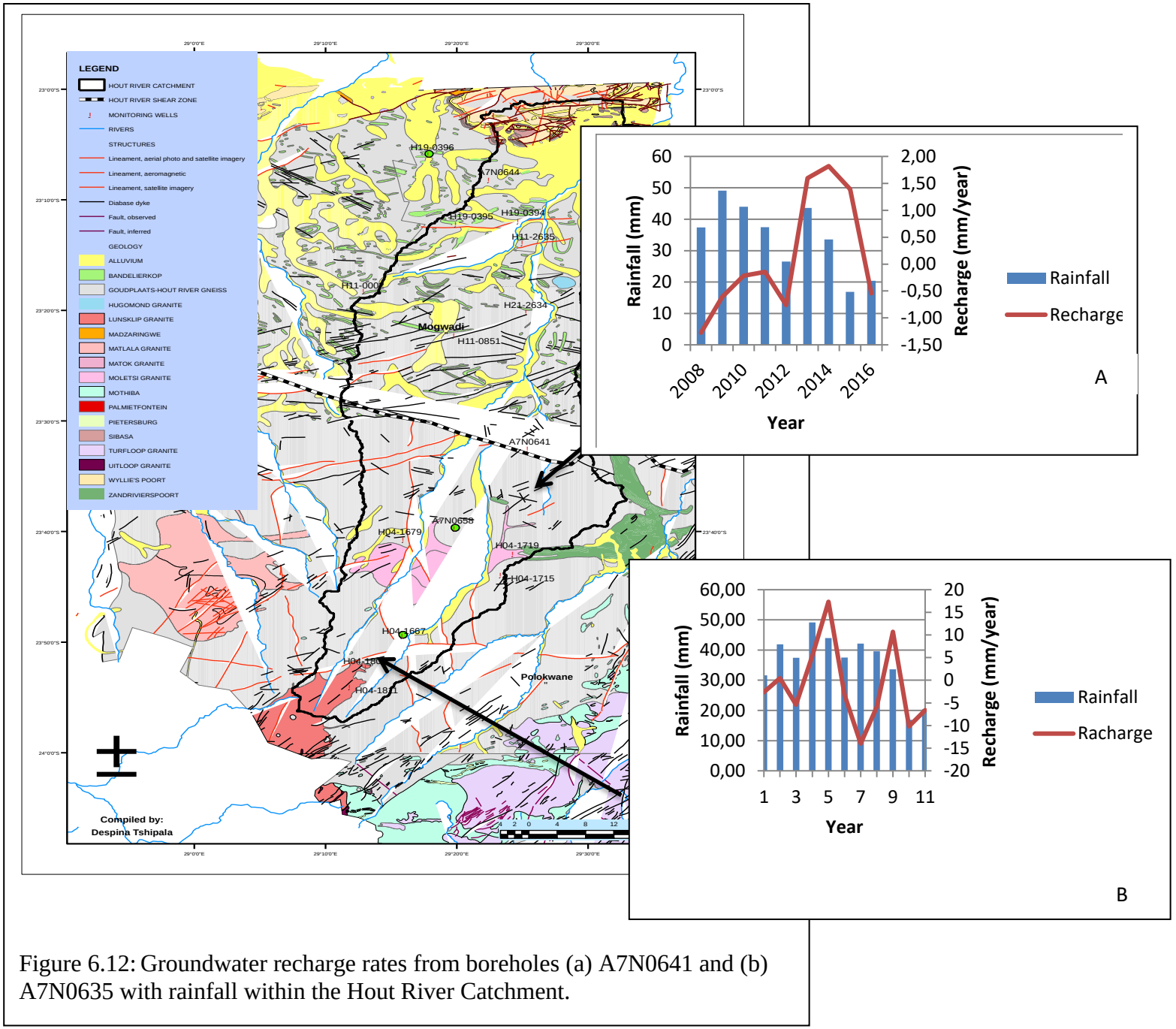


Figure 6.12: Groundwater recharge rates from boreholes (a) A7N0641 and (b) A7N0635 with rainfall within the Hout River Catchment.

6.5. Conceptual modelling of the Hout River Catchment aquifer

Conceptual model of the Hout River Catchment was computed using geological, structural, hydrogeological and hydro-chemical data collected during the research. The boundary of the study area was computed from the Hout River Catchment demarcation boundary. The Hydrostratigraphic units were constructed based on the water table deduced from the groundwater levels from the GRIP and NGA data, storage coefficients from Jolly (1986), averaged transmissivity values from Holland (2011) and lithology data obtained from the Council of Geosciences. A cross-section, which stretches from southwest towards the northeast is drawn on the surface map (Fig 6.13). A total of 12 observation boreholes were used for elevation and different lithology along the section; detailed data of the observation boreholes used for conceptual model are given in Appendix D and E.

Boreholes of different lithology and hydraulic properties were used to construct Hydrostratigraphic units (Fig 6.14). The aquifer system of the Hout River Catchment can be divided into two aquifers which occur within the weathered and fractured Goudplaats- Hout River Gneiss. The upper aquifer is unconfined and highly weathered with water table ranging from 6 m.b.g.l to 30 m.b.g.l. The interface of the weathered and fractured aquifer within the HRC were delineated based on the weathering and degree of fracturing records in the lithology data form National Groundwater Archives (Appendix E). Holland (2011) recorded transmissivities of granite at 21 m^2/day, gneiss at 31 m^2/day, dolerite dykes at 20 m^2/day and gneiss at 31 m^2/day, which were used to understand the hydraulic properties of the aquifer. Dolerite dykes are truncating the country rocks throughout the catchment.

All the components used for conceptual modelling in this study area given bellow. A conceptual representation of the HRC is given in Fig (7.15).

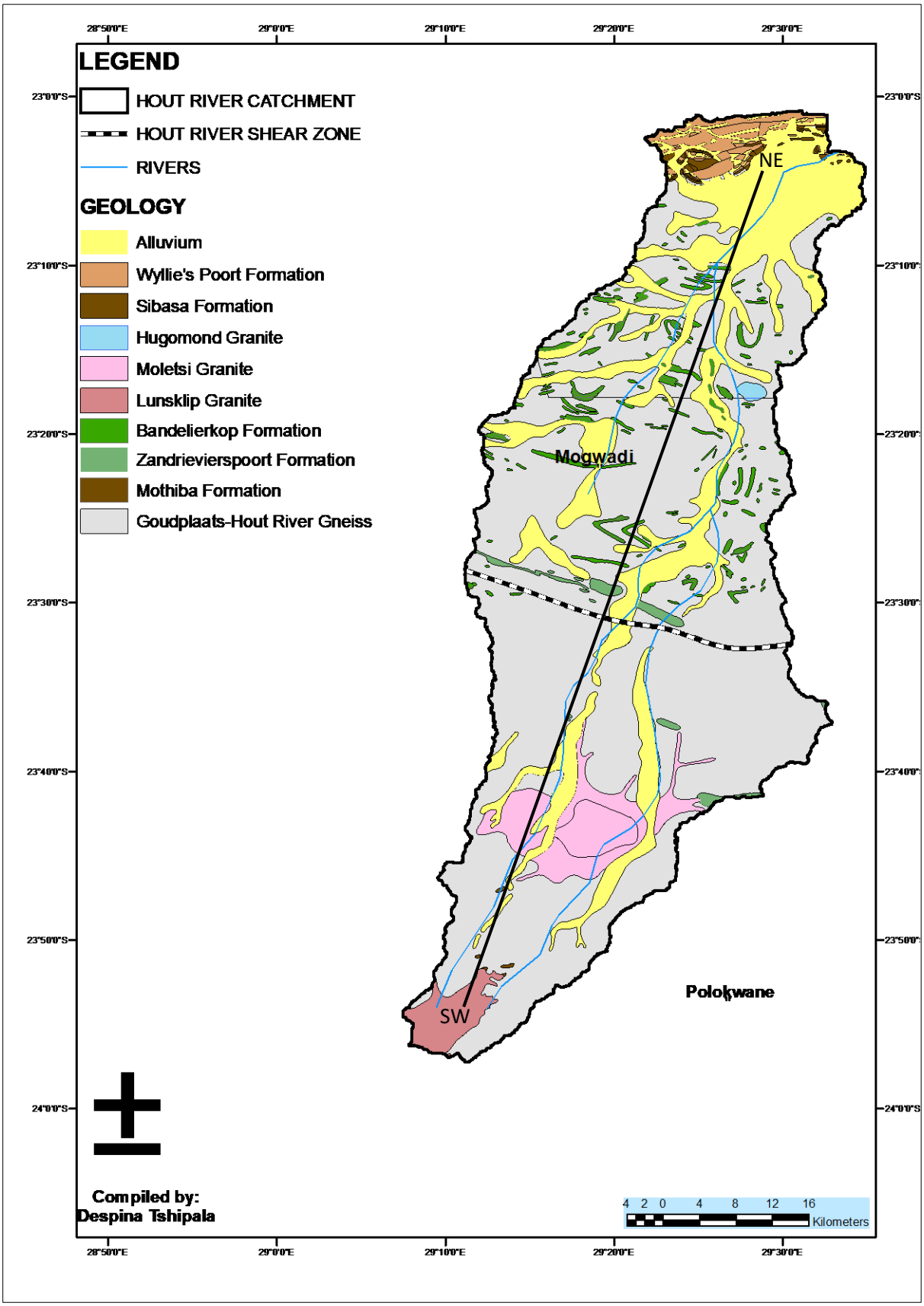


Figure 6.13: Surface delineation of the area within the catchment used for cross-section construction.

6.5.1 Structural control on groundwater flow patterns

Groundwater level analyses in the study area have shown that boreholes with shallower groundwater elevations are related to high magnetic anomalies in the aeromagnetic map coinciding with granite batholiths, Soutpansberg rocks and high dense structure concentrations like the HRSZ in the structural map as compared to areas with less structural concentrations and low magnetic anomalies. These areas have groundwater levels of less than 15 m.b.g.l. Boreholes with deeper groundwater levels seems to coincide with areas showing low magnetic anomalies. It is apparent from the structural and geophysical maps that major structural direction trends are NE-SW and less towards NW-SE, which coincide with what was previously described by Holland (2011).

6.5.2 Groundwater quality characterisation

The groundwater quality analyses based on parameters considered for this study is limited in characterising groundwater quality although still useful for understanding current state of groundwater compared to previous investigation within the catchment. Groundwater within the catchment are still palatable; however, areas showing mineralised groundwater with considerable number of dissolved solids occur in boreholes D1-D7 in the Wimpie Farm in the Mogwadi area and Mara towards the northern part of the catchment. Groundwater mineralisation with TDS ranging between 1000 and 1200 mg/l and EC also in the range of 1000 and 1400 µS/cm in the Mogwadi area is ascribed to agricultural activities and/or long-term circulation within the aquifer. In contrast, groundwater around the southern part of the catchment shows less than 300 mg/l of TDS and approximately 400 Sµ/cm of EC from borehole (D20) located within the Goudplaats-Hout Gneiss which is between the Moletsi and Luinsklip Batholiths. The results might suggest interaction with meteoric water or less weathered nature part of the aquifer. This part of the catchment is also not dominated by agricultural activities as compared to the area around the Mogwadi area. The land is used for settlements and sporadic subsidence farming. The groundwater mineralisation increases further north, whereby along the HRSZ, TDS is about 600 mg/l and EC greater than 1000 µS/cm (Fig 7.15).

6.5.3 Groundwater recharge rates and mean residence time

Tritium dating of groundwater showed that recent groundwater that recharged the aquifer after 1952 occurs along the north-western part of the catchment with ^{14}C activity above 100 pMC. Mean residence time increases towards the south-eastern part of the catchment with reduced ^{14}C activity of less than 90 pMC around the Mogwadi area, which is indicative of old groundwater greater than 1000 years mean residence time (Fig 6.15). Although it is the headwater of the surface drainage, the south-western part of the catchment gave ^{14}C activity of less than 90 pMC indicating occurrence of old groundwater. These outcomes might suggest sampled borehole tapping the lower confined aquifer with no recent recharge. However, physico-chemical analyses of the same sample showed minimal mineralisation and dissolved solids as compared to other groundwater samples within the study area, which might suggest mixture of old and younger groundwater or even much resistance of the country rocks. The rainfall data obtained records of less than 150 mm/year across the catchment.

Based on the radiogenic isotope results, recharge sources seem to emerge from the northern and southern part of the catchment part. Personal communication with farmers in the catchment showed that, groundwater levels seems to rise on boreholes proximal to river channels as compared to those distal. Highest recharge rate is associated with borehole in dolerite rocks suggesting high hydraulic conductivity. This might be influenced by high degree of weathering and fracturing. Holland (2011) showed that, pumping test analyses of boreholes that encountered dolerite dykes generally show low borehole yields as compared to those without. Boreholes located in alluvium/soil also shows higher recharge rates of 17 mm/year, which is influenced by higher hydraulic conductivity.

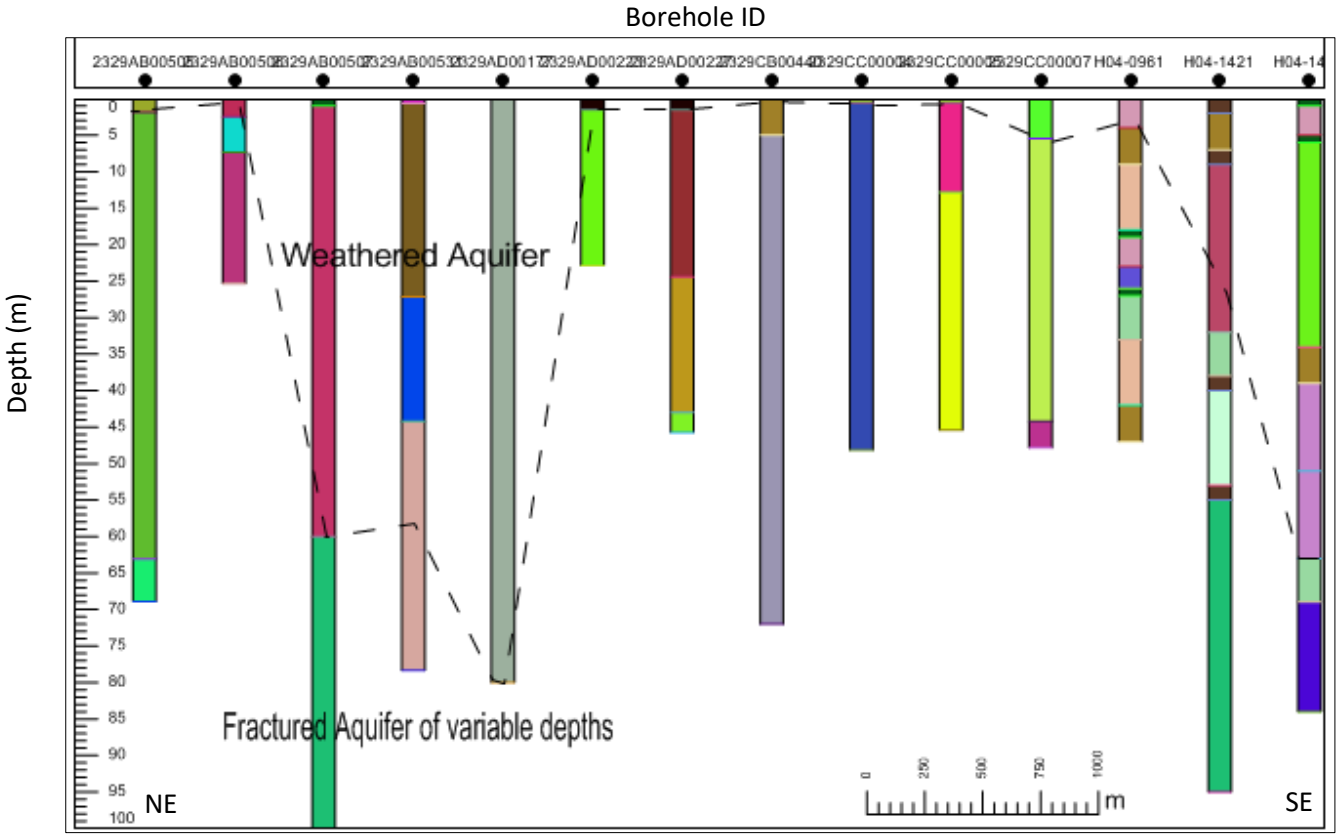


Figure 6.14: Hydrostratigraphic units of the HRC.

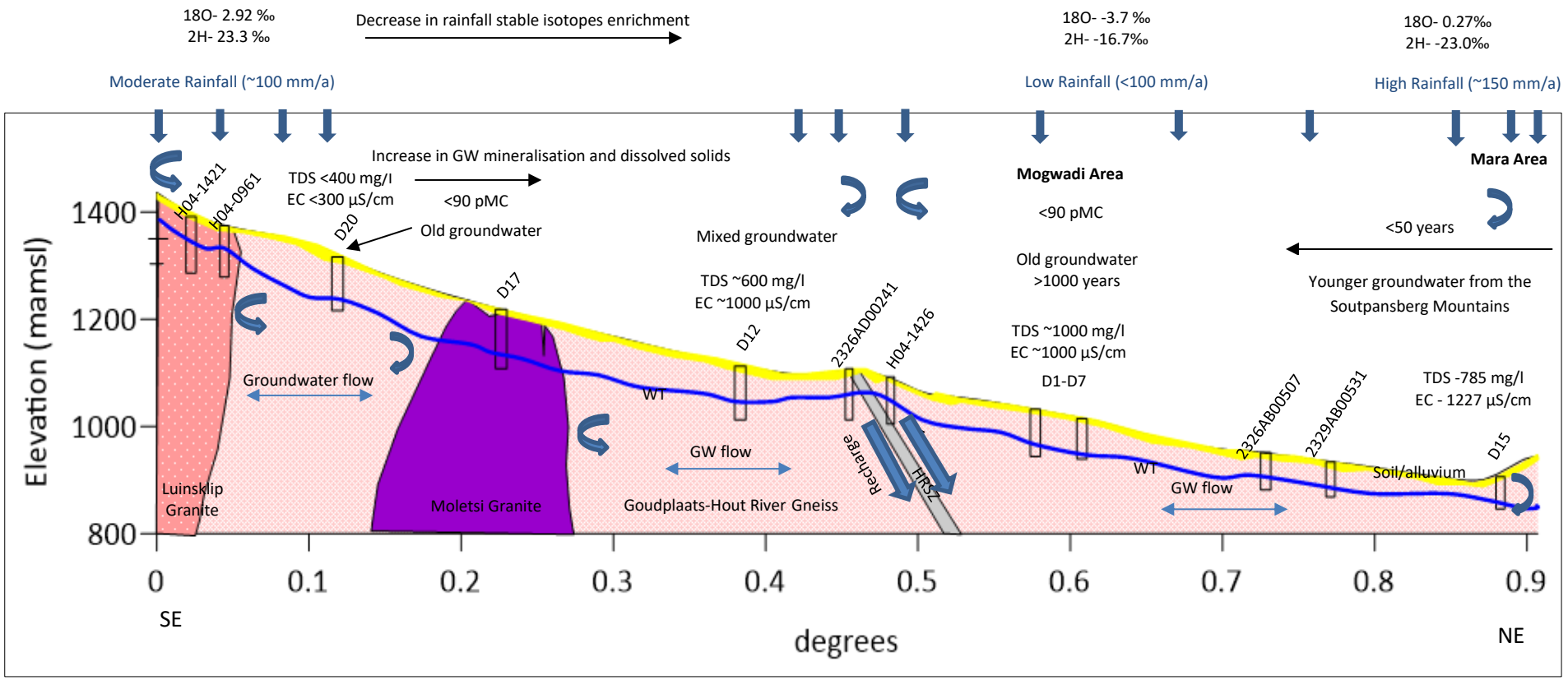


Figure 6.15: Conceptual model of the Hout River Catchment (groundwater age was determined from the tritium and C-14 results).

CHAPTER 7 : CONCLUSION AND RECOMMENDATIONS

The hydrogeological system in the Hout River catchment was conceptualised using structural and aeromagnetic data, hydrochemical data, environmental isotopes to understand the sources of recharge, quantify the amount of recharge within the aquifer and the groundwater quality. The dominant structural directions as was observed in the aeromagnetic and structural maps are in the NE and NW directions. Some of these structures are magnetic with high magnetic anomalies and some without. It is also worth mentioning that dykes and lineaments are also crosscutting the demarcation of the watershed, suggesting that groundwater could also be flowing from the neighbouring catchments through regional dykes that are fractured. Stable isotope shows that the catchment is receiving rainfall from a regional moisture source with average low deuterium excess value. The climatic data showed that mean annual rainfall has been low for many years and evapotranspiration remaining high, which resulted into low runoff and recharge. Recharge that replenished the aquifer occurred during humid conditions. After recharge, groundwater is stored in compartments forming variable sections of groundwater with short and long mean residence time. The short residence time coincide with recharge areas along the Soutpansberg Mountains. This groundwater seems to represent upper aquifer with low EC and TDS. Tritium analyses for the spring gave MRT of about 4 years. The spring water represents the upper aquifer along the northern part of the catchment. In contrast, radiocarbon dating shows that groundwater around the Mogwadi, south-eastern and southern part of the catchment recharged more than 1000 years ago. However, EC and TDS from samples in the southwestern part of the catchment shows a character of meteoric water, suggesting a possible mixing of the meteoric water with old groundwater by rainfall or less weathered conditions.

The general trend of groundwater based on the groundwater contour maps and environmental isotopes indicate that groundwater is moving from north, southwestern and north-western part of the catchment towards the southern and south-eastern part of the catchment. This groundwater flow has variable patterns with high groundwater levels associated with positive magnetic anomaly areas and moving towards areas of lower magnetic signatures. These negative magnetic anomaly areas in turn formed pockets where groundwater reside for longer periods and shows carbon-14 activity of less than 90 pMC, which suggest old groundwater.

Based on the transmissivity, environmental isotopes, groundwater levels there are two aquifers with the upper aquifer being connected along the northern part of the catchment and disconnected along the southeastern part. The lower aquifer shows no dilution by atmospheric carbon and increased dissolved solids, although groundwater samples along the southwestern part of the catchment show less dissolved solids and mineralisation. The upper aquifer shows dilution of the radiocarbon and considerable amount of tritium values, which is indicative of thermonuclear recharge. Increased TDS and EC are higher in areas of deeply weathered and fractured bedrock. The main aquifer in the catchment is the highly weathered and fractured Hout River gneiss.

The recommendations which could be an extension of this study may include:

- Tritium analyses for both rainfall and groundwater samples could be carried out for continuous years to see changes and short-term recharge variations occurring within the aquifer.
- There is also a need for consistent measurements of groundwater abstractions, surface storage and runoff in order to have water balance variables closely representing the actual field processes.
- There is a need for additional sampling of radiocarbon in groundwater such that the entire catchment is well represented since structural variations have compartmentalised the aquifer.
- There is also a need for long term and continuous measurements of groundwater levels and physicochemical parameters to understand how climate change is affecting groundwater in this catchment.
- Detailed geochemical analyses of groundwater need to be carried out in order to understand the quality of groundwater and its evolution over the years.

REFERENCES

Abiye, T., (2016). Synthesis on groundwater recharge in Southern Africa: A supporting tool for groundwater users. Groundwater for Sustainable Development, **2**, 182-189.

Acworth, R. I., (1987). The development of crystalline basement aquifers in a tropical environment. *Quarterly Journal of Engineering Geology*, **20**, 265-272.

Allen, R.G., Pereira, L. S., Raes, D., and Smith, M., (1998). Crop Evapotranspiration: Guidelines for computing crop water requirements. Irrigation and Drainage Paper No. 56. Rome: Food and Agriculture Organization of the United Nations. 326.

Anderson, M. P, Woessner, W. W., (1992). Applied groundwater modelling – Simulation of flow and advective transport. Academic Press Inc., San Dieago. 381.

Anhaeusser, C. R., (1992). Structures in granitoid gneisses and associated migmatites close to the boundary of the Limpopo Belt, *South Africa. Precambrian Res*, **55**, 81-92.

Balasubramanian, A., (2007). Methods of Groundwater Exploration.

Barker, O. B., Brandl G., Callaghan C. C., Eriksson P.G. and Van Neut., (2006). The Soutpansberg and Waterberg Groups and the Blouberg Formation. In: Johnson, M. R., Anhaeusser, C. R and Thomas R. J. (Eds.). The Geology of South Africa, *Geological Society of South Africa and the Council for Geoscience*. 302-303.

Bense, V. F., Van Balen, R. T., (2004). The effect of fault relay and clay smearing on groundwater flow patterns in the Lower Rhine Embayment. Basin Res. **16**, 397–411.

Bense, V. F., Gleeson, T., Loveless, S. E., Bour, O. and Scibek, J., (2013). Fault zone hydrogeology. *Earth-Science Reviews*, **127**, 171–192.

Bergman, F and Libby, W. F., (1957). Continental water balance, groundwater inventory and storage times, surface ocean mixing rates, and worldwide water circulation pattern from cosmic ray and bomb tritium, *Geohim Comochim Acta,* **12**, 277-296.

Beyer, M.; Morgenstern, U.; Jackson, B., (2014). Review of dating techniques for young groundwater (<100 years) in New Zealand. 53(*2*), in press.

Bird, P., Ben-Avraham, Z., Schubert, G., Andreoli, M. and Viola, G., (2006). Patterns of Stress and Strain Rate in Southern Africa. K. *Geophysics. Res*., 111(B8). B08402.

Bredenkamp, D. B., Botha, L.J., Van Tonder, G.J. and Van Rensburg, H.J., (1995). Manual on quantitative estimation of groundwater recharge and aquifer storativity WRC Report No. TT 73/95, Pretoria.

Bromley, J., Manstrom, B., Nisca, D. and Jamtlid, A. A., (1994). Airborne geophysics: application to ground-water study in Botswana. *Ground Water,* **32,** 79-90.

Bumby, A. J., Eriksson, P. G., van der Merwe, R. and Steyn, G., (2002). A half-graben setting for the Proterozoic Soutpansberg group (South Africa): evidence from the Blouberg area. Sedimentary Geology, **147**, 37–56.

Butler, J.J., Jr., (2005). Hydrogeological methods for estimation of spatial variations in hydraulic conductivity, in Hydrogeophysics, edited by Y. Rubin and S.S. Hubbard, Springer, Netherlands, 23-58.

Buttler, M., and Verhagen, B. T., (2013). Towards a Management model for the exploitation of the groundwater from the Taaibosch Karoo Graben, Limpopo Province in Abiye (2013) (Editor). The use of Isotope hydrogeology to characterize and assess water resources in Southern Africa, WRC Report TT 570/13. 53-76.

Cheney, E. S., Barton, J. M. and Brandl, G., (1990). Extent and age of the Soutpansberg sequences of southern Africa. *South African Journal of Geology*, **93**, 664–675.

Chilton, P. J. and Foster, S. S. D., (1995). Hydrological characterization and water-supply potential of basement aquifers in tropical Africa. *Hydrogeol* J **3**, 36-49.

Chinoda, G., Moyce, W., Matura, N., and Owen, R., (2009). Baseline report on the geology of the Limpopo Basin Area.

Clark, I. and Fritz, P., (1997). Environmental isotopes in hydrogeology. Lewis Publishers, New York.

Clark, L., (1985). Groundwater abstraction from Crystalline Complex areas of Africa. *Q. J. Eng. Geol*, **18,** 25-34.

Cook, P.G., (2003). A guide to regional groundwater flow in fractured rock aquifers. Seaview Press, Adelaide, Australia.

Craig, H., (1961). Isotopic variations in meteoric waters: *Science*, **133**, 1702–1703.

Dansgaard, W., (1964). Stable Isotope in Precipitation. Tellus, **16**, 436-468.

De Vries, J. J., Simmers, I., (2002). Groundwater recharge: an overview of processes and challenges. *Hydrogeology Journal*, **10**, 5–17.

Department of Water Affairs and Forestry. (1996a). South African Water Quality Guidelines: Domestic Use, Second edition, Pretoria Prepared by Ms T Belcher, Department of Water Affairs and Forestry Dr D C Grobler, CSIR Environmental Services Dr S Holmes, CSIR Environmental Services Mr J L J van der Westhuizen, Department of Water Affairs and Forestry Dr H R van Vliet, Institute for Water Quality Studies, Department of Water Affairs and Forestry

Department of Water Affairs and Forestry., (1996b). South African Water Quality Guidelines: Irrigation, Second edition, Pretoria. Prepared by Ms T Belcher, Department of Water Affairs and Forestry Dr D C Grobler, CSIR Environmental Services Dr S Holmes, CSIR Environmental Services Mr J L J van der Westhuizen, Department of Water Affairs and Forestry Dr H R van Vliet, Institute for Water Quality Studies, Department of Water Affairs and Forestry

Department of Water Affairs and Forestry., (1996c). South African Water Quality Guidelines: Livestock watering, Second edition, Pretoria. South Africa, Prepared Africa, prepared by Ms T Belcher, Department of Water Affairs and Forestry Dr D C Grobler, CSIR Environmental Services Dr S Holmes, CSIR Environmental Services Mr J L J van der Westhuizen, Department of Water Affairs and Forestry Dr H R van Vliet, Institute for Water Quality Studies, Department of Water Affairs and Forestry

Department of Water Affairs and Forestry., (2003). Internal Strategic Perspective document for the Limpopo Water Management Area. Prepared by Goba Moahloli Keeve Steyn (Pty) Ltd, Tlou and Matji Engineering and Management Services (Pty) Ltd, Golder Associates (Pty) Ltd, Charles Sellick and Associates cc.

Department of Water Affairs and Forestry., (2004). Internal Strategic Perspective document for the Limpopo Water Management Area. Prepared by Goba Moahloli Keeve Steyn (Pty) Ltd, Tlou and Matji Engineering and Management Services (Pty) Ltd, Golder Associates (Pty) Ltd, Charles Sellick and Associates cc.

Dewandel, B., Perrin, J. and Ahmed, S., (2010). Development of a tool for managing groundwater resources in semi-arid hard rock regions: application to a rural watershed in south India. *Hydrol Proc*, **24** (19), 2784–2797.

De Wit, M. J., Jones, M. G and Buchannan, D. L., (1992). The geology and tectonic evolution of the Pietersburg Greenstone Belt. South Africa. *Precambrian Research.* **55,** 123-153.

Dziembowski, Z. M., (1976). Die geohydrologie van die Dendrongebied, distrik Pietersburg. Report GH 2878. Directorate Geohydrology, Department of Water Affairs and Forestry, Pretoria.

Ebrahim, G., Villholth, K. and Boulos, M., (2016). "Modelling Groundwater Flow, Recharge and Dynamics of the Dendron (Mogwadi) Area, Limpopo River Basin, South Africa". Presentation, South Africa.

Ebrahim, G., Villholth, K. and Boulos, M., (2018). Supporting Sustainable Agricultural Groundwater Use in a Hard Rock Catchment, Hout, Limpopo Province, South Africa – Application of an Integrated Hydrogeological Model. (unpublished manuscript).

Fetter, C.W., (2001). Applied Hydrogeology, 4th ed. Prentice Hall, Inc. Upper saddle River, New Jersey, 598.

Geng, H., Brandl, G., Sun, M., Wonga, J. and Kröner, A., (2014). Zircon ages defining deposition of the Palaeoproterozoic Soutpansberg Group and further evidence for Eoarchaean crust in South Africa. *Precambrian Research.* **249**, 247–262.

Geyh, M., Amore, F.D., Darling, G., Paces, T., Pang, Z. and SILAR, J. (2000). Environmental Isotopes in the Hydrological Cycle: Principles and Applications – Volume 4: Saturated and Unsaturated Zone. IAEA, Vienna. 196.

Gustafson, G and Krásný, J (1994). Crystalline rock aquifers: Their occurrence, use and importance. *Appl. Hydrogeol*. **2**, 64-75.

Healy, R. W. and Cook, P. G., (2002). Using groundwater levels to estimate recharge. Hydrogeol. J., **10**, 91-109.

Hiscock, K. M., (2005). Hydrogeology: Principles and Practices. Blackwell Science, UK. 388.

Holland, M., (2011). Hydrogeological characterisation of crystalline basement aquifers within the Limpopo Province, South Africa (Doctoral dissertation).

Houston, J. F. T and Lewis, R. T., (1988). The Victoria Province Drought Relief Project, II Borehole Yield Relationships. Groundwater, **26**, 418-426.

International Water Management Institute (SA)., (2017): Estimated groundwater abstractions per year per farm from the WARMS data (Excel Spreadsheet).

Jolly, J. L., (1986). Borehole/irrigation survey and groundwater evaluation of the Doringlaagte drainage basin, Dendron (N.Tvl.). Report GH 3495. Directorate Geohydrology, Department of Water Affairs and Forestry, Pretoria.

Jones, M. J. (1985). The weathering zone aquifers of the basement complex areas of Africa. *Quarterly Journal of Engineering Geology*, **18**, 35-46.

Kreissig, L. Holzer and R. Frei., (2001). Geochronology of the Hout River Shear Zone and the metamorphism of the Limpopo belt, Southern Africa, *Precambrian Research,* **109**, 145–173.

Lerner, D. N., Issar, A. S., and Simmers, I., (1990). Groundwater recharge: a guide to understanding and estimating natural recharge. 8.

Letts, S., Torsvik, T.H., Webb, S. J. and Ashwal, L. D., (2011). New Paleoproterozoic palaeomagnetic data from the Kaapvaal Craton, South Africa. *Geological Society, London, Special Publications, **357**,* 9–26

Lloyd, J. W., (1986). A review of aridity and groundwater. *Hydrological Processes*, **1**, 63-78.

Maidment, D. R. and Hooper, R. P., (2005). Conceptual Framework. In: D.R. Maidment, ed. Hydrologic information system status report, chap. 2. Washington, DC: Consortium of Universities for the Advancement of Hydrologic Science, Inc (CUAHSI), 7–23.

Mandiwana, M., (2004). Geohydrologic potential and Groundwater Management in the Dendron Area, Limpopo Province. Unpublished master's thesis, University of the Witwatersrand, Johannesburg, South Africa.

Masiyandima, M., Van der Stoep, I., Mwanasawani, T., and Pfupajena, S. C., (2002). Groundwater management strategies and their implications on irrigated agriculture: the case of Dendron aquifer in Northern Province.

Matthys, A., Dippenaar Kai T., Witthu¨ser, J. and Louis Van Rooy., (2009). Groundwater occurrence in Basement aquifers in Limpopo Province, South Africa: model-setting-scenario approach. *Environ Earth Sci*, **59**,459–464.

Moghaddam, M. M., Sabseparvar, M., Mirzaei, S., and Heydarian, N., (2015). Interpretation of Aeromagnetic Data to Locate Buried Faults in North of Zanjan Province, Iran. J. *Geophys. Rem. Sens*, **4**,143.

Pietersen, K., Beekman, H. E., and Holland, M. (2011). South African Groundwater Governance Case Study. WRC Report No. KV 273/11.

Reeves, C., (2005). Aeromagnetic Survey: Principles, Practice, and Interpretation, Geosoft, Inc.

Rice, R. C., Bowman, R. S., and Jaynes, D. B., (1986). Percolation of water below an irrigated field. *Soil Science Society of America Journal*, ***50*** (4), 855-859.

Robb, L. J., Brandl, G., Anhaeusser, C. R. and Poujol, M., (2006). Archaean Granitoid Intrusions. In: Johnson, M.R., Anhaeusser, C.R., and Thomas, R.J. (Eds.). The geology of South Africa. *Geological society of South Africa*, Johannesburg/Council for Geoscience, Pretoria, 209-236.

Roering, C. Van Reeenen, D.D., Smit, C.A., Barton, J.M. Jr., De Beer, J.H., De Wit, M.J., Stettler, E.H. Van Schalwyk, J.F. Stevens, G. and Pretorius, S.J., (1992). Tectonic model for the evolution of the Limpopo Belt. *Precambrian Research*, **55**, 539-552.

Rose, S. and Long, A., (1988). Monitoring dissolved oxygen in ground water: Some basic considerations. *Ground Water Monitoring Review*, **8**, 93-97.

Rushton K, Weller J (1985) Response to pumping of a weathered-fractured granite aquifer. Journal of 625 Hydrology 80: 299-309.

Sakala, E., Tessema, A., and Nyabenze, P.K., (2014). Regional interpretation of Aeromagnetic data for groundwater exploration in Capricorn District, Limpopo, South Africa. *International journal of Modelling and Simulation*, **34**, 36-42.

Scanlon, B. R., Healy, R. W, and Cook, P. G., (2002). Choosing appropriate techniques for quantifying groundwater recharge. Hydrogeol J (in press). *DOI 10.1007/s10040-001-0176-2.*

Simmers, I., (1998). Groundwater recharge: an overview of estimation "problems" and recent development.

Smit, C. A., Roering, C. and Van Reenen, D. D., (1992). The structural framework of the southern margin of the Limpopo Belt, South Africa. *Precambrian Res*, **55**. 51- 67

Stettler, E. H., de Beer, J. H. and Blom, M.P., (1989). Crustal domains in the northern Kaapvaal as defined by magnetic lineaments. *Precambrian Res*, **45**. 263-276.

Todd MC, Washington R. 1999. Circulation anomalies associated with tropical-temperate troughs in southern Africa and the southwest Indian Ocean. Climate Dynamics 15: 937–951.

Tripathi, R. P and Singh, H. P., (1998). Soil erosion and conservation. New Age International (P) LTD Publishers, pp316.

Uken, R. and Watkeys, M. K., (1997). An interpretation of mafic dyke swarms and their relationship with major mafic magmatic events on the Kaapvaal Craton and Limpopo Belt. *S. Afr. J. Geol*, **100**(4). 341-348.

Van Biljon, W, J and Legg, J, H., (1983). The Limpopo Belt. *The Geological Society of South Africa*. **8**

Van Heerden J, Taljaard JJ. 1998. Chapter 4C. In Meteorology of the Southern Hemisphere, Karoly DJ, Vincent DG (eds). American Meteorological Society Monograph: Boston, Massachussetts, 307–336.

Van Reenen, D. D., Barton, J. M Jr., Roering, C., Smit, C. A. and Van Schalkwyk, J. F., (1987). Deep crustal response to continental collision: The Limpopo Belt of southern Africa. Geology, **15.** 11-14.

Van Reenen, D. D., Roering, C., Ashwal, L. D., and De Wit, M. J., (1992). Regional geological setting of the Limpopo Belt. *Precambrian Research*, ***55***(1-4), 1-5.

Van Reenen, D.D., Roering, C., Brandl, G., Stair, C.A. and Barton, J.M., Jr., (1990). The granulite-facies rocks of the Limpopo Belt, southern Africa. In: D. Vielzeuf and Ph. Vidal (Editors), Granulites and Crustal Evolution, Kluwer, Dordrecht, 257-289.

Van Wyk, E. (2010). Estimation of episodic groundwater recharge in semi-arid fractures hard rock aquifers. An unpublished Dissertation submitted in fulfilment of the requirements for the degree of Doctor of Philosophy in the Faculty of Natural and Agricultural Science, Department of Geohydrology, University of Free State, Bloemfontein, South Africa.

Varni, M., Comas, R., Weinzettel, P., Dietrich, S., (2013). Application of the water table fluctuation method to characterize groundwater recharge in the Pampa plain, Argentina. *Hydrological Sciences Journal*, **58** (7), 1445-1455.

Vegter, J.R. (2003). Hydrogeology of groundwater regions, Region 7, Polokwane/Pietersburg Plateau. WRC Report No. TT 209/03. Water Research Commission, Pretoria.

Verhagen, B. T., Butler, M. J., Van Wyk, E and Mutheiwana, S., (2009). A multi-tracer study of the origins, systematic and hydrological linkages of high concentrations in ground water in the Bochum District, Limpopo Province. WRC Report No. 1328/1/09. Water Research commission, Pretoria.

Verster, H., 2017. Personal communication.

Vogel, J.C. (1970). Carbon-14 dating of groundwater. Isotope hydrology 1970, Proc. Symp. IAEA, 9-13 March 1970, 225-237.

Weaver, J. M. C., Talma, A. S. and Cavé, L.S., (1999). Geochemistry and Isotopes for resource evaluation in the fractured rock aquifers of the Table Mountain Group. WRC Report No. 1009/1/03. Water Research Commission, Pretoria.

Weaver, J. M. C., Talma, A. S. and Cavé, L.S., (2007). Groundwater sampling: A comprehensive guide for sampling methods. WRC Report No. TT 303/07. Water Research Commission, Pretoria

Wilson, A. S., (2005). Hydrogeology, conceptual model and groundwater flow within alluvial aquifers of the Tenthill and Ma catchments, Lockyer Valley, Queensland (Doctoral dissertation, Queensland University of Technology).

Witthüser, K. T., Holland, M., Rossouw, T. G., Rambau, E., Bumby, A. J., Petzer, K. J., Dennis, I., Beekman, H., Van Rooy, J. L., Dippenaar, M. A., and De Wet, L.M., (2011). Hydrogeology of Basement aquifers in the Limpopo Province. WRC Report No. 1693/1/10, Pretoria.

World Health Organization (2008). World Health Organization. Guidelines for drinking water quality, (3rd Ed).

World Health Organization (2009). World Health Organization. Guidelines for drinking water quality.

Wright, E.P. (1992). The hydrogeology of crystalline basement aquifers in Africa. In: Wright, E.P. and Burgess, W.G. (eds.) Hydrogeology of Crystalline Basement Aquifers in Africa. Geological Society Special Publication No 66. Geological Society, London.

Xu, Y. and Beekman, HE. (Eds). (2003). Groundwater recharge estimation in Southern Africa. UNESCO IHP Series No. 64, UNESCO Paris. ISBN 92-9220-000-3.

Yang, X., Steward, D. R., de Lange, W. J., Lauwo, S.Y., Chubb, R. M and Bernard, E. A (2010). Data model for system conceptualization in groundwater studies. *International Journal of Geographical Information Science*, 24 (5), 677–694.

Zotarelli, L., Dukes, M. D., Romero, C. C., Migliaccio, K.W., and Morgan, K. T. (2010). Step by step calculation of the Penman–Monteith evapotranspiration (FAO-56 method). AE459. Agricultural and Biological Engineering Department, Florida Cooperative Extension Service, IFAS, UF. URL: http://edis.ifas.ufl.edu/ae 459, 12

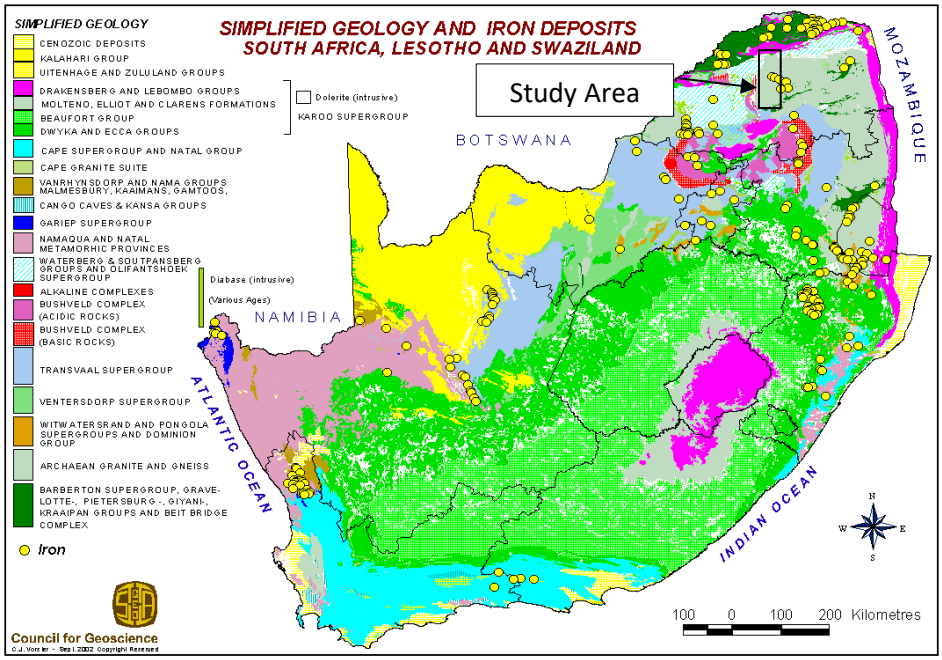
Appendix A: GRIP borehole data

GRIP borehole Number	Quaternary Catchment area	Longitude [WGS84]	Latitude [WGS84]	Borehole depth [m]	Water level [m.b.g.l]
H04-1691	A71F	29,32853	-23,6842	23,01	11
H04-1697	A71E	29,30232	-23,7404	104,05	20,84
H04-1699	A71F	29,31703	-23,7339	66,85	11,7
H04-1700	A71F	29,33839	-23,7314	48,95	14,87
H04-1702	A71F	29,37003	-23,7296	76,72	6,15
H04-1708	A71F	29,3777	-23,7306	126	18,06
H04-1710	A71F	29,38303	-23,7315	149,87	30,09
H04-1715	A71F	29,3904	-23,7319	149,78	31,14
H04-1718	A71F	29,3982	-23,7189	94,13	45,64
H04-1719	A71F	29,40614	-23,6995	66,02	9,43
H04-1803	A71E	29,20909	-23,453	0	25,64
H04-1808	A71E	29,21922	-23,8709	65,1	31,3
H04-1811	A71E	29,19886	-23,9007	44,35	2,13
H04-1857	A71F	29,4022	-23,7085	73	29,1
H04-1859	A71F	29,34823	-23,7108	70	9,65
H04-1860	A71F	29,40817	-23,6993	50	6,85
H04-1905	A71F	29,26342	-23,849	80,03	22,68
H04-1928	A71E	29,20683	-23,4529	0	23,3
H04-2098	A71F	29,2428	-23,847	71,4	13,35
H04-2149	A71E	29,24789	-23,6237	70	7,69
H04-2152	A71E	29,22168	-23,6118	75,5	11,23
H04-2163	A71E	29,2905	-23,7285	59,69	8,77
H04-2177	A71E	29,25489	-23,6293	70	3,14
H04-2178	A71E	29,2555	-23,6285	100	2,73
H04-2180	A71E	29,28931	-23,5466	107	30,46
H04-2181	A71E	29,28734	-23,5515	73	33,92
H04-2182	A71E	29,28784	-23,5485	109,64	32,45

H04-2183	A71E	29,30145	-23,54	92	46,2
H04-2184	A71E	29,29842	-23,5435	110	46,85
H04-2200	A71F	29,29006	-23,8334	42,26	20,72
H04-2201	A71E	29,20483	-23,5119	76,51	27,68
H04-2222	A71E	29,30262	-23,7484	66,14	6,93
H04-2223	A71E	29,19716	-23,8578	77,2	11,59
H04-2235	A71E	29,27719	-23,7062	78	23,24
H04-2343	A71E	29,24395	-23,8235	60	14,4
H04-2344	A71E	29,23296	-23,8174	58	8,4
H04-2345	A71E	29,21704	-23,8188	62	37,4
H04-2349	A71E	29,23676	-23,6837	78	7,08
H04-2357	A71E	29,19091	-23,4844	110	43,6
H04-2360	A71E	29,29758	-23,5974	36,38	13,92
H04-2385	A71E	29,22253	-23,6101	29,1	11,06
H04-2387	A71E	29,24631	-23,6008	28,55	8,01
H04-2411	A71E	29,24424	-23,8208	57,45	18,83
H04-2438	A71E	29,24503	-23,6278	15,73	3,89
H04-2439	A71E	29,24482	-23,628	70	3,76
H04-2447	A71E	29,24611	-23,625	99,75	5,3
H04-2448	A71E	29,24525	-23,6288	120	4,76
H04-2562	A71F	29,27582	-23,83	54	15,81
H04-2563	A71E	29,25869	-23,8186	60	22,98
H04-2577	A71F	29,32795	-23,6836	101,32	19,96
H04-2584	A71F	29,39575	-23,6615	42,58	6,21
H04-2586	A71F	29,39445	-23,6606	90,6	8,2
H04-2610	A71E	29,28675	-23,7603	59,28	10,21
H11-0737	A71G	29,21914	-23,3208	99,77	80,55
H11-0784	A71G	29,24545	-23,3069	100	81,2
H11-0785	A71G	29,24561	-23,3009	82,8	76
H11-0786	A71G	29,26641	-23,285	59	41,6
H11-0787	A71G	29,26668	-23,285	52,27	42,07
H11-0789	A71G	29,26009	-23,2814	80	47,68

H11-0790	A71G	29,26444	-23,2934	77,47	46,53
H11-0795	A71G	29,24561	-23,3122	122	76,05
H11-0796	A71G	29,25467	-23,3428	70	28,45
H11-0797	A71G	29,25	-23,3403	89,81	41,21
H11-0799	A71G	29,25981	-23,331	87,8	26,3
H11-0800	A71G	29,266	-23,3299	75,2	26
H11-0801	A71G	29,25736	-23,3411	61	44,86
H11-0802	A71G	29,24329	-23,3469	49,32	34,25
H11-0804	A71G	29,26173	-23,3226	43	26,75
H11-0805	A71G	29,23937	-23,3277	85,5	57,03
H11-0806	A71G	29,23642	-23,3142	0	80,85
H11-0807	A71G	29,2257	-23,3332	73,6	62,72
H11-0810	A71G	29,22276	-23,3249	99,2	73,7
H11-0811	A71G	29,22359	-23,3238	104,95	76,41
H11-0812	A71G	29,22248	-23,3227	102,1	82,6
H11-0813	A71G	29,22192	-23,3205	91,56	80,38
H11-0815	A71G	29,20975	-23,3319	99,73	68,99
H11-0827	A71E	29,22519	-23,4694	98,34	40,63

Appendix B: Mineral (Iron) Map of South Africa. Source: CGS



Appendix C: Estimated groundwater abstractions per year per farm from the WARMS data (Ebrahim et al, 2016)

	Total Irrigation pumping licenced volume per year per farm extracted from WARMS DATA								
Farm name	year_2007	year_2008	year_2009	year_2010	year_2011	year_2012	year_2013	year_2014	year_2015
BERGPLAATS 40 LS	46800	46800	46800	46800	46800	46800	46800	46800	46800
BUISDORP 37 LS	16000	16000	16000	16000	16000	16000	16000	16000	16000
BUISHOEK 54 LS	69500	69500	69500	69500	69500	69500	69500	69500	69500
KAALBULT 53 LS	507500	507500	507500	507500	507500	507500	507500	507500	507500
YORK 93 LS	283700	283700	283700	283700	283700	283700	283700	283700	283700
NIMMERSAULT 109 LS	232780	232780	232780	232780	232780	232780	232780	232780	232780
DEDROOM 112 LS	74000	74000	74000	74000	74000	74000	74000	74000	74000
ALTENBURG 111 LS	218959	218959	218959	218959	218959	218959	218959	218959	218959
BORNST 107 LS	364000	364000	364000	364000	364000	364000	364000	76000	76000
BAVIAANSPOORT 130 LS	510270	510270	510270	510270	510270	510270	510270	407770	407770
NE PLUS ULTRA 110 LS	595540	595540	595540	595540	595540	595540	595540	595540	595540
BLOEMPJES VLEI 125 LS	282485	282485	282485	282485	282485	282485	282485	282485	282485
NEW HANOVER 124 LS	15000	15000	15000	15000	15000	15000	15000	15000	15000
WALDBURG 126 LS	62582	62582	62582	62582	62582	62582	62582	62582	62582
GROOTHOEK 129 LS	103500	103500	103500	103500	103500	103500	103500	103500	103500

CLAUDIUS 106 LS	360500	360500	360500	360500	360500	360500	360500	360500	360500
	269378	269378	269378	269378	269378	269378	269378	269378	269378
POTSDAM 128 LS	206900	206900	206900	206900	206900	206900	206900	206900	206900
GELUKSFONTEIN 127 LS	360544	360544	317044	257044	257044	257044	257044	257044	251222
KLEIN COLLIE 123 LS	161056	161056	161056	135287	135287	135287	135287	135287	135287
BELLEVUE 122 LS	164500	164500	164500	164500	164500	164500	164500	164500	164500
JAN ANTONIE 121 LS	32500	32500	32500	32500	32500	32500	32500	32500	32500
ANEX ALION 170 LS	706100	706100	706100	668850	668850	668850	668850	668850	668850
DUITSCHLAND 169 LS	147000	147000	147000	147000	147000	147000	147000	147000	147000
TWEEFONTEIN 166 LS	556600	556600	556600	556600	556600	556600	556600	556600	556600
DIDEMUS 171 LS	474790	474790	474790	431290	431290	431290	431290	431290	431290
GOEDGENOEG 185 LS	1757241	1757241	1757241	1757241	1757241	1757241	1757241	1757241	1757241
KRAAIFONTEIN 186 LS	387731	387731	387731	387731	387731	387731	387731	387731	387731
KWAGGASBULT 187 LS	526000	526000	526000	526000	526000	526000	526000	526000	526000
PATRYSPAN 207 LS	207900	207900	207900	207900	207900	207900	207900	207900	207900
SOHO 204 LS	202000	202000	202000	202000	101000	101000	101000	101000	101000
LEKKERLACH 206 LS	201000	201000	201000	201000	201000	201000	201000	201000	201000
KALKBULT 183 LS	816700	816700	816700	816700	816700	816700	816700	816700	816700
KALKBANK 182 LS	442141	442141	442141	442141	442141	442141	442141	442141	442141
KALKFONTEIN 173 LS	908387	908387	908387	908387	908387	908387	908387	908387	908387
RECHTDAAR 175 LS	151500								

TOMMY 119 LS	74750	74750	74750	25500	25500	25500	25500	25500	25500
VOORSCHOTEN 115 LS	153700	153700	153700	153700	153700	153700			
AMSTERDAM 116 LS	279948	279948	279948	279948	279948	279948	279948	279948	279948
VERDWAALPAN 181 LS	155184	155184	155184	155184	155184	155184	155184	155184	155184
BRAKSPRUIT 211 LS	1183000	1183000	1183000	1183000	1183000	1183000	1183000	1183000	1183000
ONVERWACHT 209 LS	198720	198720	198720	198720	198720	198720	198720	198720	198720
DELOSKOP 205 LS	1071134	1071134	1071134	1071134	1071134	1071134	1071134	1071134	1071134
VISCHGAT 555 LS	52000	52000	52000	52000	52000	52000	52000	52000	52000
KALKGAT 554 LS	1208356	1208356	1208356	1208356	1208356	1208356	850178	835178	835178
ENKELDEBOSCH 572 LS	207250	207250	207250	207250	207250	207250	207250	207250	207250
KALKFONTEIN 573 LS	1094990	1094990	1094990	1094990	1094990	1094990	1094990	1094990	1094990
OUDOORNBULT 571 LS	270610	270610	270610	270610	270610	270610	270610	270610	270610
PALMIETFONTEIN 609 LS	22080	22080	22080	22080	22080	22080	22080	22080	22080
LANGGEREKT 610 LS	284000	284000	284000	284000	284000	284000	284000	284000	284000
DE PUT 611 LS	362101	362101	362101	362101	362101	362101	362101	362101	362101
WITKLIP 556 LS	657000	657000	657000	657000	657000	657000	328500	328500	328500
KALKLAAGTE 214 LS	474984	474984	474984	474984	474984	474984	304492	304492	304492
SPRINGFORBI 557 LS	746852	746852	746852	746852	746852	746852	481852	481852	481852
RUIGTEVLEI 559 LS	126984	126984	126984	126984	126984	126984	63492	63492	63492
GROENVLAKTE 560 LS	30060	30060	30060	30060	30060	30060	30060	30060	30060
MAKOUWLAAGTE 561 LS	165000	165000	165000	165000	165000	165000	165000	165000	165000

GOEDGEDACHT 49 LS	1024382	1024382	1024382	1024382	1024382	1024382	1024382	1024382	1024382
SPITSKOP 217 LS	573000	573000	573000	573000	573000	573000	573000	573000	573000
KALKOVEN 299 LS	2424144	2424144	2424144	2424144	2424144	2424144	2424144	2424144	2424144
SODOM 300 LS	304299	304299	304299	304299	304299	304299	304299	304299	304299
HOUT RIVIER 50 LS	206570	206570	206570	206570	206570	206570	206570	206570	206570
PROESERPINA 301 LS	378847	378847	378847	378847	378847	378847	378847	378847	378847
NEUSTADT 113 LS	264000	264000	264000	264000	264000	264000	264000	264000	264000
LEYDEN 114 LS	924612	924612	924612	924612	924612	924612	924612	924612	924612
RADE VORUE WALDA 349 LS	160832	160832	132782	132782	132782	132782	132782	132782	132782
PLATKLIPFONTEIN 179 LS	54500	54500	54500	54500	54500	54500	54500	54500	54500
DRAAIFONTEIN 180 LS	125000	125000	125000	125000	125000	125000	125000	125000	125000
HAAKDOORNBULT 215 LS	361080	361080	361080	361080	361080	361080	180540	180540	180540
MAROELAPAN 613 LS	42320	42320	42320	42320	42320	42320	42320	42320	42320
KALKFONTEIN 615 LS	13500	13500	13500	13500	13500	13500	13500	13500	13500
STETTIN 133 LS	40000	40000	40000	40000	40000	40000	40000	40000	40000
MEANDERTHAL 188 LS	184380	184380	184380	184380	184380	184380	184380	184380	184380
ZANDPUT 202 LS	50000	50000	50000	50000	50000	50000	50000	50000	50000
VISCHKUIL 545 LS	43920	43920	43920	43920	43920	43920	43920	43920	43920
MACHICHAANS 709 LS	18000	18000	18000	18000	18000	18000	18000	18000	18000
DIEPLAAGTE 708 LS	8000	8000	8000	8000	8000	8000	8000	8000	8000
KLIPKOPJES 707 LS	5000	5000	5000	5000	5000	5000	5000	5000	5000

GROENFONTEIN 706 LS	171590	171590	171590	171590	171590	171590	171590	171590	109095
TONDERSHOEK 658 LS	133400	133400	133400	133400	133400	133400	133400	133400	133400
COMBRO 163 LS	103000	103000	103000	103000	103000	103000	103000	103000	103000
APPELFONTEIN 189 LS	903500	903500	903500	903500	903500	903500	903500	903500	903500
MALIETZIES 606 LS	117340	117340	117340	117340	117340	117340	117340	117340	117340
GOEDVERWACHT 224 LS	157490	157490	157490	157490	157490	157490	157490	157490	157490
Total (million cubic meter per annum)	**30.034**	**29.883**	**29.811**	**29.596**	**29.495**	**29.495**	**27.975**	**27.569**	**27.501**

Appendix D: Lithology data used to construct a cross-section.

ID	Easting	Northing	Elevation	starting	Ending	Lithology	GeositeInfo_Farm
H04-0963	-23.82687	29.21727	1293	0	2	SOIL	VAALKOP PORTION VAALKOP
H04-0963	-23.82687	29.21727	1293	2	5	Dolerite	VAALKOP PORTION VAALKOP
H04-0963	-23.82687	29.21727	1293	5	20	Dolerite	VAALKOP PORTION VAALKOP
H04-0963	-23.82687	29.21727	1293	20	35	Dolerite	VAALKOP PORTION VAALKOP

H04-0963	-23.82687	29.21727	1293	35	40	Dolerite	VAALKOP PORTION VAALKOP
H04-0963	-23.82687	29.21727	1293	40	47	Dolerite	VAALKOP PORTION VAALKOP
H04-0962	-23.82576	29.21894	1321	0	1	SOIL	
H04-0962	-23.82576	29.21894	1321	42	47	Gneiss	VAALKOP PORTION VAALKOP
2329AD00243	-23.29853	29.44312	968	0	2.13	SOIL	MALIETZIES GED GA-MAKIBELO
2329AD00243	-23.29853	29.44312	968	2.13	14.32	Granite	
2329AD00243	-23.29853	29.44312	968	14.32	16.45	NO SAMPLE	TWEEFONTEIN
2329AD00243	-23.29853	29.44312	968	16.45	56.08	Granite	TWEEFONTEIN
2329AD00181	-23.2977	29.44783	969	0	4	Granite	HUGOMOND
2329AD00181	-23.2977	29.44783	969	4	55	Granite	HUGOMOND
2329AD00230	-23.29025	29.49004	982	0	7.62	SOIL	HUGOMOND
2329AD00230	-23.29025	29.49004	982	7.62	19.81	Granite	
2329AD00230	-23.29025	29.49004	982	19.81	35.66	Dolerite	HUGOMOND
2329AD00230	-23.29025	29.49004	982	35.66	63.7	Granite	

H04-1421	H04-1421	H04-1421	H04-1421	H04-1421	H04-1421	H04-1421
53	40	38	32	9	7	2
55	53	40	38	32	9	7
2	13	2	6	23	2	5
Schist	Granite	Schist	Granite	Granite	Schist	Granite
Schist	Granite	Schist	Granite	Granite	Schist	Granite
53	40	38	32	9	7	2
Consolidated	Consolidated	Consolidated	Consolidated	Consolidated	Consolidated	Consolidated
Unweathered	Unweathered	Unweathered	Unweathered	Highly	Highly	Highly
				Moderately		Moderately
29,18921	29,18921	29,18921	29,18921	29,18921	29,18921	29,18921
-23,8541	-23,8541	-23,8541	-23,8541	-23,8541	-23,8541	-23,8541
1322	1322	1322	1322	1322	1322	1322
1269	1282	1284	1290	1313	1315	1320
1267	1269	1282	1284	1290	1313	1315
722954	722954	722954	722954	722954	722954	722954
7360204	7360204	7360204	7360204	7360204	7360204	7360204
Rho	Rho	Rho	Rho	Rho	Rho	Rho

2329CC00004	2329CB00440	2329CB00440	H04-1426	H04-1426	H04-1426	H04-1421
0,6	5	0	69	63	51	55
48,15	72	5	84	69	63	95
47,55	67	5	15	6	12	40
Granite	Quartzite	Quartzite	Granite	Granite	Granite	Granite
Granite	Quartzite	Quartzite	Granite	Granite	Granite	Granite
0,6	5	0	69	63	51	55
Consolidated	Consolidated	Consolidated	Consolidated	Consolidated	Consolidated	Consolidated
		Highly	Unweathered	Highly	Highly	Unweathered
29,19643	29,32144	29,32144	29,26149	29,26149	29,26149	29,18921
-23,9394	-23,5158	-23,5158	-23,5259	-23,5259	-23,5259	-23,8541
1469	1097	1097	1127	1127	1127	1322
1468,4	1092	1097	1058	1064	1076	1267
1420,85	1025	1092	1043	1058	1064	1227
723542,8	737035,8	737035,8	730894,6	730894,6	730894,6	722954
7350747	7397467	7397467	7396445	7396445	7396445	7360204
Rho	Rho	Rho	Rho	Rho	Rho	Rho

2329AD 00227	2329AD 00227	2329AD 00223	2329AD 00223	2329CC0 0005	2329CC0 0005	2329CC0 0005
24,38	1,52	1,52	0	12,8	0,6	0
42,97	24,38	22,86	1,52	45,41	12,8	0,6
18,59	22,86	21,34	1,52	32,61	12,2	0,6
NO SAMPL	Granite	Granite	Granite	Granite	Granite	SOIL
NO	Granite	Granite	Granite	Granite	Granite	SOIL
24,38	1,52	1,52	0	12,8	0,6	0
	Consolid ated	Consolid ated	Consolid ated	Consolid ated	Consolid ated	Unconsol idated
	Highly		Highly		Highly	
29,49008	29,49008	29,49006	29,49006	29,22033	29,22033	29,22033
-23,2902	-23,2902	-23,2902	-23,2902	-23,9077	-23,9077	-23,9077
989	989	989	989	1394	1394	1394
964,62	987,48	987,48	989	1381,2	1393,4	1394
946,03	964,62	966,14	987,48	1348,59	1381,2	1393,4
754693,9	754693,9	754691,9	754691,9	726031,2	726031,2	726031,2
7422165	7422165	7422165	7422165	7354217	7354217	7354217
Rho	Rho	Rho	Rho	Rho	Rho	Rho

2329AB00531	2329AB00506	2329AB00506	2329AB00507	2329AB00507	2329AD00177	2329AD00227
0,61	7,32	2,44	60	1	0	42,97
27,13	25,3	7,32	100	60	80	45,72
26,52	17,98	4,88	40	59	80	2,75
Granite	Granite	Quartzite	Granite	Granite	Granite	Granite
Granite	Granite	Quartzite	Granite	Granite	Granite	Granite
0,61	7,32	2,44	60	1	0	42,97
Consolidated	Consolidated	Consolidated	Consolidated	Consolidated	Consolidated	Consolidated
				Highly	Highly	
29,39893	29,38949	29,38949	29,37338	29,37338	29,49005	29,49008
-23,0827	-23,1577	-23,1577	-23,1896	-23,1896	-23,2899	-23,2902
996	937	937	944	944	989	989
995,39	929,68	934,56	884	943	989	946,03
968,87	911,7	929,68	844	884	909	943,28
745746,1	744642,5	744642,5	742934,8	742934,8	754691,4	754693,9
7445308	7437016	7437016	7433505	7433505	7422196	7422165
Ms	Rho	Rho	Rho	Rho	Rho	Rho

Geosite	2329AB00531	2329AB00531
Depth Top	44,2	27,13
Depth	78,33	44,2
thickness	34,13	17,07
FORMATION	Granite	Dolerite
STRATUM	Granite	Dolerite
top string	44,2	27,13
Material Type	Consolidated	Consolidated
Weathering		
Fracturing		
Longitude	29,39893	29,39893
Latitude	-23,0827	-23,0827
Elevation	996	996
Top elevation	951,8	968,87
Bot_elevation	917,67	951,8
utmX	745746,1	745746,1
utmY	7445308	7445308
CHRONOSTRA	Ms	Ms